Groundwater-stream water interactions: point and distributed measurements and innovative upscaling technologies

Inaugural-Dissertation to obtain the academic degree

Doctor of Philosophy (Ph.D.) in River Science
Submitted to the Department of Biology, Chemistry and Pharmacy of

Freie Universität Berlin
by

GAONA GARCÍA, JAIME

Berlin, 2019

The work of this doctoral thesis was conducted from 1st of December 2015 to 23th April 2019 under the supervision of PD Dr. rer. nat. habil. Jörg Lewandowski (Leibniz Institute of Freshwater Ecology and Inland Fisheries / Humboldt Universität Berlin) and Prof. Dr. Alberto Bellin (University of Trento, Italy). The work was carried out at the Leibniz Institute of Freshwater Ecology and Inland Fisheries Berlin, Germany, at the Free University Berlin, Germany and at the University of Trento, Italy.

1st Reviewer: **PD Dr. Jörg Lewandowski**

2nd Reviewer: **Prof. Dr. Klement Tockner**

Date of defence: 27 June 2019

The SMART Joint Doctorate Programme

Research for this thesis was conducted with the support of the Erasmus Mundus Programme, within the framework of the Erasmus Mundus Joint Doctorate (EMJD) SMART (Science for Management of Rivers and their Tidal systems). EMJDs aim to foster cooperation between higher education institutions and academic staff in Europe and third countries with a view to creating centres of excellence and providing a highly skilled 21st century workforce enabled to lead social, cultural and economic developments. All EMJDs involve mandatory mobility between the universities in the consortia and lead to the award of recognized joint, double or multiple degrees.

The SMART programme represents collaboration among the University of Trento, Queen Mary University of London and Free University Berlin. Each doctoral candidate within the SMART programme has conformed to the following during the 3 years of study:

(i) Supervision by a minimum of two supervisors in two institutions (their primary and secondary institutions).

(ii) Study for a minimum period of 6 months at their secondary institution.

(iii) Successful completion of a minimum of 30 ECTS of taught courses.

(iv) Collaboration with an associate partner to develop a particular component/application of their further research that is of mutual interest.

(v) Submission of a thesis within 3 years of commencing the programme.

The SMART Erasmus Mundus Joint Doctoral Programme has been funded by the European Commission, SGA 2015-1628. This publication reflects the views only of the authors, and the Commission cannot be held responsible for any use which may be made of the information contained therein.

"Education is to bring people to themselves,
and at the same time, know how to conform to the limits.
But with discipline, there must also be intuition and love"

Mlle. Nadia Boulanger

Table of contents

Summary

The need to consider groundwater and surface water as a single resource has fostered the interest of the scientific community on the interactions between surface water and groundwater. The region below and alongside rivers where surface hydrology and subsurface hydrology concur is the hyporheic zone. This is the region where water exchange determines many biogeochemical and ecological processes of great impact on the functioning of rivers. However, the complex processes taking place in the hyporheic zone require a multidisciplinary approach.

The combination of innovative point and distributed techniques originally developed in separated disciplines is of great advantage for the indirect identification of water exchange in the hyporheic zone. Distributed techniques using temperature as a tracer such as fiber-optic distributed temperature sensing can identify the different components of groundwater-surface water interactions based on their spatial and temporal thermal patterns at the sediment-water interface. In particular, groundwater, interflow discharge and local hyporheic exchange flows can be differentiated based on the distinct size, duration and sign of the temperature anomalies. The scale range and resolution of fiber-optic distributed temperature sensing are well complemented by geophysics providing subsurface structures with a similar resolution and scale. Thus, the use of fiber-optic distributed temperature sensing to trace flux patterns supported by the exploration of subsurface structures with geophysics enables spatial and temporal investigation of groundwater-surface water interactions with an unprecedented level of accuracy and resolution.

In contrast to the aforementioned methods that can be used for pattern identification at the interface, other methods such as point techniques are required to quantify hyporheic exchange fluxes. In the present PhD thesis, point methods based on hydraulic gradients and thermal profiles are used to quantify hyporheic exchange flows. However, both methods are one-dimensional methods and assume that only vertical flow occurs while the reality is much more complex. The study evaluates the accuracy of the available methods and the factors that impact their reliability. The applied methods allow not only to quantify hyporheic exchange flows but they are also the basis for an interpretation of the sediment layering in the hyporheic zone.

For upscaling of the previous results three-dimensional modelling of flow and heat transport in the hyporheic zone combines pattern identification and quantification of fluxes into a single framework. Modelling can evaluate the influence of factors governing groundwater-surface water interactions as well as assess the impact of multiple aspects of model design and calibration of high impact on the reliability of the simulations. But more importantly, this modelling approach enables accurate estimation of water exchange at any location of the domain with unparalleled resolution. Despite the challenges in 3D modelling of the hyporheic zone and in the integration of point and distributed data in models, the benefits should encourage the hyporheic community to adopt an integrative approach comprising from the measurement to the upscaling of hyporheic processes.

Zusammenfassung

Die Notwendigkeit, Grundwasser und Oberflächenwasser als eine zusammenhängende Ressource zu betrachten, hat das Interesse der Wissenschaft für die Wechselwirkungen zwischen Grundwasser und Oberflächenwasser geweckt. Die Grenzzone unterhalb und entlang von Flüssen, in denen Oberflächenwasser-Hydrologie und Untergrund-Hydrogeologie zusammen treffen, wird hyporheische Zone genannt. Der Wasser-Fluxe in der hyporheischen Zone sind für viele biogeochemische und ökologische Prozesse entscheidend und haben einen großen Einfluss auf das Funktionieren des Ökosystems Fluss. Ein Verständnis der komplexen Vorgänge in der hyporheischen Zone erfordert einen multidisziplinären Ansatz.

Die Kombination aus innovativen, punktuellen und flächig-verteilten Messtechniken, die ursprünglich in unterschiedlichen Disziplinen entwickelt wurden, ist für die Untersuchung des Wasseraustauschs in der hyporheischen Zone von großem Vorteil. Flächig-verteilte Messtechniken, bei denen die Temperatur als Tracer verwendet wird wie z. B. die faseroptische Temperaturmessung, können die verschiedenen Komponenten von Grundwasser-Oberflächenwasser Wechselwirkungen anhand ihrer räumlichen und zeitlichen thermischen Muster an der unmittelbaren Sediment-Wasser-Grenzfläche identifizieren. Insbesondere Grundwasser, Zwischenabfluss und lokaler hyporheischer Austausch können aufgrund der spezifischen Größe, Dauer und dem Vorzeichen der Temperaturanomalien unterschieden werden. Der Skalenbereich und die räumliche Auflösung der faseroptischen Temperaturmessung wird gut durch die Geophysik ergänzt, da sie Daten mit vergleichbarer raumlicher Auflösung und auf vergleichbarer Skala liefert. Somit ermöglicht die Kombination der beiden Techniken, also der faseroptischen Temperaturmessung zur Mustererkennung und der Geophysik zur Erfassung der Untergrundstrukturen, ein Prozessverständnis der Grundwasser-Oberflächenwasser Wechselwirkungen mit einer bisher unerreichten Genauigkeit und Auflösung.

Im Gegensatz zu den zuvor genannten Methoden, die für eine Mustererkennung der Grundwasser-Oberflächenwasser Wechselwirkungen geeignet sind, können Punktmessungen genutzt werden, um den hyporheischen Wasseraustausch zu quantifizieren. In der vorliegenden Doktorarbeit habe ich Punktmessungen basierend auf hydraulischen Gradienten

und thermischen Sedimenttiefenprofilen genutzt, um den hyporheischen Austausch zu quantifizieren. Beide Methoden sind allerdings eindimensionale Methoden und setzen voraus, dass nur vertikale Fluxe auftreten. Die Realität ist wesentlich komplexer. Die angewendeten Methoden erlauben nicht nur, die hyporheischen Fluxe genau zu quantifizieren, sondern geben auch Aufschluss über die Strukturen des Sediments und ergänzen damit die geophysikalische Erkundung.

Um die Ergebnisse hoch zu skalieren, wurden die identifizierten Muster und die quantifizierten Fluxe in einer dreidimensionale Modellierung des Wasser- und Wärmetransports in der hyporheischen Zone kombiniert. Die Modellierung kann genutzt werden, um die Faktoren zu evaluieren, die die Wechselwirkungen zwischen Grundwasser und Oberflächenwasser steuern. Noch wichtiger ist es jedoch, dass dieser Modellierungsansatz eine genaue Abschätzung des Wasseraustauschs an jedem Ort des Modellgebietes mit einer beispiellosen Auflösung ermöglicht. Obwohl es Herausforderungen bei der Implementierung der 3D-Modellierung hyporheischer Zonen sowie bei der Integration von Punkt- und flächig-verteilten Daten in die Modelle gibt, sollten der mögliche Nutzen die hyporheische Wissenschaftsgemeinschaft dazu ermutigen, weitere Forschungsanstrengungen in dieser Richtung zu unternehmen.

Thesis outline

This thesis is composed of five chapters. The first chapter is the general introduction (Chapter 1). The following three chapters (Chapters 2 to 4) are manuscripts of scientific publications, either published, submitted or close to submission. Each manuscript contains its own abstract, introduction, material and methods, results, discussion and conclusions sections together with the associated references. Given the sequential nature of the work developed along these three chapters on identification, quantification and extrapolation of groundwater-surface water interactions, the last chapter (Chapter 5) is devoted to the simultaneous discussion of the findings of the chapters in the context of the general objectives of the thesis.

Chapter 1:

General introduction

Chapter 2:

Jaime Gaona, Karin Meinikmann and Jörg Lewandowski (2019). Identification of groundwater exfiltration, interflow discharge and hyporheic exchange flows by fiber-optic distributed temperature sensing supported by electromagnetic induction geophysics. *Hydrological Processes,* 2019; 1– 13. https://doi.org/10.1002/hyp.13408 (published)

Author's contributions: **JG** and JL designed the study. **JG,** KM and JL collected the data. **JG** processed the data. **JG**, KM and JL interpreted the data and conceptualized the manuscript. **JG** wrote the manuscript and all authors contributed to the text. **JG**, KM and JL revised the manuscript.

Chapter 3:

Jaime Gaona, Jörg Lewandowski. (To be submitted). Quantification of vertical hyporheic exchange flows under strong upwelling in a heterogenous streambed: comparison of hydraulic and thermal methods.

Ready for submission to peer-review journals.

Author's contributions: **JG** and JL designed the study. **JG** collected the data. **JG** processed the data. **JG** and JL interpreted the data and conceptualized the manuscript. **JG** wrote the manuscript and JL contributed to the text.

Chapter 4:

Jaime Gaona, Alberto Bellin. (To be submitted). Flow and heat transport modelling in the hyporheic zone based on high-resolution temperature and geophysics datasets.

Ready for submission to peer-review journals.

Author's contributions: **JG** and AB designed the study. **JG** collected the data. **JG** processed the data. **JG** and AB interpreted the data and conceptualized the manuscript. **JG** wrote the manuscript and AB contributed to the text.

Chapter 5:

General discussion

List of figures

List of tables

Chapter 1: General introduction

1.1 Groundwater-surface interactions

Surface water hydrology and groundwater hydrology are getting closer each day. The traditionally separated perception of groundwater (GW) and surface water (SW) is no longer accepted. Groundwater and surface water are a single resource: surface and subsurface hydrology come together by the investigation of GW-SW interactions (Winter et al., 1999). These interactions take place in the area beneath and alongside the river called the hyporheic zone (HZ) (Harvey & Bencala, 1993; White, 1993). In the HZ, hydrological processes are controlled by both surface drivers (climate, geomorphology, obstacles to the flow) and underground drivers (hydrogeological conditions, sediment properties…). The flows between GW and SW are called hyporheic exchange flows (HEF) (Wondzell & Swanson, 1999). HEF comprises groundwater discharging to the overlying water body, surface water infiltrating into the aquifer and the portion of surface water that enters the sediment, remains for a certain residence time in the HZ flowing through the sediment, and finally re-entering to the surface water body. The coincidence of surface water conditions and groundwater conditions in the hyporheic zone results in complex interactions and overlap of characteristics and processes of both adjacent compartments (Sophocleous, 2002). Thus, the HZ is the interface where not only water exchange occurs but also biogeochemical and ecological processes show characteristics of both GW and SW (Fleckenstein et al., 2008; Tonina & Bufigton, 2009).

Despite the widespread perception of groundwater as a key factor of river functioning, there is still some lack of knowledge about the existence and relevance of GW-SW interactions (Boulton, 2000). GW-SW interactions are a key component of the water cycle and require careful consideration by water resources managers (Gorelick, 1986). The lack of accurate estimates of the volumes exchanged between rivers and aquifers put at risk the efficacy of water management policies (e.g. environmental flows requirements of the EU Water Framework Directive). GW-SW interactions impact not only water balances but also crucial chemical and ecological processes. HEF influence transformation rates of organic matter (Findlay et al., 1993) and nutrients (Grimm, 1984). They also determine nutrient

retention and release (Triska et al., 1989) and pollutant retention (Lewandowski et al., 2011; Schaper et al., 2018). The estimation of HEF is also required for ecologic studies (Stanford & Ward, 1993; Findlay, 1995; Zarnetske & Haggerty, 2015) especially for fish ecologists determining the optimal spawning locations based on upwelling or downwelling (Baxter & Hauer, 2000; Malcolm et al., 2002). Beyond the ecological functioning of the ecosystem (Brunke & Gonser, 1997), there are implications related to human impacts on the hydrological cycle, which tend to concentrate in the HZ (Hancock, 2002). Better identification and quantification of hyporheic processes can help to develop better policies to avoid the degradation of rivers caused by river straightening, bank reinforcement, removal of woody debris (Blaen et al., 2018), unsustainable depletion of water tables (Boulton & Hancock, 2006), dam operation (Sawyer et al., 2009) or climate change (Stanley & Valett, 1992).

The scientific community has collected a vast number of hyporheic datasets on different scales (Magliozzi et al., 2018) but the available datasets are site-specific and usually limited to the topic of the study. There is a general lack of datasets comprising multi-scale observations of GW-SW interactions. This is particularly true for studies devoted to the identification and quantification of the spatial patterns and temporal changes of GW-SW interactions (Wondzell & Swanson, 1996; Sophocleous, 2002).

1.2 Challenges of HEF investigation

Several challenges are inherent to the investigation of hyporheic exchange flows. First of all, HEF occur in the subsurface, inaccessible to direct observation. There are no direct methods to measure HEF, i.e. flow paths and velocities in the HZ.

Seepage meters are the only direct method able to measure fluxes across the sediment-water interface. The method is based on collecting exfiltrating water at the sediment-water interface of lakes (McBride & Pfannkuch, 1975) and rivers (Lee & Hynes, 1977). However, the limited applicability of seepage meters, particularly in flowing water, prevents a widespread use (Murdoch & Kelly, 2003).

The alternative to the direct point measurement method is indirect measurement of processes related to HEF, e.g. temperature gradients or pressure gradients across the

sediment-water interface. Comprehensive reviews of such methods can be found elsewhere, e.g. Kalbus et al. (2006), Rosenberry et al. (2015). However, in contrast to methods for measuring flow across the sediment-water interface, methods for flow determination in the HZ itself are much more challenging. For example, chemical tracing measures the concentrations of specific conservative substances to determine the path and magnitude of HEF in the HZ (Harvey & Bencala, 1993). Conversely, chemical tracing lacks the capacity to provide detailed spatial distributions of exfiltration at sediment-water interfaces and detailed temporal evolution of water exchange (Stream Solute Workshop, 1990; Harvey et al., 1996). However, this information is relevant to distinguish the different components of HEF as well as the impacts of subsurface heterogeneity.

The limitations of chemical tracing illustrate how studying of HZ processes are frequently limited by the scale range of the techniques applied (Hakenkamp et al., 1993). The limited range of scales measurable with single techniques undermines the identification of hyporheic processes, which overlap at different scales (Poole et al., 2006). Factors such as geomorphology, subsurface geology, the flow and the sediment regime can impact hyporheic processes from local to basin scales (Stanford & Ward, 1993, Wroblicky et al., 1998; Kasahara & Wondzell, 2003; Boano et al., 2006; Wondzell, 2006). The local hydraulic gradients and properties of the HZ can also have impacts from the bedform to the reach scale (Packman et al., 2004; Wondzell, 2006; Cardenas & Wilson, 2007; Buffington & Tonina, 2009; Sawyer et al., 2011). To cover such wide range of scales different hyporheic measurement techniques suitable for the multi-scale investigation are required (Krause et al., 2012; Briggs et al., 2012; Unland et al., 2013). Based on such investigations it is possible to identify the spatial patterns of HEF across scales. Furthermore, it is also necessary to measure hyporheic processes across temporal scales due to the non-stationarity of the HZ processes (Käser et al., 2009). This increases the requirements on the techniques in addition to the multi-scale approach.

1.3 Multiscale approach

As outlined at the end of the previous chapter, a multi-scale approach is required to understand the complex processes and process interactions occurring on different spatial scales (Magliozzi et al., 2017). There are innovative techniques that contribute to multi-scale

investigations of hyporheic processes. Among them, fiber-optic distributed temperature sensing (FO-DTS) and geophysics are useful for pattern identification across scales. While FO-DTS is useful to identify discharge patterns at the immediate sediment-water interface, geophysics can be applied to study subsurface structures that cause the observed subsurface flow patterns. Both methods are not useful to quantify fluxes. However, in combination with point techniques, they have remarkable strengths for quantification and understanding of HEF.

Distributed temperature sensing and geophysics for pattern identification

Several methods to study GW-SW interactions are based on temperature as a natural tracer. While GW temperatures are more or less constant in the course of the year (approximately 10 °C in Germany) the surface water is warmer than the groundwater in summer and colder in winter. Thus, the temperature at the interface depends on the flow of GW and SW at the interface (Constantz & Stonestrom, 2003). Fortunately, there has been a lot of technical development during the last decades that allows fast and easy temperature measurements. Furthermore, measurements of temperature are inexpensive, reliable and non-destructive (Anderson, 2005). Vertical fluxes can be quantified based on the thermal depth gradients in the sediment (White et al., 1987).

Temperature sensing provides also the chance to identify regions of GW-SW interaction based on the spatial and temporal thermal patterns observed at the immediate sediment-water interface (Evans & Petts, 1997). Even though continuous monitoring (in time) of temperature is simple, fast and inexpensive with data loggers, capturing the spatial thermal patterns demands the use of distributed techniques such as fiber-optic distributed temperature sensing (FO-DTS) (Lowry et al., 2007). The technique operates sending laser pulses along a fiber cable and measuring the back-scattered light in the Stokes and Anti-Stokes range of the light spectrum of the emitted pulse. The difference between both ranges depends on temperature (Dakin, 1987) and the travel time of the light pulse depends on the location in the cable, i.e. distance between laser source/detector and location in the cable where back-scattering occurs. These optical fundamentals enable high precision temperature measurements with sub-meter resolution to kilometer scale. The current laser units can sample these long distances in such short time periods with sufficient reliability that it is

possible to distinguish temporal temperature change at time scale of minutes. This wide spatial and temporal range of FO-DTS demonstrates its potential for investigating thermal patterns of water exchange across scales (Selker et al., 2006).

Geophysics can also contribute to multi-scale indirect observation of variables related to HEF, i.e. properties of the subsurface materials (Binley et al., 2015). Among the multiple techniques applied in hydrogeophysics, electromagnetic induction (EMI) provides fast, economic and non-invasive exploration of the subsurface (Robinson et al., 2008). Heterogeneity is relevant in hyporheic studies since it impacts the distribution of HEF on multiple scales (Fleckenstein et al., 2006). EMI geophysics reveals heterogeneity from the local streambed scale to the geologic scale. The technique is also of great value to support the multi-scale thermal measurements using FO-DTS. EMI geophysics reveal distributed information about the geologic controls of the exchange while FO-DTS registers the distributed thermal consequences of HEF at the sediment-water interface (Mansoor et al., 2006; Lowry et al., 2007; Rosenberry et al., 2016). The complementary dimensions of these techniques, spatial in the case of FO-DTS and volumetric in the case of geophysics support the multi-scale approach.

The advantages of combining point techniques for quantification of exchanges

The quantification of HEF with techniques such as FO-DTS is only possible when different levels of the sediment are measured to capture the thermal gradients. Few studies of this type (Shanafield et al., 2016) are available due to their high demand of time and resources. Combining FO-DTS with point measurement techniques and transfer function is a possibility to provide preliminary quantification over large areas (Lautz & Ribaudo, 2012, Blume et al., 2013). However, the limited accuracy of these transfer functions explain why point techniques remain as the prevalent methods to quantify hyporheic exchange flows. Among point techniques, both the measurement of hydraulic and thermal gradients in depth of the sediment enable vertical flux estimation of water exchanges (Conant, 2004).

Temperature-depth profiles provide information about fluxes across the sediment-water interface. Steady-state one-dimensional (1D) heat transport methods assume that the temperature-depth profile is constant over time and use the curvature of the gradient at the sediment-water interface to calculate water fluxes (Stallman, 1965; Bredehoeft &

Papadopoulos, 1965). The daily cycles of temperature time series of depth profiles can also be used to estimate vertical fluxes. The methods are based on the amplitude attenuation and/or phase shift of the temperatures cycles propagating into the sediment. Numerous heat transport analytical solutions (Hatch et al., 2006; Keery et al., 2007; McCallum et al., 2012; Luce et al., 2013) as well as a few numerical models (Healy & Ronan, 1996; Koch et al., 2015) were developed in recent decades, spreading the use of point temperature (gradients) for flux quantification (Kurylyk et al., 2019). However, the irregular transmission of temperature in heterogeneous sediments and the irregular water fluxes due to the heterogeneous distribution of hydraulic conductivities can significantly reduce the reliability of the flux estimates. Furthermore, the estimates are based on the assumption that only vertical fluxes, i.e. fluxes parallel to the temperature-depth profile, occur. However, hyporheic zones are characterized by a strong horizontal flow component.

To deal with these challenges, combined interpretation of the hydraulic and thermal gradients improves the interpretation of the vertical flux estimates in relation to the sediment heterogeneity (Schmidt et al., 2006). Data from point hydraulic and thermal measurement techniques provide small scale hyporheic knowledge useful for modelling (Stonedahl et al., 2010). The combination of point and distributed data widens the range of scales at which hyporheic modelling can be applied for the goal of upscaling.

The value of integrating point and distributed data into modelling of HZ processes

However, transfer functions represent a simplified approach for quantifying fluxes. Their results are generally dimensionally limited to the sediment-water interface or the other levels of the hyporheic zone where data were collected. Quantifying fluxes beyond the dimension of the collected data and the scope of transfer functions requires adopting three-dimensional (3D) flow and heat transport modelling of the hyporheic zone. 3D modelling of the hyporheic zone requires sufficient information to parametrize and to calibrate the model (Wondzell et al., 2009). Including data from the scale ranges covered by the aforementioned point and distributed methods is of great advantage to accurately define and evaluate 3D models. With such a wide range of scales of the datasets, models help to test the distribution of exchange observed at the sediment-water interface (Shanafield et al., 2016) and to

investigate the influence of subsurface heterogeneity (Wondzell et al., 2009). Additionally, given the fact that 3D models of the HZ outperform 1D methods for vertical flux estimation (Brookfield & Sudicky, 2012), modelling has the potential for upscaling the distribution of HEF across scales (Stonedahl et al., 2010; Gomez-Velez & Harvey, 2014). Finally, the integration of point and distributed data into 3D models of the HZ can boost the upscaling potential of 3D modelling, in line with the increasingly interdisciplinary and multi-scale approaches required in hyporheic studies (Krause et al., 2010; Mouhri et al., 2013).

1.4 Gaps in HEF estimation

In view of the challenges and opportunities described in previous sections, the present PhD thesis addresses the following specific research gaps:

i. The first research gap is the separation of HEF components based on their origin (Sophocleous, 2002). The global net exchange in/across the HZ can be useful for summarizing the impacts of GW-SW interactions but is insufficient to understand the related hydraulic, chemical and ecologic processes. So far, only modelling studies target the separation of groundwater and the other HEF components (Bhaskar et al., 2012). Apart from the need to distinguish these components for a profound process understanding, it is also required to investigate their specific spatial and temporal patterns (Fleckenstein et al., 2010).

ii. The second research gap is the reliable quantification of HEF. The quantification of HEF is crucial for estimating the exfiltrating/infiltrating volumes at the sediment-water interface and for evaluating the transport and transformation processes taking place in the hyporheic zone. This is a challenging task due to the subsurface location of HEF, inaccessible for direct observation (Palmer, 1993). Despite the development of different hydraulic and thermal methods for the vertical quantification of HEF (Kurylyk et al., 2019), there is need to review their capabilities and limitations under strong upwelling and heterogeneous conditions.

iii. The third research gap is the need to improve 3D flow and transport modelling of the HZ to upscale the quantification of HEF (Gomez-Velez & Harvey, 2014). To achieve a successful flow and heat transport modelling additional gaps need to be addressed: (a) It is required to integrate point and distributed data into 3D models (Shanafield et al.,

2016). (b) It is necessary to improve the capabilities of models to integrate data of subsurface heterogeneity such as from geophysical data because subsurface heterogeneity severely impacts HEF (Crook et al., 2008).

Altogether, these research gaps determine a sequence of needs for the investigation of hyporheic exchange flows that define the objectives and structure of the thesis.

1.5 Objectives and structure of the thesis

The general target of the present study is the identification and quantification of groundwater-surface water interactions in streams by a combination of innovative measurement techniques. This includes the integration of point and distributed data into 3D models aiming to upscale HEF estimates.

The **second chapter** targets the identification of the different components of HEF (groundwater discharge, interflow discharge and local up-/downwelling) by differentiating their particular spatial and temporal thermal patterns. Geophysics support the classification of the components of HEF by providing evidence that the geological/sedimentary configuration impacts on the distribution of exchange.

The **third chapter** comprises different hydraulic and thermal analytical and numerical methods for quantifying the vertical component of HEF. The methods use point data obtained from hydraulic heads and temperature-depth profiles at locations of strong upwelling which are typical for the study site. The chapter tests the capabilities and limitations of the methods and provides accurate quantification of the vertical flow components of HEF.

The **fourth chapter** combines the two previous chapters by integrating the distributed and point data into a 3D numerical model of the HZ. The first aim of the model is to reproduce both the spatial distribution of the components of exchange identified in Chapter 2 and the point estimates of vertical fluxes provided by the 1D methods in Chapter 3. By successfully identifying the patterns and quantifying the magnitude of the water exchange, the model aims to upscale HEF beyond the scale of the point estimates obtained from 1D methods. Secondly, the model focuses on assessing the contribution of distributed data from the geophysical exploration of the site to reduce the impact of heterogeneity on the accuracy

of HEF estimates. Finally, the model evaluates the benefits of integrating multiple data sets of different types and scales for improving the parametrization and calibration of 3D models of the HZ.

The final chapter is devoted to the discussion of the main findings of each chapter. In particular, the discussion highlights the advantages of distributed measurement techniques for large scale identification of GW-SW interactions (Chapter 2), the challenges on quantifying these interactions despite the advances of 1D methods (Chapter 3) and the potential of 3D modelling of the HZ for upscaling the quantification of hyporheic exchange flows (Chapter 4). The discussion of these findings aims to increase our understanding of hyporheic processes and the factors governing it across scales.

With this structure in mind, I invite the reader to read the following chapters that aim, on one hand, to improve methods for quantification of local and overall hyporheic fluxes and on the other hand hyporheic process understanding.

1.6 References

Alley, W. M., Winter, T. C., Harvey, J. W., & Franke, O. L. (1999). Groundwater and surface water: A single resource. *US Geological Survey, Circular 1139*, Denver, CO, 79 pp.

Anderson, M. P. (2005). Heat as a Ground Water Tracer. *Groundwater*, 43: 951-968. https://doi.org/10.1111/j.1745-6584.2005.00052.x

Bhaskar, A. S., Harvey, J. W., & Henry, E. J. (2012). Resolving hyporheic and groundwater components of streambed water flux using heat as a tracer. *Water Resources Research*, 48(8). https://doi.org/10.1029/2011WR011784

Baxter, C. V., Hauer, F. R., (2011) Geomorphology, hyporheic exchange and selection of spawning habitat by bull trout. *Canadian Journal of Fisheries and Aquatic Sciences*, *2000, 57*(7): 1470-1481. https://doi.org/10.1139/f00-056

Bencala, K. E. (1984). Interactions of solutes and streambed sediment: 2. A dynamic analysis of coupled hydrologic and chemical processes that determine solute transport. *Water Resources Research*, *20*(12), 1804-1814. https://doi.org/10.1029/WR020i012p01804

Binley, A., Hubbard, S. S., Huisman, J. A., Revil, A., Robinson, D. A., Singha, K., & Slater, L. D. (2015). The emergence of hydrogeophysics for improved understanding of subsurface processes over multiple scales. *Water Resources Research*, *51*(6), 3837-3866. https://doi.org/10.1002/2015WR017016

Blaen, P. J., Kurz, M. J., Drummond, J. D., Knapp, J. L., Mendoza‐Lera, C., Schmadel, N. M., ... & Ward, A. S. (2018). Woody debris is related to reach‐scale hotspots of lowland stream ecosystem respiration under baseflow conditions. *Ecohydrology, 11*(5), e1952. https://doi.org/10.1002/eco.1952

Boano, F., Camporeale, C., Revelli, R., & Ridolfi, L. (2006). Sinuosity-driven hyporheic exchange in meandering rivers. *Geophysical Research Letters*, *33*(18). https://doi.org/10.1029/2006GL027630

Boulton, A. J. (2000). River Ecosystem Health Down Under: Assessing Ecological Condition in Riverine Groundwater Zones in Australia. *Ecosystem Health*, *6*(2), 108–118. https://doi.org/10.1046/j.1526-0992.2000.00011.x

Boulton, A. J., & Hancock, P. J. (2006). Rivers as groundwater-dependent ecosystems: a review of degrees of dependency, riverine processes and management implications. *Australian Journal of Botany*, *54*(2), 133-144. https://doi.org/10.1071/BT05074

Briggs, M. A., Lautz, L. K., & McKenzie, J.M. (2012). A comparison of fiber-optic distributed temperature sensing to traditional methods of evaluating groundwater inflow to streams. *Hydrological Processes, 26*(9): 1277-1290.

https://doi.org/10.1016/j.jhydrol.2011.11.053

Brookfield, A. E., & Sudicky, E. A. (2012). Implications of hyporheic flow on temperature-based estimates of groundwater/surface water interactions. *Journal of Hydrologic Engineering, 18*(10), 1250-1261. https://doi.org/10.1061/(ASCE)HE.1943-5584.0000726

Brunke, M., & Gonser, T. O. M. (1997). The ecological significance of exchange processes between rivers and groundwater. *Freshwater Biology*, *37*(1), 1-33. https://doi.org/10.1046/j.1365-2427.1997.00143.x

Buffington, J. M., & Tonina, D. (2009). Hyporheic exchange in mountain rivers II: effects of channel morphology on mechanics, scales, and rates of exchange. *Geography Compass*, *3*(3), 1038-1062. https://doi.org/10.1111/j.1749-8198.2009.00225.x

Cardenas, M. B. and J. L. Wilson (2007). Thermal regime of dune-covered sediments under gaining and losing water bodies. *Journal of Geophysical Research: Biogeosciences, 112*(G4). https://doi.org/10.1016/j.jhydrol.2007.08.019

Conant Jr, B. (2004). Delineating and quantifying groundwater discharge zones using streambed temperatures. *Groundwater*, *42*(2), 243-257. https://doi.org/10.1111/j.1745-6584.2004.tb02671.x

Constantz, J., & Stonestrom, D. A. (2003). Heat as a tracer of water movement near streams. *US Geological Survey Circular*, *1260*, 1-96.

Crook, N., Binley, A., Knight, R., Robinson, D. A., Zarnetske, J., & Haggerty, R. (2008). Electrical resistivity imaging of the architecture of substream sediments. *Water Resources Research, 44*(4). https://doi.org/10.1029/2008WR006968

Dakin, J. P. (1987). Multiplexed and distributed optical fiber sensor systems. *Journal of Physics E*: *Scientific Instruments, 20*(8), 954.

Evans, E. C., & Petts, G. E. (1997). Hyporheic temperature patterns within riffles. *Hydrological Sciences Journal*, *42*(2), 199-213. https://doi.org/10.1080/02626669709492020

Findlay, S., Strayer, D., Goumbala, C., & Gould, K. (1993). Metabolism of streamwater dissolved organic carbon in the shallow hyporheic zone. *Limnology and Oceanography*, *38*(7), 1493-1499. https://doi.org/10.4319/lo.1993.38.7.1493

Fleckenstein, J. H., Niswonger, R. G., & Fogg, G. E. (2006). River-aquifer interactions, geologic heterogeneity, and low-flow management. *Groundwater, 44*(6), 837-852. https://doi.org/10.1111/j.1745-6584.2006.00190.x

Fleckenstein, J.H., Frei, S., Niswonger, R.G. (2008). Simulating river-aquifer exchange: the missing scale. *In British Hydrological Society National Meeting on Hyporheic Hydrology*, Birmingham.

Fleckenstein, J. H., Krause, S., Hannah, D. M., & Boano, F. (2010). Groundwater-surface water interactions: New methods and models to improve understanding of processes and dynamics. *Advances in Water Resources, 33*(11), 1291-1295. https://doi.org/10.1016/j.advwatres.2010.09.011

Gaona, J., Meinikmann, K., Lewandowski, J. (2019). Identification of groundwater exfiltration, interflow discharge and hyporheic exchange flows by fiber-optic distributed temperature sensing supported by electromagnetic induction geophysics. *Hydrological Processes*. https://doi.org/10.1002/hyp.13408

Gomez-Velez, J. D., and J. W. Harvey (2014). A hydrogeomorphic river network model predicts where and why hyporheic exchange is important in large basins. *Geophysical Research Letters*, 41, 6403–6412. https://doi.org/10.1002/2014GL061099

Gorelick, S.M. (1986). Conjunctive water use: understanding and managing groundwater-surface water interactions. *International Association of Hydrologic Sciences, Publication No.* 156*,* 547pp, Wallingford.

Grimm, N. B., & Fisher, S. G. (1984). Exchange between interstitial and surface water: implications for stream metabolism and nutrient cycling. *Hydrobiologia*, *111*(3), 219-228. https://doi.org/10.1007/BF00007202

Hakenkamp, C. C., Valett, H. M., & Boulton, A. J. (1993). Perspectives on the Hyporheic Zone: Integrating Hydrology and Biology. Concluding Remarks. *Journal of the North American Benthological Society*, *12*(1), 94–99. https://doi.org/10.2307/1467690

Hancock, P. (2002). Human Impacts on the Stream–Groundwater Exchange Zone. *Environmental Management* (29) 763. https://doi.org/10.1007/s00267-001-0064-5

Harvey, J. W., & Bencala, K. E. (1993). The effect of streambed topography on surface-subsurface water exchange in mountain catchments. *Water Resources Research*, *29*(1), 89-98. https://doi.org/10.1029/96WR01268

Harvey, J. W., Wagner, B. J., & Bencala, K. E. (1996). Evaluating the reliability of the stream tracer approach to characterize stream-subsurface water exchange. *Water Resources Research*, *32*(8), 2441-2451. https://doi.org/10.1029/96WR01268

Hatch, C. E., Fisher, A. T., Revenaugh, J. S., Constantz, J., & Ruehl, C. (2006). Quantifying surface water-groundwater interactions using time series analysis of streambed thermal records: Method development. *Water Resources Research, 42(10).* https://doi.org/10.1029/2005WR004787

Kasahara, T., & Wondzell, S. M. (2003). Geomorphic controls on hyporheic exchange flow in mountain streams. *Water Resources Research*, *39*(1), SBH-3. https://doi.org/10.1029/2002WR001386

Healy, R. W., & Ronan, A. D. (1996). Documentation of computer program VS2DH for simulation of energy transport in variably saturated porous media: Modification of the US Geological Survey's computer program VS2DT (pp. 96-4230). *US Geological Survey.* https://pubs.usgs.gov/wri/1990/4025/report.pdf

Kalbus, E., Reinstorf, F., & Schirmer, M. (2006). Measuring methods for groundwater? surface water interactions: a review. *Hydrology and Earth System Sciences Discussions*, *10*(6), 873-887. https://doi.org/10.1.1.371.8802

Käser, D. H., Binley, A., Heathwaite, A. L., & Krause, S. (2009). Spatio-temporal variations of hyporheic flow in a riffle-step-pool sequence. *Hydrological Processes: An International Journal*, *23*(15), 2138-2149. https://doi.org/10.1002/hyp.7317

Keery, J., Binley, A., Crook, N., & Smith, J. W. (2007). Temporal and spatial variability of groundwater-surface water fluxes: development and application of an analytical method using temperature time series. *Journal of Hydrology, 336(1), 1-16.* https://doi.org/10.1016/j.jhydrol.2006.12.003

Koch, F. W., Voytek, E. B., Day-Lewis, F. D., Healy, R., Briggs, M. A., Lane, J. W., & Werkema, D. (2015). 1DTempPro V2: New Features for Inferring Groundwater/Surface-Water Exchange. *Groundwater, 54(3), 434-439.* https://doi.org/10.1111/gwat.12369

Krause, S., Hannah, D. M., Fleckenstein, J. H., Heppell, C. M., Kaeser, D., Pickup, R., ... & Wood, P. J. (2011). Inter‐disciplinary perspectives on processes in the hyporheic zone. *Ecohydrology, 4*(4), 481-499. https://doi.org/10.1002/eco.176

Krause, S., T. Blume and N. Cassidy (2012). Investigating patterns and controls of groundwater up-welling in a lowland river by combining Fiber-optic Distributed

Temperature Sensing with observations of vertical hydraulic gradients. *Hydrology and Earth System Sciences 16*(6): 1775-1792. https://doi.org/10.5194/hess-16-1775-2012

Kurylyk, B.L., Irvine, D.J., Bense, V.F. (2019). Theory, tools, and multidisciplinary applications for tracing groundwater fluxes from temperature profiles. *WIREs Water* 6:e1329. https://doi.org/10.1002/wat2.1329

Lee, D.R., & Hynes, H.B.N. (1978). Identification of groundwater discharge zones in a reach of Hillman Creek in southern Ontario. *Water Quality Research Journal, 13.1* (1978): 121-134. https://doi.org/10.2166/wqrj.1978.010

Lewandowski, J., Hoehn, E., Kalbus, E., Nützmann, G., Radke, M., Saenger, N. & Schimdt, C. (2009). *Hyporheisches Netzwerk. Poster, DGL-Jahrestagun Oldenburg*, 28.09-02.10.09.

Lewandowski, J., Putschew, A., Schwesig, D., Neumann, C., & Radke, M. (2011). Fate of organic micropollutants in the hyporheic zone of a eutrophic lowland stream: results of a preliminary field study. *Science of the Total Environment*, *409*(10), 1824-1835. https://doi.org/10.1016/j.watres.2018.04.040

Lowry, C. S., J. F. Walker, R. J. Hunt and M. P. Anderson (2007). Identifying spatial variability of groundwater discharge in a wetland stream using a distributed temperature sensor. *Water Resources Research*, *43*(10). https://doi.org/10.1029/2007WR006145

Luce, C. H., Tonina, D., Gariglio, F., & Applebee, R. (2013). Solutions for the diurnally forced advection‐diffusion equation to estimate bulk fluid velocity and diffusivity in streambeds from temperature time series. *Water Resources Research, 49*(1), 488-506. https://doi.org/10.1029/2012WR012380

Magliozzi, C., Grabowski, R., Packman, A. I., & Krause, S. (2017). Scaling down hyporheic exchange flows: from catchments to reaches. *Hydrology and Earth System Sciences Discussions*, 1-53. https://doi.org/10.5194/hess-2016-683

Magliozzi, C., Coro, G., Grabowski, R., Packman, A. I., & Krause, S. (2018). A multiscale statistical method to identify potential areas of hyporheic exchange for river restoration planning. *Environmental Modelling & Software*. https://doi.org/10.1016/j.envsoft.2018.09.006

Malcolm, I., C. Soulsby and A. Youngson (2002). "Thermal regime in the hyporheic zone of two contrasting salmonid spawning streams: ecological and hydrological implications." *Fisheries Management and Ecology*, *9*(1): 1-10. https://doi.org/10.1046/j.1365-2400.2002.00276.x

Mansoor, N., Slater, L., Artigas, F., & Auken, E. (2006). High-resolution geophysical characterization of shallow-water wetlands. *Geophysics*, *71*(4), B101-B109. https://doi.org/10.1190/1.2210307

McBride, M. S., and H. O. Pfannkuch (1975). The distribution of seepage within lakebeds. *J. Research US Geological Survey* 3.5 (1975): 505-512.

McCallum, A. M., Andersen, M. S., Rau, G. C., & Acworth, R. I. (2012). A 1 ‐ D analytical method for estimating surface water-groundwater interactions and effective thermal diffusivity using temperature time series. *Water Resources Research, 48*(11). https://doi.org/10.1029/2012WR012007

Mouhri, A., Flipo, N., Rejiba, F., de Fouquet, C., Bodet, L., Kurtulus, B., … Goblet, P. (2013). Designing a multi-scale sampling system of stream-aquifer interfaces in a sedimentary basin. *Journal of Hydrology*, *504*, 194–206. https://doi.org/10.1016/j.jhydrol.2013.09.036

Murdoch, L. C., & Kelly, S. E. (2003). Factors affecting the performance of conventional seepage meters. *Water Resources Research*, *39*(6). https://doi.org/10.1029/2002WR001347

Poole, G. C., Stanford, J. A., Running, S. W., & Frissell, C. A. (2006). Multiscale geomorphic drivers of groundwater flow paths: subsurface hydrologic dynamics and hyporheic habitat diversity. *Journal of the North American Benthological Society*, *25*(2), 288-303. https://doi.org/10.1899/0887-3593(2006)25[288:MGDOGF]2.0.CO;2

Packman, A. I., Salehin, M., & Zaramella, M. (2004). Hyporheic exchange with gravel beds: basic hydrodynamic interactions and bedform-induced advective flows. *Journal of Hydraulic Engineering*, *130*(7), 647-656. https://doi.org/10.1061/(ASCE)0733-9429(2004)130:7(647)

Palmer, M. A. (1993). Experimentation in the hyporheic zone: challenges and prospectus. *Journal of the North American Benthological Society*, *12*(1), 84-93. https://doi.org/10.2307/1467689

Robinson, D. A., Binley, A., Crook, N., Day‐Lewis, F. D., Ferré, T. P. A., Grauch, V. J. S., ... & Nyquist, J. (2008). Advancing process‐based watershed hydrological research using near‐surface geophysics: A vision for, and review of, electrical and magnetic geophysical methods. *Hydrological Processes*, *22*(18), 3604-3635. https://doi.org/10.1002/hyp.6963

Rosenberry, D. O., Lewandowski, J., Meinikmann, K., & Nützmann, G. (2015). Groundwater‐the disregarded component in lake water and nutrient budgets. Part 1: effects of groundwater on hydrology. *Hydrological Processes, 29*(13), 2895-2921. https://doi.org/10.1002/hyp.10403

Rosenberry, D. O., Briggs, M. A., Voytek, E. B., & Lane, J. W. (2016). Influence of groundwater on the distribution of dwarf wedgemussels (Alasmidonta heterodon) in the upper reaches of the Delaware River, northeastern USA. *Hydrology and Earth System Sciences, 20*(10), 4323-4339. https://doi.org/10.5194/hess-20-4323-2016

Sawyer, A., Cardenas, M.B., Bomar, A. & Mackey, M. (2009). Impact of dam operations on hyporheic exchange in the riparian zone of a regulated river. *Hydrological Processes*, *23*: 2129-2137. https://doi.org/10.1002/hyp.7324

Sawyer, A. H., Bayani Cardenas, M., & Buttles, J. (2011). Hyporheic exchange due to channel‐spanning logs. *Water Resources Research*, *47*(8). https://doi.org/10.1029/2011WR010484

Schaper, J. L., Seher, W., Nützmann, G., Putschew, A., Jekel, M., & Lewandowski, J. (2018). The fate of polar trace organic compounds in the hyporheic zone. *Water Research, 140*, 158-166. https://doi.org/10.1016/j.watres.2018.04.040

Schmidt, C., Bayer-Raich, M., & Schirmer, M. (2006). Characterization of spatial heterogeneity of groundwater-stream water interactions using multiple depth streambed

temperature measurements at the reach scale. *Hydrology and Earth System Sciences Discussions*, 3(4), 1419-1446. https://doi.org/10.5194/hess-10-849-2006

Selker, J. S., Thévenaz, L., Huwald, H., Mallet, A., Luxemburg, W., van de Giesen, N., Stejskal, M., Zeman, J., Westhoff, M. and Parlange, M. B. (2006). Distributed fiber-optic temperature sensing for hydrologic systems. *Water Resouces Research*, *42*, W12202. https://doi.org/10.1029/2006WR005326.

Shanafield, M., McCallum, J. L., Cook, P. G., & Noorduijn, S. (2016). Variations on thermal transport modelling of subsurface temperatures using high-resolution data. *Advances in water resources*, *89*, 1-9. https://doi.org/10.1016/j.advwatres.2015.12.018

Sophocleous, M. (2002). Interactions between groundwater and surface water: the state of the science. *Hydrogeology Journal*, *10*: 52. https://doi.org/10.1007/s10040-001-0170-8

Stallman, R. W. (1965). Steady one‐dimensional fluid flow in a semi‐infinite porous medium with sinusoidal surface temperature. *Journal of Geophysical Research*, *70*(12), 2821-2827. https://doi.org/10.1029/JZ070i012p02821

Stanford, J. A., & Ward, J. V. (1993). An ecosystem perspective of alluvial rivers: connectivity and the hyporheic corridor. *Journal of the North American Benthological Society*, *12*(1), 48-60. https://doi.org/10.2307/1467685

Stonedahl, S. H., J. W. Harvey, A. Wörman, M. Salehin, and A. I. Packman (2010). A multiscale model for integrating hyporheic exchange from ripples to meanders. *Water Resources Research*, *46*, W12539. https://doi.org/10.1029/2009WR008865.

Stream Solute Workshop (1990). Concepts and Methods for Assessing Solute Dynamics in Stream Ecosystems. *Journal of the North American Benthological Society,* Vol. 9, No. 2 (Jun. 1990), pp. 95-119 (25 pages). https://doi.org/10.2307/1467445

Tonina, D. and Buffington, J. M. (2009), Hyporheic Exchange in Mountain Rivers I: Mechanics and Environmental Effects. *Geography Compass*, *3*: 1063-1086. https://doi.org/ 10.1111/j.1749-8198.2009.00226.x

Triska, F. J., Kennedy, V. C., Avanzino, R. J., Zellweger, G. W., & Bencala, K. E. (1989). Retention and transport of nutrients in a third-order stream in northwestern California: Hyporheic processes. *Ecology*, *70*(6), 1893-1905. https://doi.org/10.2307/1938120

Unland, N. P., Cartwright, I., Rau, G. C., Reed, J., Gilfedder, B. S., Atkinson, A. P., & Hofmann, H. (2013). Investigating the spatiotemporal variability in groundwater and surface water interactions: a multi-technique approach. *Hydrology and Earth System Sciences*, *17*(9), 3437. https://doi.org/10.5194/hess-17-3437-2013

White, D. S. (1993). Perspectives on Defining and Delineating Hyporheic Zones. *Journal of the North American Benthological Society*, *12*(1), 61–69. https://doi.org/10.2307/1467686

White, D. S., Elzinga, C. H., & Hendricks, S. P. (1987). Temperature patterns within the hyporheic zone of a northern Michigan river. *Journal of the North American Benthological Society, 6*(2), 85-91. https://doi.org/10.2307/1467218

Wondzell, S., & Swanson, F. J. (1996). Seasonal and Storm Dynamics of the Hyporheic Zone of a 4th-Order Mountain Stream. I: Hydrologic Processes. *Journal of the North American Benthological Society, 15*, no. 1, 3-19. https://doi.org/10.2307/1467429

Wondzell, S. M., and F. J. Swanson (1999), Floods, channel change, and the hyporheic zone. *Water Resources Research, 35*(2), 555–567. https://doi.org/10.1029/1998WR900047.

Wondzell, S. M. (2006), Effect of morphology and discharge on hyporheic exchange flows in two small streams in the Cascade Mountains of Oregon, USA. *Hydrological Processes*, *20*: 267-287. https://doi.org/10.1002/hyp.5902

Wondzell, S. M., LaNier, J., & Haggerty, R. (2009). Evaluation of alternative groundwater flow models for simulating hyporheic exchange in a small mountain stream. *Journal of Hydrology, 364*(1-2), 142-151. https://doi.org/10.1016/j.jhydrol.2008.10.011

Wroblicky, G. J., Campana, M. E., Valett, H. M., & Dahm, C. N. (1998). Seasonal variation in surface-subsurface water exchange and lateral hyporheic area of two stream-

aquifer systems. *Water Resources Research*, *34*(3), 317-328. https://doi.org/10.1029/97WR03285

Zarnetske, J. P., Haggerty, R., & Wondzell, S. M. (2015). Coupling multiscale observations to evaluate hyporheic nitrate removal at the reach scale. *Freshwater Science*, *34*(1), 172-186. https://doi.org/10.1086/680011

1

Chapter 2:

Identification of groundwater-surface water interactions

J. Gaona [1,2,3], K. Meinikmann[1], J. Lewandowski [1,4]

[1] Leibniz Institute of Freshwater Ecology and Inland Fisheries (IGB), Müggelseedamm 310, 12587, Berlin, Germany. [2] Freie Universität Berlin, Dahlem Research School, Hittorfstraße 16, 14195, Berlin, Germany. [3]University of Trento, Department of Civil, Environmental and Mechanical Engineering, Via Messiano 77, 31123, Trento, Italy. [4]Humboldt University Berlin, Faculty of Mathematics and Natural Sciences, Geography Department, Rudower Chaussee 16, 12489 Berlin, Germany.

Article published as:

Gaona, J., Meinikmann, K., Lewandowski, J. (2019). Identification of groundwater exfiltration, interflow discharge and hyporheic exchange flows by fiber-optic distributed temperature sensing supported by electromagnetic induction geophysics. *Hydrological Processes,* 2019 (1-13). https://doi.org/10.1002/hyp.13408

2.1 Abstract

Water exchange across the sediment-water interface of streams impresses a characteristic thermal pattern at the interface. The use of fiber-optic distributed temperature sensing (FO-DTS) at the sediment-water interface in a small sand-bed stream identifies such temperature patterns. Groundwater and interflow can be differentiated based on the temporal evolution of temperature patterns. Additionally, sudden temperature changes at the sediment-water interface observed during the transit of floods enable spatial identification of local up- and downwelling. Electromagnetic induction geophysics (EMI) can detect subsurface texture structures that support groundwater-surface water exchange. Our results show that areas of permanent temperature anomalies observed with FO-DTS match areas of comparatively homogeneous electrical conductivity. This indicates groundwater discharge and enables differentiating groundwater discharge from interflow and local downwelling.

2.2 Introduction

The sediment-water interface is one of the crucial interfaces in the water cycle. There, water exchange determines environmentally important chemical and biological processes (Lewandowski et al., 2011). The interface underlying streams where groundwater and surface water mix and which contains variable portions of surface water (SW) and groundwater (GW) is called the hyporheic zone (HZ). Flow in this zone is termed hyporheic exchange flows (HEF). HEF is exchanged across the streambed in both directions. Water flowing in the stream channel flows into the subsurface (downwelling), in the hyporheic zone and then returns to the stream (upwelling) (Winter, 1998; Bencala, 2005). While groundwater exfiltration originates in the saturated zone, interflow is the lateral movement of water in the unsaturated zone. Interflow occurs when water infiltrates into the subsurface, hydraulic conductivity decreases with depth, and lateral flow proceeds downslope (Lyon et al., 2004). Both, groundwater and interflow might enter the hyporheic zone, and might discharge into the SW as a portion of the HEF.

Studying downwelling, upwelling, GW exfiltration and interflow discharge is challenging. A powerful approach is the use of temperature as a tracer of water exchange (Constantz & Stonestrom, 2003; Anderson, 2005). GW and interflow have temperature

regimes defined by climatic conditions while SW temperatures respond to weather conditions and additionally to the percentage share of its runoff components. GW exfiltration, interflow discharge and local upwelling and downwelling leave source-specific spatially and temporally variable temperature patterns at the sediment-water interface which we call "thermal footprint". To cope with the spatial heterogeneity of the exchange either laborious point or distributed measurement techniques such as fiber-optic distributed temperature sensing (FO-DTS) is required.

FO-DTS is capable of mapping temperature variations at the sediment-water interface based on the temperature-dependent (Raman) backscattering of a laser pulse in the fiber-optic cable used as a distributed sensor (Dakin, 1987). First, FO-DTS was applied in lakes (Selker et al., 2006a) and later on in rivers (Selker et al., 2006a; Westhoff et al., 2007) and other water bodies such as wetlands (Lowry et al., 2007) to study GW-SW interactions. Multi-linear layouts of the fiber-optic cable provide valuable 2D information about location, shape and scale of HEF patterns (Mwakanyamale et al., 2012; Blume et al., 2013) taking advantage of the sub-meter resolution of FO-DTS (Henderson et al., 2009). This high resolution provided by FO-DTS applied in a 3D layout even enabled investigation on thermal transport in the hyporheic zone (Shanafield et al., 2016). Recent studies combining FO-DTS with other techniques such as piezometers, temperature-depth profiles, ground-penetrating radar … revealed a large potential of such combinations for studies of GW-SW exchange in complex environments (Briggs et al., 2012a; González-Pinzón et al., 2015; Hare et al., 2015). Geophysical techniques are particularly powerful to explore the geologic variability of the riverbed controlling GW-SW exchange (Hare et al., 2017; Slater et al., 2010).

In contrast to other geophysical techniques such as electrical resistivity imaging (ERI) or georadar (Crook et al., 2006; Day-Lewis et al., 2006), there are few EMI applications in stream sediments (Gourry et al., 2003; Mansoor et al., 2006; Binley et al., 2013; Rosenberry et al., 2016) despite its advantages for quick and economic exploration of subsurface structures (Robinson et al., 2008). Advantages of EMI compared to ERI are its readiness and flexibility to explore large subsurface areas in detail without requiring much manpower, resources or time.

The physics of the EMI technique consist of the induction of a magnetic field that creates a secondary electromagnetic field in the sediment. The phase shift of the secondary magnetic field (quadrature) recorded back in the device is inverted to provide electrical conductivity results depending on pore water composition and sediment texture (Boaga, 2017). The depth of investigation depends on the excitation frequency or/and the separation of the electromagnetic coils (Binley et al., 2013). EMI helps to differentiate between fine and coarse sediment based on differences of electrical conductivity (Lesch et al., 2005) under the prerequisite that pore water conductivity and other conductivity variations of sediment (clay) are negligible compared to the texture range of the streambed.

The present study applies a multi-linear 2D layout of FO-DTS to identify the intensity and spatial distribution of the different HEF components ((a) GW exfiltration, (b) interflow discharge and (c) local down-/upwelling of SW) by capturing temperature maps of the sediment-water interface. In addition, similarly to the works of Rosenberry et al. (2016) at coarse-grained fluvial settings, we test the potential of EMI geophysics for exploring the subsurface structures of a heterogeneous sandy stream to support the interpretation of GW-SW exchange based on the thermal footprints observed with FO-DTS.

2.3 Materials and methods

2.3.1 Study site

The study site is located at the upper River Schlaube, a second-order stream in Brandenburg, Germany (Figure 2.1a). The study reach is located in a funnel glacial valley carved in a plateau of sandy materials. The depressed location of the river (altitude contrast 30-50 m) results in high piezometric heads. Multiple permanent springs can be observed along the river banks in areas upstream and downstream of the study site. These springs indicate a close connection between interflow, groundwater and SW. The average width of the river is approximately 4 m and the slope of the river is s=0.005 m/m at the study site (Figure 2.1b). The streamflow shows only small variations because it is naturally regulated by Lake Wirchensee located 1400 m upstream of the study site. The measured flow regime (Table 2.1) during our study oscillated between 18 and 35 L/s.

At the 45 m long reach of the study site, diverse hydro-geomorphologic sections (straight, meandering and multi-channel) with different riverbed structures (planar sections, riffle-pool and bars) exist. Based on these geomorphic changes of the stream, we define four transects (Figure 2.1b). TR1 is located where the stream shows a main straight channel of quick current and a muddy meandering secondary channel of slow flow reincorporated to the main channel a few meters downstream. TR2 pinpoints the area where a fallen log isolates the left side of the channel from the current, which remains flooded depending on the stream level. TR3 is located downstream a narrow section of the stream, between a pool and riffle sequence. TR4 covers a sandy point bar in the last curve of the study site. There is a variety of sediment textures (from clean gravels to fine organic deposits, with hydraulic conductivities between $2.43 \cdot 10^{-4}$ m/s and $2.31 \cdot 10^{-6}$ m/s (21 m/d and 0.2 m/d) of the uppermost sediment layers). Woody debris is present in the streambed.

2.3.2 Fiber-optic distributed temperature sensing

FO-DTS was applied to distinguish GW exfiltration, interflow discharge and local up-/downwelling of SW contributing to the thermal patterns observed at the sediment-water interface. Details about FO-DTS operation for river thermal investigation can be found elsewhere (e.g. Selker et al., 2006a; Tyler et al., 2009). Figure 2.1b visualizes the 2D-layout of the FO-DTS cable in 10 parallel lines deployed along a river reach of ≈ 50 m length. The lines were transversally separated 20-50 cm depending on the stream's width. 590 m fiber-optic cable (Brugg BRUusens 2 x MMF metallic armoured 4.6 mm Red 25/125 nm) were buried 3-8 cm deep in the sediment to measure sediment-water interface temperatures instead of SW temperatures (Lowry et al., 2007; Krause et al., 2012). Only in case of obstacles, such as roots or logs, the cable emerged from the sediment and was in contact with SW or air. The depth of the cable in the sediment was qualitatively monitored by plastic ties of known length fixed to the cable to account for scouring and sediment deposition. Two loops of 25 m length at each end of the cable submerged in a mixed ice-bath were used to conduct the calibration of the control unit Silixa Ultima (Silixa Ltd., Hertfordshire, UK).

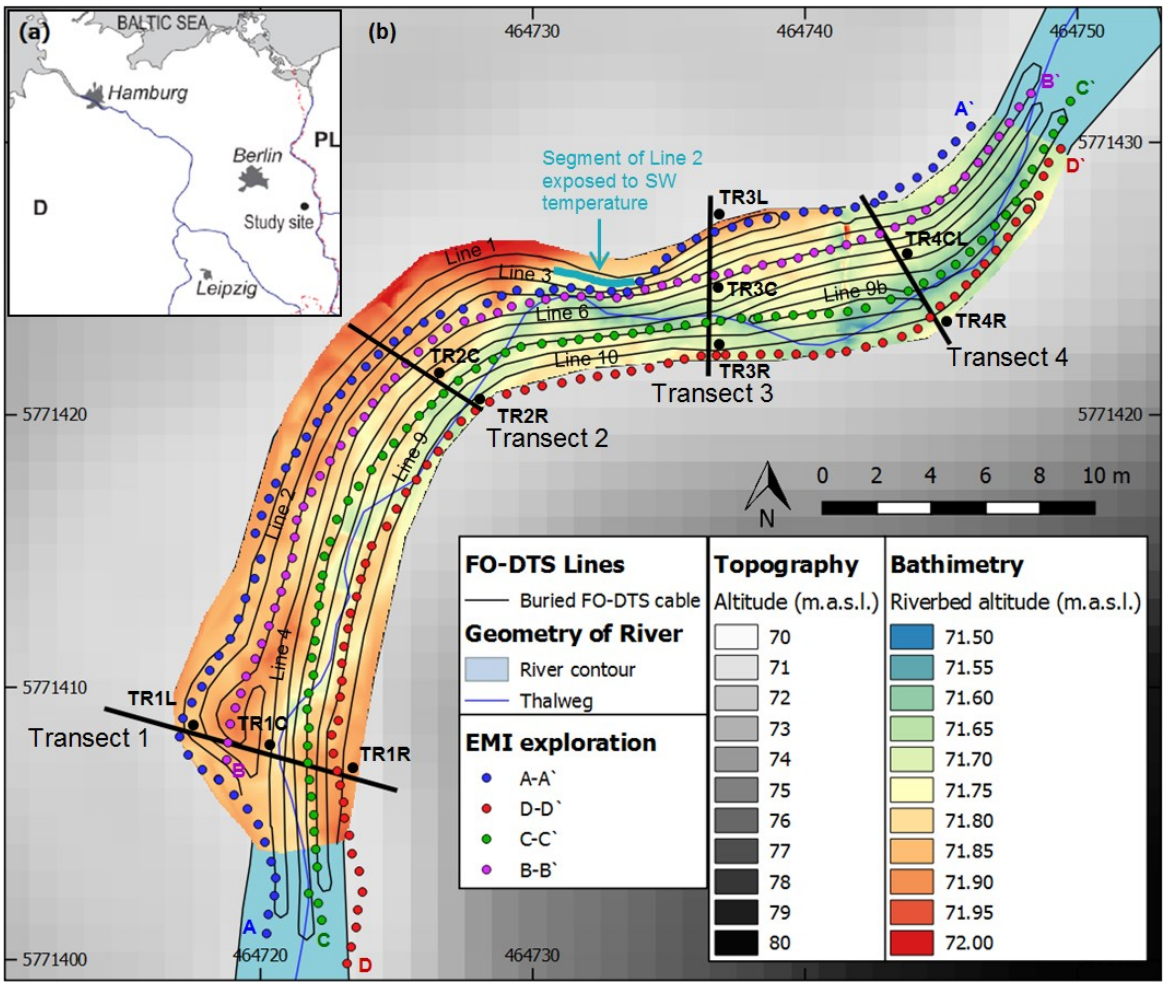

Figure 2.1: Study site. (a) Location of the study site in northeast Germany. (b) Detailed elevation map including bathymetry of the River Schlaube, layout of FO-DTS cable and lines of EMI measurements. Transects are locations of additional measurements as described in Table 1. TRij location (e.g. TR4C) defines transect i at its transversal position j in the direction of flow (L: left, C: center, CL: center-left, R: right).

The cable was operated in a single-ended mode in both directions. The FO-DTS system has a spatial resolution of ≈ 0.3 m and achieves a temperature resolution < 0.05 °C for measurement durations of 4 to 5 minutes. Measurements analyzed in the present study where conducted especially in summer and winter when temperature contrasts between GW and SW were largest (3 - 6 °C), i.e. on 25 Jul 2016, 15 Sep 2016, 18 Jan 2017, plus the 48 h long period between 1 Jul 2017, 0:00 h and 2 Jul 2017, 24:00 h (Table 2.1). The measurement periods covered diverse weather, streamflow, interflow and GW conditions (Figure 2.2).

The cable location was georeferenced by a tachymetric survey with a Leica TPS1200 (Leica Geosystems AG, Hesse, Germany). To define start and end points of each DTS line in the raw measurement file, start and end points of each line, as well as other intermediate relevant points along the fiber, were manually warmed. The other relevant points included areas in contact with air or stream water. Some of the sections of the cable in contact with streamflow were used as references of SW temperatures while sections in contact with the atmosphere were eliminated from the dataset (e.g. 'Log' areas in Figure 2.2 and Figure 2.3).

In addition to FO-DTS, pressure data loggers Schlumberger Mini-Diver™ (Schlumberger Ltd., Texas, USA) monitored GW (filter screen 70 cm below the sediment-water interface) and SW pressure heads at Transects TR1 and TR3 (Figure 2.1b). At those two transects, streamflow velocity and cross-sectional bed morphology were additionally measured with the electromagnetic sounder OTT-MFpro (OTT Hydromet GmbH, Austria) to calculate streamflow. Air and SW temperatures were recorded with HOBO Tidbitv2™ data loggers (Onset Computer Coorp., Massachusetts, USA). Furthermore, we took sediment samples of the upper 5 cm of the streambed 0.5 to 1 m downstream of each transect to determine hydraulic and thermal properties of the hyporheic sediment (Table 2.1). An additional Tidbit2™ data logger measured GW temperature at the source of the strongest spring upstream of the study site.

Table 2.1: Technical specifications of the instruments and measurement setups

Parameter	**Device**		**Details**	**Date (hours measured / N number of time steps)**
Sediment-water interface temperature	FO-DTS: Silixa Ultima control unit (4 km range, 2 channels) 590 m Brugg BRUsens armoured fiber-optic cable (2 x MMF metallic 4.6 mm, 25/125 nm)	10 longitudinal lines in 50 m long stream section, separated 20-50 cm, buried 3 - 8 cm in the streambed	Sampling rate: 4 min (2016) 5 min (2017) Longitudinal resolution ≈ 0.3 m, (sample points every 0.127 m) Temperature resolution ≈ 0.03 °C Time series of temperature for 3611 points in the riverbed	25 Jul 2016 (4.5h/N=68) Flood event 1 15 Sep 2016 (7.5h/N=60) 18 Jan 2017 (4.5h/N=54) 2-3 Jul 2017 (continuous: 48h/N=576) Flood events 2 and 3 (Within the quasi-continuous period 30 Jun-4 Jul 2017)
Piezometric head	Hand-made multi-level piezometers	3 in Transect 1, 2 in Transect 2, 3 in Transect 3, 2 in Transect 4	Resolution: 0.01 cm H_2O, Accuracy: 0.5 cm H_2O Depth of filter screens: (v2016: 5/15/25/35/45/55 cm deep) (v2017: 1/8/14/23/31/48/65/82 cm)	1 Aug 2016 – 4 Jul 2017

Air and water temperature	2 HOBO Tidbits v2	Transect 1	Resolution: 0.02 °C at 25 °C Accuracy: ± 0.21 °C from 0 - 50 °C	5 Mar - 30 Aug 2016 Sampling rate: 15 min
Streamflow velocity	Hydromet OTT-OTT MF pro	Transect 1, Transect 3, Transect 4	Accuracy: ± 2 % flow value ± 0.015 m/s speed (0-3 m/s)	15 Sep 2016, 20 Feb 2017, 2-3 Jul 2017
Electrical conductivity of sediment	CMD-Explorer	4 longitudinal lines of 45 m length, measurement points separated 0.6 m.	Sampling rate: 10 s Effective depth of exploration: (H) 2.2-4.2-6.7 m/(L) 1.1-2.1-3.3 m EC resolution = 0.1 mS/m EC accuracy = ±4% at 50 mS/m Temperature stability= ±0.1 mS/m/°C	4 Jul 2017 17 Oct 2017
Electrical conductivity of pore water	Greissinger GMH3410 conductivity meter	80 samples in sets of 8 from the 10 multi-level piezometers	Range of conductivity: 0 – 200mS/cm Accuracy: (the larger value applies) ± 0.5% of reading ± 0.3% full scale ± 2 mS/cm	4 Jul 2017
Saturated hydraulic conductivity K_s, Thermal conductivity λ, thermal diffusivity κ, volumetric thermal capacity C, thermal resistivity ρ and porosity of sediment	Co. UMS (now Co. METER) K-SAT dynamic head permeameter & Co. Decagon (now Co. METER) K2PRO thermal probe	24 sediment samples of 50 cm height were collected in metal Rings from the upper 5 cm of the streambed in 0.5 and 1 m distance downstream of each transect	KSAT: Range of K_s: 0.01 - 5000 cm d^{-1}, Inaccuracy: 2-10% KD2PRO: Resolution / range / accuracy λ: 7% / 0.02-2 W m^{-1} K^{-1} / ± 10% κ: 7% / 0.1-1 mm^2 s^{-1} / ± 10% C: 5% / 0.5-4 MJ m^{-3} K^{-1} / ± 10% ρ: 5% / 50-5000 cm K W^{-1} / ± 0.01% Porosity by weighting and drying the samples of known volume (250 ml of the sample KSAT rings) in an oven for 48 hours (105 °C).	Summer 2016 Winter 2017
Sediment structure and layering	Pürckhauer soil borer	Down to 1.50 m in the sediment along the Thalweg of the stream each 5 m downstream	Qualitative description of the type of material Approximate description of sediment layering	Summer 2018

2.3.3 Identification of groundwater and interflow discharge

Lowry et al. (2007) first proposed the identification of GW discharge based on temperature anomalies and their temporal variability at the sediment-water interface (SWI). The authors demonstrate how the interpretation of temperature anomalies facilitates identifying areas of diffuse and focused groundwater discharge. Krause et al., (2012) also localizes water discharge at the SWI with temperature anomalies $A_T(SWI_i)$ $(°C)$ and describes additional indicators for temporal analysis. In the present study, the temperature anomaly $A_T(SWI_i)$ of any point i along the fiber buried in the sediment is calculated by subtracting the

spatially averaged SW temperature $\overline{T(SW)}$ (°C) from the measured SWI temperature at point i $T(SWI_i)$ (°C) (Equation 2.1). The $\overline{T(SW)}$ used as reference is averaged from 15 measurement points along 2 m of Line 2 of the setup, upstream of transect TR3 (Figure 2.1), where the fiber lies unburied over roots in full contact with SW. The quick and deep current of the stream where Line 2 remains unburied ensures intensive mixing of the SW supporting the representativeness of the measured SW temperatures. This approach also enables identifying interflow discharge by analysis of SWI temperatures in the margins.

Equation 2.1 $$A_T(SWI_i) = T(SWI_i) - \overline{T(SW)}$$

$A_T(SWI_i)$, $T(SWI_i)$ and $\overline{T(SW)}$ values are calculated for every 5 minutes measurement interval. Table 2 summarizes the use of A_T to identify areas of the SWI influenced either by GW exfiltration or interflow discharge. Groundwater discharge occurs in areas with year to seasonal persistence of temperature anomalies. The temporal evolution of temperature anomalies at time scales from hours to weeks is used to identify interflow discharge after heavy rainfalls.

The areas attributed to GW and interflow discharge based on their distinct temperature anomalies are labelled according to the source of water identified on them (GW: groundwater, INTF: interflow) and their transect location. Other areas take the name of the observed hydrologic state such as emerged (Ei) or stagnated waters (Si). In this way, GW3 means an area of temperature anomaly attributed to GW discharge located at transect 3. Being i= the transect where they are located, i=i-j means located between two transects.

2.3.4 Identification of small-scale downwelling patterns during floods

Natural flood events in River Schlaube are rare due to the strong regulating effect of upstream located lakes and the dense forest canopy in the basin. Despite the steady nature of the streamflow, we noticed several small peaks and periods of slightly increased SW levels in the recorded surface water level time series. In order to distinguish which periods of increased flow can be considered floods, we calculated the seasonal, trend and random components of the surface water level time series averaged at daily time steps. We obtained standard deviations of 2.35 cm, 0.35 cm and 0.67 cm, respectively, for the seasonal, trend and random components (R package “stats v.3.5.1”, function “decompose” based on Kendall

et al. (1983)). Moreover, the comparison of the random component with the rainfall time series points out differences attributable to artificial flow operation, especially during periods of summer baseflow. Indeed, the cause of these surface water level fluctuations was the operation of a weir at the outflow of the upstream located lake, an infrastructure capable of triggering man-made flood pulses. Artificial flood events caused by an increased discharge from the warm, upstream located lake cause a peak of increased SW temperatures quickly propagating downstream (Watson et al., 2018). As soon as the thermal peak reaches the study site, SW temperatures increase abruptly. SW temperatures propagate particularly fast into the sediment where significant SW downwelling takes place (Cardenas & Wilson, 2007).

The artificial events included in the present study show water level rises of 2.5 cm, 4 cm and 5 cm in less than 20 minutes. These level rises represent flood events of respectively 3.7, 6 and 7.5 times the standard deviation of the natural daily random component. The spatial and temporal analysis of the abrupt temperature changes occurring in certain areas of the shallow streambed enables the localization of local SW downwelling. We propose the identification of areas of local SW downwelling based on the different resilience of particular regions of the SWI to temperature change induced by artificial flood events. The spatially variable temperature changes at the SWI can be mapped as rates of temperature change $\Delta T/\Delta t$ (°C/h) during each time step Δt. The delineation of down-/upwelling areas is based on their respective resilience to flood-induced temperature changes. Downwelling areas show fast adaption towards high values of $\Delta T/\Delta t$ during flood conditions. Upwelling areas experience little change in $\Delta T/\Delta t$ both under baseflow and flood conditions.

In summer the forest canopy causes a mosaic of sunlight reaching the valley bottom. The analysis of $\Delta T/\Delta t$ caused by this mosaicked radiation during the period prior to each flood's arrival allows defining a threshold between the range of $\Delta T/\Delta t$ caused by radiation and the one determined by the sudden warming due to the flood. We define that the 95-percentile of the $\Delta T/\Delta t$ observed during the steady-state before the flood ($\Delta T/\Delta t_{95\%}$) defines the positive threshold for $\Delta T/\Delta t$ caused by radiation, the main source of heat affecting the SWI under steady conditions. The assumption implies that $\Delta T/\Delta t > \Delta T/\Delta t_{95\%}$ are caused by a heat source (e.g. SW inflow) different from radiation with a 95% confidence interval. Downwelling areas, where SW infiltration prevails, should show $\Delta T/\Delta t > \Delta T/\Delta t_{95\%}$ while upwelling areas should remain below the threshold.

2.3.5 Subsurface exploration using EMI geophysics

EMI exploration of the subsurface was conducted in four longitudinal transects of ≈ 50 m length that follow the curvature of the river which is constrained by the slopes (Figure 2.1). We used a CMD Explorer (GF Instruments, Brno, Czech Republic) for surveying the longitudinal transects in manual mode in steps separated 0.6 m. Multi-depth low induction number devices such as the CMD-Explorer have multiple receiver coils separated from the transmitter coil (Villeneuve et al., 2015) operating at the same frequency. Low induction number electromagnetic devices of unique-frequency operate a linear calibration applicable at low to moderate ranges of electrical conductivity of subsurface materials (≤ 100 mS/m) (Brosten et al., 2010).

The limited GPS positioning capabilities under dense forest canopy forced to locate the CMD locations with the total station Leica TPS 1200 which lasted at least 10 seconds per location. Thus, we chose a measurement time of 10 s also for the CMD Explorer. The device enables a theoretical exploration depth of approximately 6 m with the horizontal coplanar configuration (full-depth range). On-the-fly 1D inversion of the apparent electrical conductivity is provided by the CMD Explorer. However, RES2Dinv (Geotomo Software SDN BHD, Malaysia) has been used for the 2D inversion of the data. The EMI data were loaded into the software as a fictional electrical resistivity survey configured in a pole-pole array (type 6) according to the CMD's manual. From the multiple parametrization options of the software, we adopted the finite-difference mode to calculate the apparent resistivity. We have chosen the non-linear smoothness-constrained least-squares optimization technique (L2 norm) (Loke et al., 2003) regarding the assumed smooth transition from low to high values of resistivity in a streambed without identified bedrock. The model achieves this smoothing by minimizing the square of the changes in resistivity (L2 norm). The range of dampening factors is assumed 0.01-0.1 with initial values of 0.1. The horizontal flatness filter ratio used was 1; no diagonal filter was used. The option of the finest node configuration of 4 nodes in between electrodes was chosen. The layer depth definition of the mesh increases with depth from 0.05 cm in the upper layers to 1 m in the lower ones. The convergence limit was set to 3% after 4 iterations. The software provides RMS error fit and noise statistics.

EMI response depends on electrical conductivity (EC) of pore water, sediment structure/texture, and water saturation. Below the streambed the latter is 100 %, i.e. constant and thus negligible. For the correct interpretation of the EMI data, the electrical conductivity of the pore water is required to assure that difference of electrical conductivity observed with EMI are due to subsurface texture changes and not due to different pore water EC. Therefore, we collected 80 pore water samples from the eight different depths of the ten multi-level piezometers (Table 2.1) located at the four transects. Unfortunately, soils with clay content may invert the proportional relation between EC and porosity and the associated hydraulic conductivity (Slater & Lesmes, 2002). Sediment coring with a 1.5 m Pürckhauer type auger (Table 2.1) was conducted to unveil subsurface clay deposits taking advantage of the fact that clays remain in this narrow corer type while sandy and coarser materials tend to be lost in the overlying water column during retrieval of the corer.

2.4 Results and discussion

2.4.1 FO-DTS-based identification of groundwater and interflow discharge

Areas GW3 and GW4 (Figure 2.2) show persistent positive temperature anomalies A_T of up to 3.5 °C (hot spots) during winter and negative A_T down to -3.5 °C (cold spots) in summer. Both regions experience small variations of their area ($\Delta Area$ = ± 21 % at GW3 and ± 15.5 % at GW4) and average temperature anomaly ($\Delta|A_T|$ = ±0.4 °C at GW3 and ±0.26 °C at GW4 during baseflow conditions the 15 Sep 2016 and 18 Jan 2017, Figure 2.2a and b). Note that the delineation of the area is temporally changing and thus the number of averaged values of the temperature anomalies is also varying.

Conversely, the increase of the areas during the periods after rainfall (2 Jul 2017, Figure 2.2c) reaches $\Delta Area$ = + 176 % of the baseflow area at GW3 and + 140 % at GW4. The increase of the temperature anomaly in these circumstances becomes ΔA_T = -1.36 °C at GW3 and -0.83 °C at GW4. Pressure transducers at Transects 3 and 4, respectively (Figure 2.1), indicate higher piezometric heads of subsurface water compared to SW. Area GW3 at TR3 is located in a pool. It is well known that groundwater discharge is diverted to such pool areas by hyporheic flow paths (Cardenas & Wilson, 2007). As described by Kasahara & Hill (2007b), the downstream part of convex shorelines as they occur at GW3 and at GW4 result

in increased GW discharge from the riparian aquifer. These findings support that GW discharge causes the temperature anomalies at GW3/GW4.

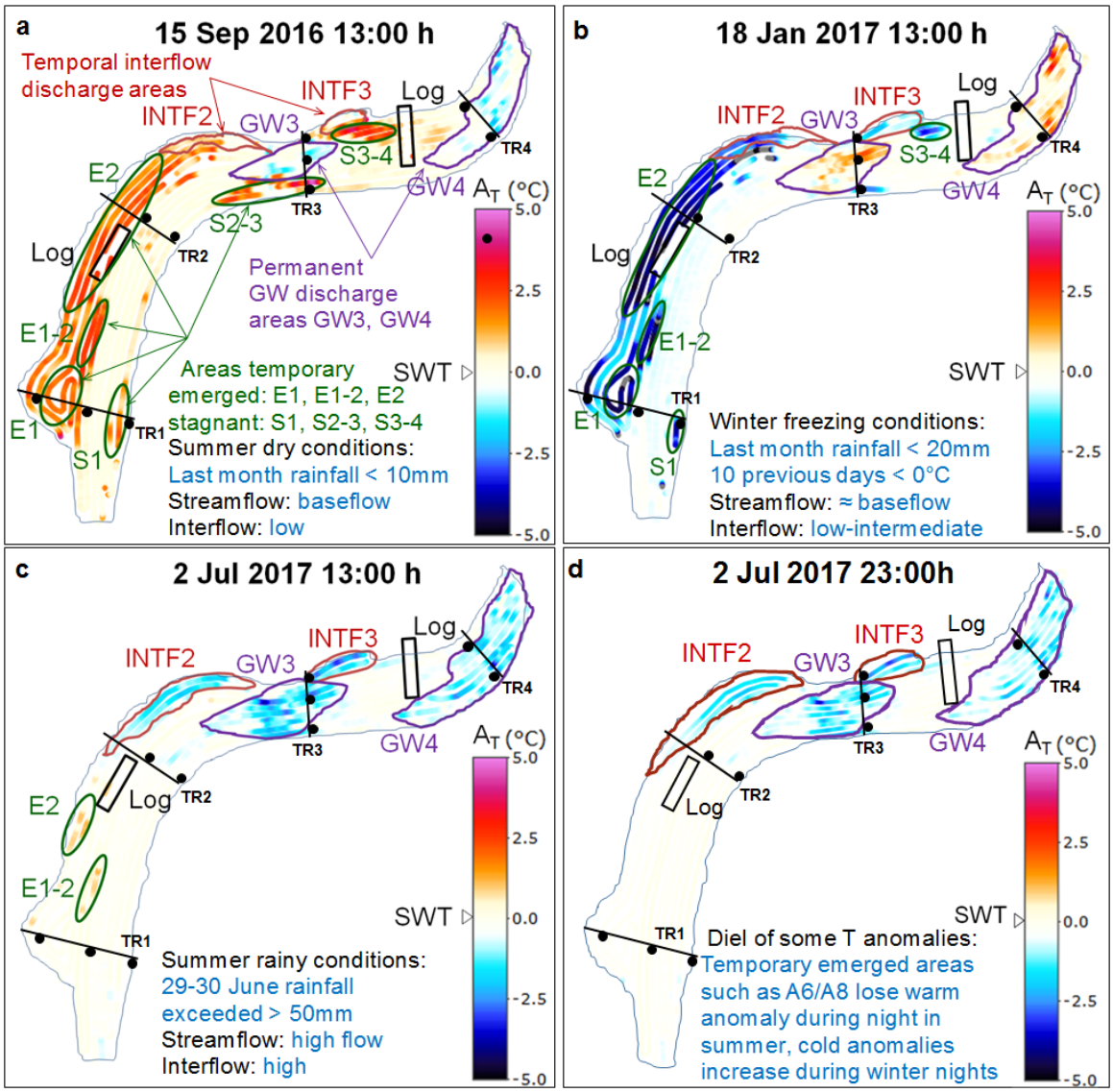

Figure 2.2: (a, b, c) Maps of temperature anomalies A_T (°C) at the SWI (deviation of the SWI temperature from the SW temperature) under (a) dry summer conditions with low river stage and strong radiation, (b) winter conditions with ice formation in stagnant areas, (c) summer wet conditions with interflow discharge after rainfalls, and (d) the temporal disappearance of the temperature anomalies of temporary emerged areas (E1, E1-2, E2) due to the absence of radiation during night.

Areas INTF2 and INTF3 show temporary cold A_T (independent of the season (Figure 2.2a-c)) that increase sharply both in intensity and extent in the hours to days after rain events and progressively fade away within days (Figure 2.3d-g).

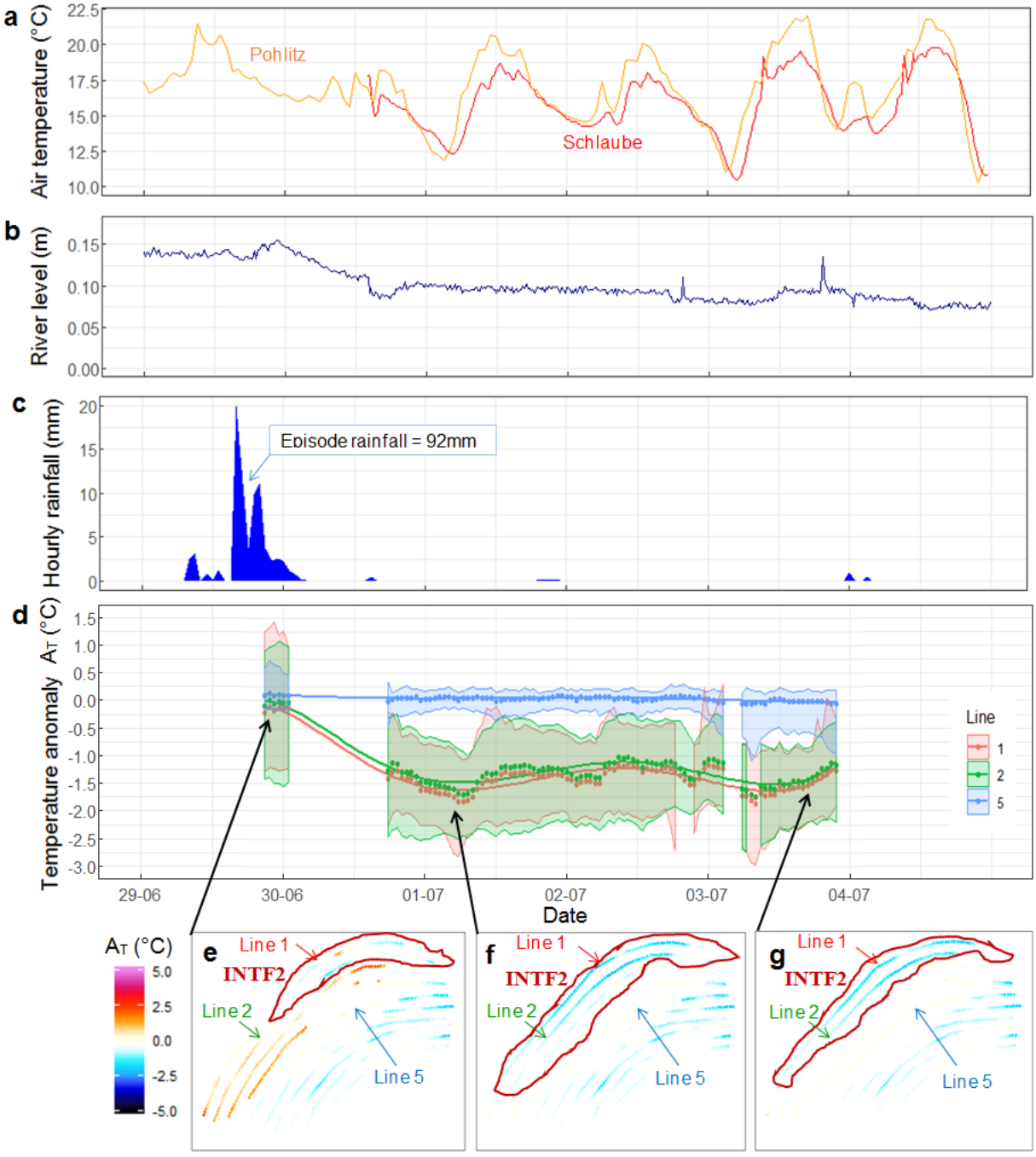

Figure 2.3: Time series of environmental conditions and interflow during and after the intense rainfall episode on 29 Jun 2017. (a) Air temperatures at Schlaube (red line) and the closest (8 km) German Meteorological Service (DWD) station 3967 at Pohlitz (orange line)

show increasing daily temperature amplitudes after the end of the rainfall episode. (b) The streamflow barely responds to the intense rainfall episode. Overall, there is a trend of a temporarily decreasing river stage. (c) Hourly rainfall measured by DWD in Pohlitz. Other stations farther from the study site show consistently heavy regional rainfalls. (d) Time series of spatially averaged temperature anomalies AT of the FO-DTS fiber for the sections in area INTF2 of Lines 1, 2 and 5 (panels e-g). Note that the delineation of area INTF2 is temporally changing and thus the number of averaged values of the temperature anomalies is also varying. Shaded areas are 95% confidence intervals of the mean temperature anomaly of the points from each line included in region INTF2 on each time step. Surface water and groundwater discharge prevail outside of area INTF2, which explains the quasi-constant temperature anomaly of the approximately 30 points of Line 5 parallel to INTF2. Conversely, DTS lines 1 and 2 located close to the left shoreline (e-g) reveal a sharp temperature decrease in the first day after the rainfall episode and recover steadily afterwards; a phenomenon that is consistent with the temporal evolution of interflow discharge. (e-g) Section of study site with area INTF2 visualizing the spatial pattern of the temperature anomalies and their temporal evolution. The change of INTF2 occurs preferably along the margin, consistent with the origin of interflow.

The spatial extent of INTF2 and INTF3 increases significantly (more than four times for INTF2 and almost two times for INTF3) from its minimum extent at dry weather to a maximum extent during periods of and shortly after periods of precipitation (15 Sept 2016, Figure 2.2a vs. 2 Jul 2016, Figure 2.2c, Figure 2.3e-g). The average temperature anomaly A_T in INTF2 increases from - 0.07 °C (almost non-existent) during dry periods to - 1.57 °C during wet periods. In INTF3, A_T is -0.17 °C during dry periods and - 1.79 °C during wet periods.

The pulse-like discharge pattern after rain events followed by flow recession shown in Lines 1 and 2 of Figure 2.3e, f, g indicates that shallow interflow discharge is the driving force of the temperature anomaly at INTF2 for those lines. The lack of clear correlation between AT and environmental conditions such as air temperature or river stage fluctuations supports the interflow origin, too. Visually identified springs on the streambank after periods of precipitation are further support of the occurrence of intense interflow at the study site.

Emerged areas (Ei) and areas of stagnant water (Si) show larger values of A_T (>3 °C) than INTF2/INTF3 during days of large daily temperature amplitudes (e.g. 15 Sep 2016, Figure 2.2a, or 18 Jan 2017, Figure 2.2b). Additionally, the anomalies disappear partly during night time (Figure 2.2d). Probably radiation is the driving force of the observed temperature anomalies. E1, E1-2, E2 are temporarily emerged areas depending on SW levels while S1, S2-3, S3-4 comprise pools of stagnant water. The temporal disconnection of E1, E1-2 and E2 from the streamflow and the shallow slow flow at S1, S2-3, S3-4 favour the increasing relevance of radiation on their thermal response and explains the large value of A_T. Table 2.2 summarizes how to distinguish different types of subsurface discharge at the SWI based on ranges of $A_T(SWI_i)$, and additionally, the ranges observed for emerged/stagnant areas showing the daily temperature cycle of $A_T(SWI_i)$ due to solar radiation.

2.4.2 FO-DTS differentiation of local SW down-/upwelling during floods

Three flood events were measured with FO-DTS (Table 2.2, Figure 2.4a-f). Flood events raised both SW temperatures (Figure 4) and SWI temperatures, the latter in some areas up to 1.4 °C within 20 minutes ($\Delta T/\Delta t$ 3-5 °C/h) (Figure 2.4b, d, f). We calculated the threshold $\Delta T/\Delta t_{95\%} \approx 1$ °C/h (Figure 2.4a, c, e) under baseflow conditions based on the periods shortly before floods in which radiation is the main source of warming (1.4°C/h on 25 Jul 2016, 0.8 °C/h on 2 Jul 2017, 0.9 °C/h on 3 Jul 2017, Figure 2.4b, d, f). The threshold distinguishes warming due to floods from the range of warming caused by the ubiquitous impacts of solar radiation and air temperature fluctuation. Additionally, areas of the SWI experiencing $\Delta T/\Delta t < 1$ °C/h both during baseflow and flooding conditions correspond to the areas GW3/GW4 of prevalent groundwater upwelling.

The flood from 25 Jul 2016 exhibits the largest overall increase of both SW level and SW temperature (5 cm and 1.4 °C) among the three floods (Figure 2.4b). The increase of the SW level caused the prevalence of downwelling areas at the SWI ($\Delta T/\Delta t$ shift from 0-1 °C/h before to 1.5-3.5 °C/h during the flood). Only areas corresponding to GW discharge (GW3/GW4) identified in Section 2.3.2 do not experience $\Delta T/\Delta t > 1.5$ °C/h.

The second flood (2 Jul 2017, Figure 2.4c and d) is the smallest in terms of water level rise (2.5 cm) and SW temperature increase (0.3 °C). Downwelling is less widespread compared to 25 Jul 2016, despite $\Delta T/\Delta t_{95\%}$ being lower (0.8 °C/h). However, both the second

and the third flood, enabled a clear spatial identification of down-/upwelling areas (Figure 2.4d-f), showing that the $\Delta T/\Delta t_{95\%}$-approach can be successfully applied even for small flood events with low overall temperature and water level increase.

Table 2.2: Interpretation of temperature patterns at the SWI.

Flow pattern [Example area]	Temperature anomaly A_T (°C) [Example dates]	Rates of temperature change at the SWI caused by flood-induced changes of SW temperatures $\Delta T/\Delta t$ (°C/h)
Groundwater discharge [Area GW3/GW4, Figure 2.2a-c]	Permanent cold anomaly (A_T<0) in summer [15 Sep 2016, Figure 2.2a/c] Permanent warm anomaly (A_T>0) in winter [18 Jan 2017, Figure 2.2b] (Quasi-constant permanent temperature anomalies)	na
Interflow discharge [Area INTF2/INTF3, Figure 2.2a-c]	Temporary cold anomaly (A_T<0) in winter [18 Jan 2017, Figure 2.2b] and summer [2 Jul 2017, Figure 2.2c] with receding extension/intensity after the end of a rainfall event [15 Sep 2016, Figure 2.2a] (Temperature anomalies increasing in area and intensity: (1) sharp decrease of T during rainfall event and (2) steady decrease recovery from hours to weeks scale after the rainfall episode)	na
Local SW downwelling [Areas delimited with red contour, Figure 2.4b/d/f]	$A_T \approx 0$, i.e. areas with temperatures non-distinguishable from SW temperatures	Fast response, with values over the threshold of $\Delta T/\Delta t_{95\,\%}$ calculated based on measurements shortly before the flood event: 1.4 °C/h [25 Jul 2016, Figure 2.4b b] 0.8 °C/h [2 Jul 2017, Figure 2.4b d], 0.9 °C/h [3 Jul 2017, Figure 2.4b f]
Local SW upwelling [Areas outside the red contour delimiting areas of local SW downwelling, Figure 2.4b/d/f]	[All baseflow dates]	Slow response, with values below the threshold $\Delta T/\Delta t_{95\%}$ both under baseflow conditions [Figure 2.4b/d/f] and flood conditions [Figure 2.4b/d/f].
Temporary emerged areas [Area E1, E1-2, E2, Figure 2.2] Temporary stagnant waters [Area S1, S2-3, S3-4, Figure 2.2]	Strong warm anomalies during the daily cycle (A_T>0) when exposed to radiation [15 Sep 2016, Figure 2.2a] Strong temporally persistent cold anomalies (A_T<0) when affected by freezing of stagnant waters in winter [18 Jan 2017, Figure 2.2b] No anomalies (A_T≈0) when connected to streamflow [2 Jul 2017, Figure 2.2c]	Slow with values below the threshold $\Delta T/\Delta t_{95\%}$ under baseflow [Figure 2.2d/f/h] or flood conditions [Figure 2.2e/g/i] due to clogging.

(na: not applicable)

Although all three floods are small (=< 5 cm) their different intensities result in different sizes of downwelling areas. This reveals that care is required when interpreting the data. Areas identified as downwelling might only be downwelling during the flood event

because of the altered hydraulic gradients due to the flood. Thus, the down-/upwelling distribution portrayed during floods may differ from the one during baseflow conditions. Instead, a sudden modification of the SW temperature without altering the flow would be useful to delineate downwelling areas during baseflow.

It turned out that the sequence of down-/upwelling areas identified with the $\Delta T/\Delta t_{95\%}$-threshold resembles the streambed morphology of the study site, except for areas GW3/GW4 where GW upwelling withstands the flood perturbation. Riffle-pool sequences (R and P labels in Figure 2.4b, d, f) such as the one upstream of the log and transect TR4 reveals the agreement between $\Delta T/\Delta t$ and streambed morphology. In detail, this riffle area upstream of the log before transect TR4 shows high $\Delta T/\Delta t$ indicative of downwelling while downstream, where the $\Delta T/\Delta t$ values remain primarily below the threshold, pools prevail. Other high values of $\Delta T/\Delta t$ occur in areas of quick streamflow (QS label in Figure 2.4b, d, f) over irregular bedforms such as upstream of transect TR1 and in the bend of the stream between transects TR2 and TR3 can be related to increased downwelling in areas of high streamflow speed (Packman & Salehin, 2003; Wu et al., 2018). This approach of combining morphological and unsteady thermal information has the potential to provide further insights into the thermal exchange in bedforms under varying flow conditions. High precision surveys of the streambed would be an advantage for this purpose (e.g. laser scanning).

2.4.3 Combined interpretation of FO-DTS, EMI and direct subsurface exploration to identify subsurface structures.

The inversion of EMI geophysics data provides electrical conductivity (EC) values of the streambed as an indicator of texture changes in the sediment under the prerequisite that the variability of the EC of the pore water can be neglected. The 0.75% and 2.5% misfit statistics values obtained for profiles A-A' and D-D' with the L2 norm method (Figure 2.5a$_1$ and a$_2$) are close to the ideal values of misfit of around 1%. Figure 5a & 5b displays the inverted values of EC obtained from the EMI survey in a range from 5 to 23 mS/m. The electrical conductivity values obtained from 72 pore water samples collected from the multi-level piezometers (at depths -0.01, -0.14, -0.18, -0.23, -0.31, -0.48, -0.65, -0.82 m) show a range of EC between 21 and 45 mS/m. Locations with a larger range of EC values in the

vertical profile of the pore water samples (such as TR1L) show a similar range width in the EMI values.

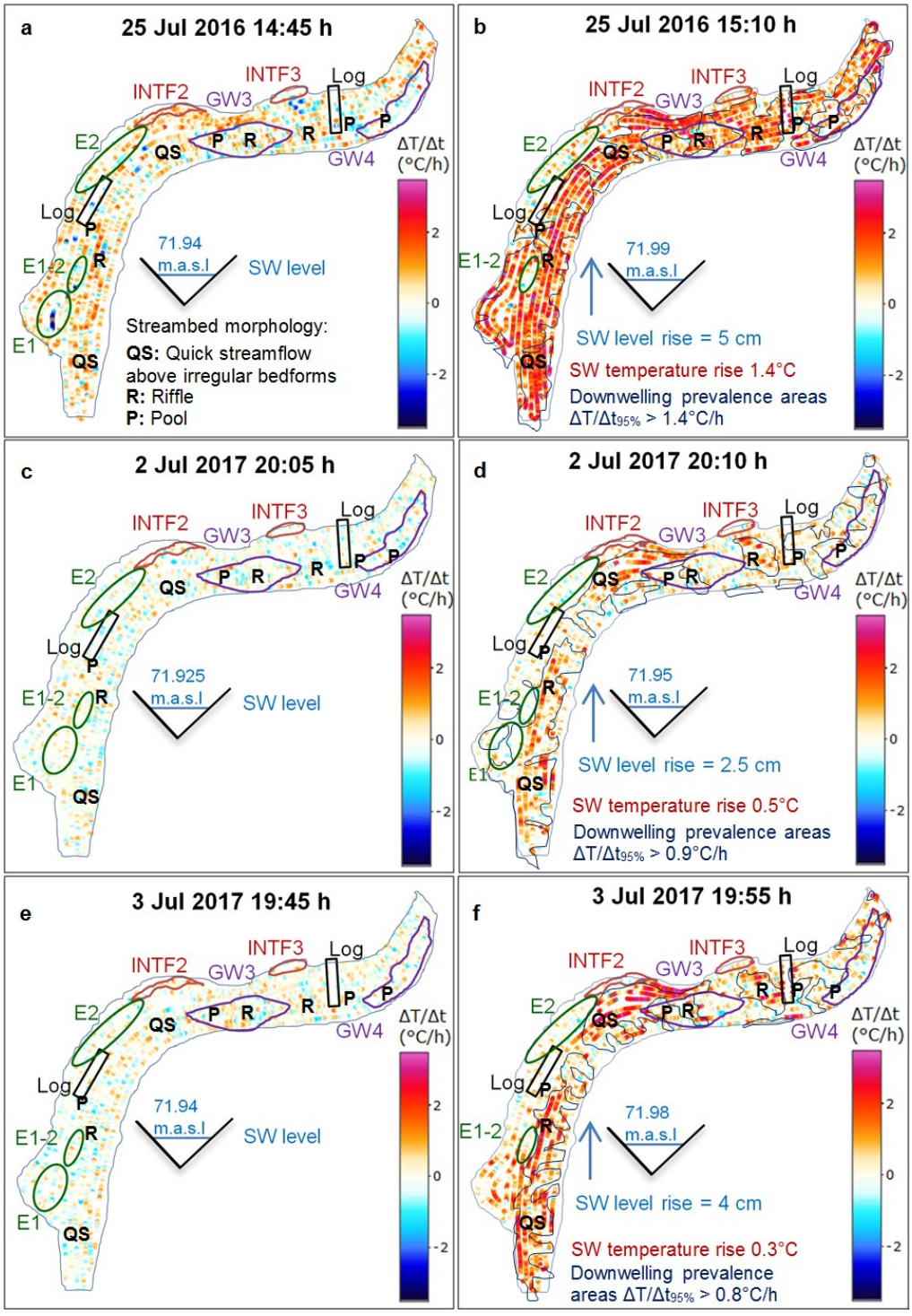

Figure 2.4: Rates of temperature change ΔT/Δt (°C/h) under no-flood (a, c, e) and flood (b, d, f) conditions for three events recorded with FO-DTS: (a, b) 25 Jul 2016, (c, d) 2 Jul 2017,

(e, f) 3 Jul 2017. Warming rates previous to flood transit are higher in the case of 25 Jul 2016 compared to the other two dates due to high radiation (up to 1 °C/h) at midday, but much lower than flood warming rates (up to 3.5 °C/h). Areas, where downwelling prevails, are delineated in (b, d, f) with dark blue lines based on the calculated thresholds of $\Delta T/\Delta t95\%$. The most relevant morphological features of the streambed are labelled with QS (quick streamflow above irregular bedforms), R (riffles) and P (pools).

Even though the EC range is similar between techniques, the offset between both methods suggests uncertain accuracy of the universal calibration of the EMI device for the specific subsurface characteristics of the streambed of River Schlaube. The correlation between the fluid conductivity and the bulk conductivity of the soil obtained with geophysics is weak, R^2=0.152, and smaller than the R^2=0.34 reported in Brosten et al. (2010). Such small correlation indicates the negligible effect of fluid conductivity changes on the distribution of electrical conductivities observed with geophysics. Thus, the EC values and their spatial changes observed with EMI are indicative of texture heterogeneity.

An abrupt transition in downstream direction of the longitudinal EC profiles can be observed from high EC values (in red) at transect TR1 to the low values at TR3/TR4 (in blue). Such discontinuities exist also with depth at TR1 and TR2 indicating stratification of materials. Low EC values prevail along transects TR3/TR4 with TR3 showing a region of slightly higher EC with vertical continuity (denoted in light blue) embedded in low EC materials (in dark blue). The high EC values at the left side of TR1 (Figure 2.5a_1 and a_2) suggest the presence of either a conductive region or materials causing electric effects such as clay.

The diel-driven A_T observed at TR1 at the SWI (upper face of Figure 2.5b_1 and b_2) show no permanent patterns attributable to GW discharge but to radiation, which suggests the existence of a layer blocking the flow. Additional evidence about the resistive nature of the high EC materials found in TR1 is provided from the vertical exploration of the sediment with the Pürckhauer corer (Figure 2.5c and Table 2.1). At both TR1 and TR2, fine clay and organic materials were retrieved in deep layers, stuck into the narrow section of the corer.

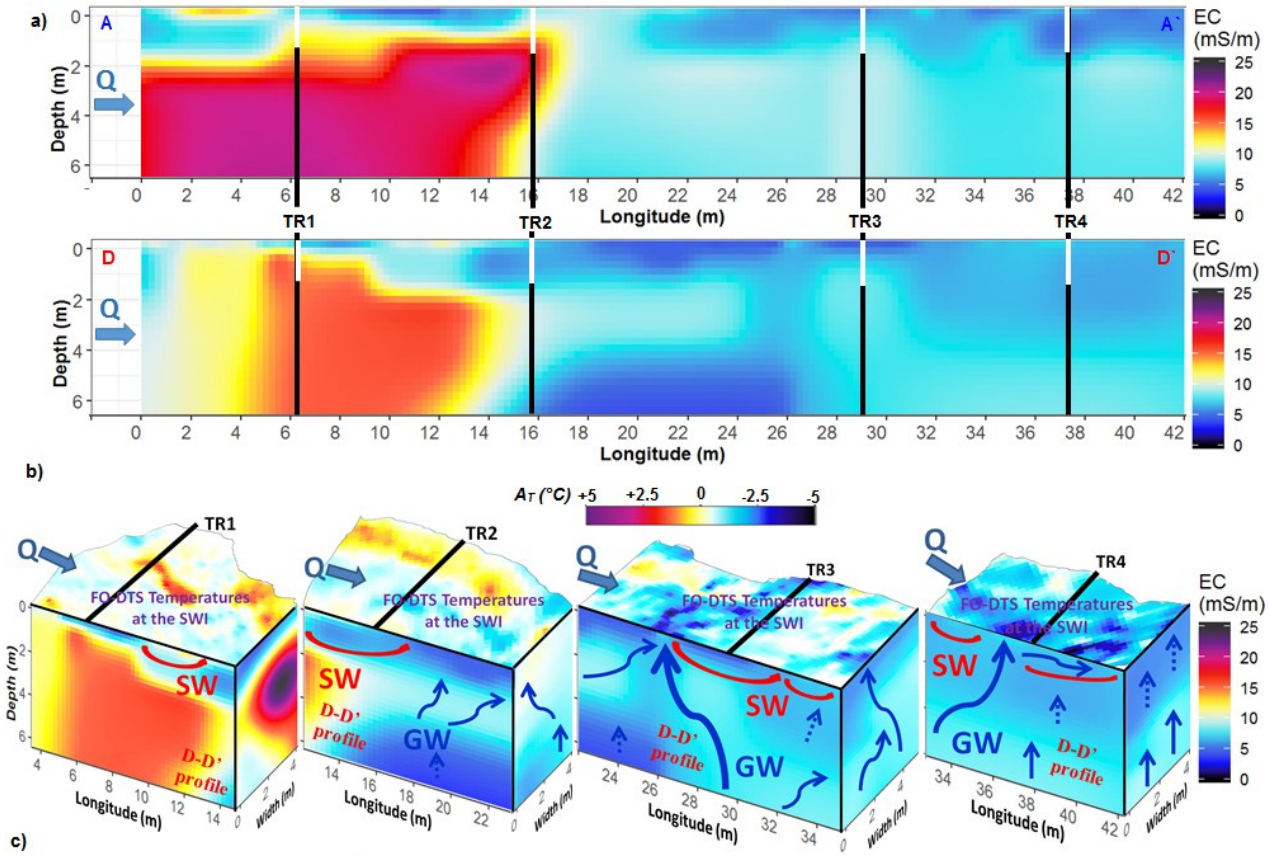

TR1

Depth (cm)	Sediment description
0-10	Sand with small gravel
0-30	Sand with wood and leaves
30-50	Sand with small gravel
50-60	Fine organic matter with gravel
60-120	Clay with fine organic matter
120-135	Fine organic matter with sand

TR2

Depth (cm)	Sediment description
0-20	Fine sand
20-30	Sand with fine organic matter
30-65	Core lost
65-80	Sand, clay and organic matter
80-145	Clay with fine organic matter

TR3

Depth (cm)	Sediment description
0-20	Medium sand
20-50	Fine sand with gravel and wood
50-145	Core lost

TR4

Depth (cm)	Sediment description
0-30	Fine to medium sand
30-55	Medium sand with gravel
55-145	Core lost

Figure 2.5: (a) Longitudinal profiles A-A` and D-D` (compare Figure 1b) of electrical conductivity (mS/m) down to approximately 6 m depth obtained from the 2D inversion of EMI geophysics data along approx. 50 m of the study site. (b) Prismatic models of the riverbed at transects TR1, TR2, TR3 and TR4 representing FO-DTS temperature anomalies at the SWI in the upper face of the prisma (horizontal) and electrical conductivity profiles in the lateral faces of the prisma (vertical). The blue and red arrows conceptualize the paths of groundwater (GW) and surface water (SW) flows based on both, subsurface structures detected in the EMI survey and temperature anomalies observed at the SWI by FO-DTS. The Q arrow represents the direction of streamflow and indicates the location of the Thalweg. (c)

Subsurface stratification and sediment types based on cores collected at transects TR1-TR4 with a Pürckhauer corer (Table 2.1). Location and length of cores are indicated in (a) panels as white lines. Lost segments of cores correspond to medium to coarse permeable sands that were washed out of the corer in the overlying stream during retrieving the corer.

The presence of clays below permeable sands and gravels agrees with the abrupt vertical transition from low to high EC values observed in the EMI profiles at around 1 m depth. The assimilation of high EC values to fine materials (in the absence of bedrock) is consistent with EMI geophysics observations of Rosenberry et al. (2016). Downstream, cores at TR3 and TR4 indicate the absence of fine-textured materials such as clay or organic deposits. As sands tend to be washed out from the corer in the overlying stream while retrieving the corer, the lost sediment of TR3 and TR4 can be considered as permeable material. This vertical continuity of permeable sediment of TR3 and TR4 corresponds well to the homogeneity of EC values displayed in the EMI profiles and to the presence of A_T at the SWI observed by FO-DTS (upper face of Figure 2.5b of TR3 and TR4).

The combined interpretation of FO-DTS, EMI and direct sediment exploration enables reliable testing of consistencies between methods. The FO-DTS-based identification of areas GW3 and GW4 as permanent temperature anomalies is indicative of GW discharge. These findings correspond well with the sandy materials retrieved from cores along transects TR3 and TR4 where also EMI profiles indicate homogenous conditions of the aquifer at meter to decimeter scales. The vertical continuity of low values of EC at TR3 and TR4 representing coarse materials supports the identification of areas of GW discharge GW3 and GW4 at those transects. The agreement underlines the reliability of FO-DTS for the identification of groundwater exchange based on temperature patterns.

The absence of significant temperature anomalies attributable to groundwater or interflow discharge at transect TR1 is in correspondence with the high EC region identified in the first half of the EMI profiles as the fine materials of low hydraulic conductivity extracted from the lower layers of the soil cores. In view of the successful identification of the two distinct areas of clogged materials at TR1 and TR2 and conductive ones at TR3 and TR4, EMI also succeeded in revealing the meter to decameter scale of spatial heterogeneity

of the aquifer. These findings are consistent with the reported impacts of intermediate-scale aquifer heterogeneity on groundwater seepage (Fleckenstein et al., 2006).

However, due to the spatial averaging of the electromagnetics induced by such a wide EMI device (almost 4 m wide), the EC values obtained are limited in resolution (Binley et al., 2015). We are aware that the small scale heterogeneity of the subsurface, in particular at the upper layers caused by scour and deposition, remains undetected. Given the strong impact of this small heterogeneity in the sub-meter water exchange of the HZ (Krause et al., 2012), detailed subsurface exploration is recommended.

EMI surveys or other geophysical techniques with decimeter or even centimeter resolution of shallow subsurface are also necessary to support our findings of FO-DTS about local SW downwelling during floods. Similarly, high-resolution topographic monitoring of bedforms as described in Brasington et al. (2012) could help to distinguish the particular impacts of the thermal, morphological and sedimentary controls on the local hyporheic exchange.

In the present study, EMI has only been applied to study subsurface structure underneath the stream. However, the method could also be applied to study subsurface structures alongside the stream. Time series of EMI investigations at the slopes of the Schlaube valley might be useful to investigate interflow since a changing water saturation of the soil can be easily identified with EMI time series (Robinson et al., 2008).

2.5 Conclusions

A high-density mesh of FO-DTS installed at the sediment-water interface shows capabilities for the differentiation of groundwater and interflow components based on spatial and temporal analysis of the temperature patterns. The high spatial and temporal resolution of FO-DTS allows observing the alteration of the exchange during transient states such as rain events and floods. In particular, transient conditions enable (1) the identification of interflow based on the temporal evolution of the temperature anomalies and (2) local surface-water downwelling based on their low resilience to temperature and pressure changes in the overlying water. However, the technique has limited capability to infer the factors causing the observed spatial heterogeneity of the temperature patterns. Aiming to overcome this

limitation of FO-DTS and prove the source of the groundwater component, geophysical techniques, such as electromagnetic induction (EMI), can provide in-depth exploration of the sediment. The electrical conductivity profiles and maps provided by the EMI technique can qualitatively infer texture changes in the sediment. This capability is particularly useful to identify streambed structures relevant for connectivity/disconnectivity of groundwater and surface water, which enables to check the validity of the identification of the areas of water exchange distinguished with FO-DTS. We encourage the hyporheic community to address the challenging steps ahead to extend FO-DTS capabilities as well as to foster the combined use and evaluation of the different techniques to improve our understanding of GW-SW exchange across scales.

2.6 Acknowledgements

This research is funded by the SMART (Science for MAnagement of Rivers and Tidal systems) Joint Doctoral Erasmus Mundus Programme, funded by the European Commission, SGA 2015-1628. This publication reflects the views only of the authors, and the Commission cannot be held responsible for any use which may be made of the information contained therein. We thank Christine Sturm, Anne Mehrtens, Wiebke Seher, Jason Galloway, Hannah Schulz and Birgit Müller for their help with fieldwork and specially Amaia Marruedo and Silvia Folegot for their FO-DTS training, as well as the Nature Park Schlaubetal for allowing access to River Schlaube. We must extend our gratitude to Fernando A. Monteiro Santos (University of Lisbon) for the invaluable insights he shared about the accurate procedure to survey and process EMI data. Finally, we thank two anonymous reviewers whose comments/suggestions helped to improve and clarify the present manuscript.

2.7 References

Anderson, M. P. (2005). Heat as a groundwater tracer. *Groundwater*, *43*(6), 951-968. https://doi.org/10.1111/j.1745-6584.2005.00052.x

Bencala, K. E. (2005). 113: Hyporheic exchange flows. *Encyclopedia of Hydrological Sciences, 1-7.*

Binley, A., Ullah, S., Heathwaite, A. L., Heppell, C., Byrne, P., Lansdown, K., … & Zhang, H. (2013). Revealing the spatial variability of water fluxes at the groundwater-surface water interface. *Water Resources Research*, *49*(7), 3978–3992. https://doi.org/10.1002/wrcr.20214

Binley, A., Hubbard, S. S., Huisman, J. A., Revil, A., Robinson, D. A., Singha, K., & Slater, L. D. (2015). The emergence of hydrogeophysics for improved understanding of subsurface processes over multiple scales. *Water resources research, 51*(6), 3837-3866. https://doi.org/10.1002/2015WR017016

Blume, T., Krause, S., Meinikmann, K., & Lewandowski, J. (2013). Upscaling lacustrine groundwater discharge rates by fiber-optic distributed temperature sensing. *Water Resources Research*, *49*(12), 7929-7944. https://doi.org/10.1002/2012WR013215

Boaga, J. (2017). The use of FDEM in hydrogeophysics. *Journal of Applied Geophysics*, *139*, 36-46. https://doi.org/10.1016/j.jappgeo.2017.02.011

Brasington, J., Vericat, D., & Rychkov, I. (2012). Modelling river bed morphology, roughness, and surface sedimentology using high-resolution terrestrial laser scanning. *Water Resources Research, 48*(11). https://doi.org/10.1029/2012WR012223

Briggs, M. A., Lautz, L. K., & McKenzie, J. M. (2012a). A comparison of fiber-optic distributed temperature sensing to traditional methods of evaluating groundwater inflow to streams. *Hydrological Processes*, *26*(9), 1277-1290. https://doi.org/10.1002/hyp.8200

Briggs, M. A., Lautz, L. K., McKenzie, J. M., Gordon, R. P. & Hare, D. K. (2012b). Using high-resolution distributed temperature sensing to quantify spatial and temporal variability in vertical hyporheic flux. *Water Resources Research*, *48*(2). https://doi.org/10.1029/2011WR011227

Brosten, T. R., Day-Lewis, F. D., Schultz, G. M., Curtis, G. P., & Lane Jr, J. W. (2011). Inversion of multi-frequency electromagnetic induction data for 3D characterization of hydraulic conductivity. *Journal of Applied Geophysics*, *73*(4), 323-335. https://doi.org/10.1016/j.jappgeo.2011.02.004

Cardenas, M. B., & Wilson, J. L. (2007). Thermal regime of dune-covered sediments under gaining and losing water bodies. *Journal of Geophysical Research: Biogeosciences*, *112*(G4). https://doi.org/10.1029/2007JG000485

Constantz, J., & Stonestrom, D. A. (2003). Heat as a tracer of water movement near streams. *US Geological Survey Circular*, *1260*, 1-96.

Crook, N., Binley, A., Knight, R., Robinson, D. A., Zarnetske, J., & Haggerty, R. (2008). Electrical resistivity imaging of the architecture of substream sediments. *Water Resources Research*, *44*(4). https://doi.org/10.1029/2008WR006968

Dakin, J. (1987). Multiplexed and distributed optical fiber sensor systems. *Journal of Physics E: Scientific Instruments*, *20*(8), 954. https://doi.org/10.1088/0022-3735/20/8/002

Day-Lewis, F. D., White, E. A., Johnson, C. D., Lane Jr, J. W., & Belaval, M. (2006). Continuous resistivity profiling to delineate submarine groundwater discharge: Examples and limitations. *The Leading Edge*, *25*(6), 724-728. https://doi.org/10.1190/1.2210056

Fleckenstein, J. H., Niswonger, R. G., & Fogg, G. E. (2006). River-aquifer interactions, geologic heterogeneity, and low-flow management. *Groundwater*, *44*(6), 837-852. https://doi.org/10.1111/j.1745-6584.2006.00190.x

González-Pinzón, R., Ward, A. S., Hatch, C. E., Wlostowski, A. N., Singha, K., & Brock, J. T. (2015). A field comparison of multiple techniques to quantify groundwater-surface-water interactions. *Freshwater Science*, *34*(1), 139-160. https://doi.org/10.1086/679738

Gourry, J. C., Vermeersch, F., Garcin, M. & Giot, D. (2003). Contribution of geophysics to the study of alluvial deposits: a case study in the Val d'Avaray area of the River Loire, France". *Journal of applied geophysics*, *54*, 35-49. https://doi.org/10.1016/j.jappgeo.2003.07.002

Hare, D. K., Briggs, M. A., Rosenberry, D. O., Boutt, D. F., & Lane, J. W. (2015). A comparison of thermal infrared to the fiber-optic distributed temperature sensing for evaluation of groundwater discharge to surface water. *Journal of Hydrology*, *530*, 153-166. https://doi.org/10.1016/j.jhydrol.2015.09.059

Hare, D. K., Boutt, D. F., Clement, W. P., Hatch, C. E., Davenport, G. (2017). Hydrogeological controls on spatial patterns of groundwater discharge in peatlands. *Hydrology and Earth System Sciences, 21*(12) 6031–6048. https://doi.org/10.5194/hess-21-6031-2017

Henderson, R. D., Day-Lewis, F. D., & Harvey, C. F. (2009). Investigation of aquifer-estuary interaction using wavelet analysis of fiber-optic temperature data. *Geophysical Research Letters*, *36*(6). https://doi.org/10.1029/2008GL036926

Kasahara, T., & Hill, A. R. (2007). Lateral hyporheic zone chemistry in an artificially constructed gravel bar and a re-meandered stream channel, Southern Ontario, Canada. *Journal of the American Water Resources Association*, *43*(5), 1257-1269. https://doi.org/10.1111/j.1752-1688.2007.00108.x

Kendall, M., Stuart, A., & Ord, J. K. (1983). *The advanced theory of statistics*, Vol.*3*, pp. 410-414.

Krause, S., Blume, T., & Cassidy, N. (2012). Investigating patterns and controls of groundwater up-welling in a lowland river by combining Fiber-optic Distributed Temperature Sensing with observations of vertical hydraulic gradients. *Hydrology and Earth System Sciences*, *16*(6), 1775-1792. https://doi.org/10.5194/hess-16-1775-2012

Lesch, S. M., Corwin, D. L., & Robinson, D. A. (2005). Apparent soil electrical conductivity mapping as an agricultural management tool in arid zone soils. *Computers and Electronics in Agriculture*, *46*(1-3), 351-378. https://doi.org/10.1016/j.compag.2004.11.007

Lewandowski, J., Angermann, L., Nützmann, G., & Fleckenstein, J. H. (2011). A heat pulse technique for the determination of small-scale flow directions and flow velocities in the streambed of sand-bed streams. *Hydrological Processes*, *25*(20), 3244-3255. https://doi.org/10.1002/hyp.8062

Loke, M. H., Acworth, I., & Dahlin, T. (2003). A comparison of smooth and blocky inversion methods in 2D electrical imaging surveys. *Exploration Geophysics*, *34*(3), 182-187. https://doi.org/10.1071/EG03182

Lowry, C. S., Walker, J. F., Hunt, R. J., & Anderson, M. P. (2007). Identifying spatial variability of groundwater discharge in a wetland stream using a distributed temperature sensor. *Water Resources Research*, *43*(10). https://doi.org/10.1029/2007WR006145

Mansoor, N., Slater, L., Artigas, F., & Auken, E. (2006). High-resolution geophysical characterization of shallow-water wetlands. *Geophysics*, *71*(4), B101-B109. https://doi.org/10.1190/1.2210307

Mwakanyamale, K., Slater, L., Day-Lewis, F.D., Elwaseif, M., & Johnson, C. (2012). Spatially variable stage-driven groundwater-surface water interaction inferred from time-frequency analysis of distributed temperature sensing data. *Geophysical Research Letters*, *39*(6). https://doi.org/10.1029/2011GL050824

Packman, A. I., & Salehin, M. (2003). Relative roles of stream flow and sedimentary conditions in controlling hyporheic exchange. *Hydrobiologia*, *494*(1-3), 291-297. https://doi.org/10.1023/A:102540342

Robinson, D. A., Binley, A., Crook, N., Day-Lewis, F. D., Ferré, T. P. A., Grauch, V. J. S., ... & Nyquist, J. (2008). Advancing process-based watershed hydrological research using near-surface geophysics: A vision for, and review of, electrical and magnetic geophysical methods. *Hydrological Processes*, *22*(18), 3604-3635. https://doi.org/10.1002/hyp.6963

Robinson, D. A., Lebron, I., Kocar, B., Phan, K., Sampson, M., Crook, N. & Fendorf, S. (2009). Time-lapse geophysical imaging of soil moisture dynamics in tropical deltaic soils: An aid to interpreting hydrological and geochemical processes, *Water Resources Research*, *45*, https://doi.org/10.1029/2008WR006984

Rosenberry, D.O., Briggs, M.A., Voytek, E.B., & Lane, J.W. (2016). Influence of groundwater on the distribution of dwarf wedgemussels (Alasmidonta heterodon) in the upper reaches of the Delaware River, northeastern USA. *Hydrology and Earth System Sciences 20*(10)*: 4323–4339.* https://doi.org/10.5194/hess-20-4323-2016

Selker, J. S., Thévenaz, L., Huwald, H., Mallet, A., Luxemburg, W., Van De Giesen, N., ... & Parlange, M. B. (2006a). Distributed fiber-optic temperature sensing for hydrologic systems. *Water Resources Research*, *42*(12). https://doi.org/10.1029/2006WR005326

Selker, J. S., Van de Giesen, N., Westhoff, M., Luxemburg, W., & Parlange, M. B. (2006b). Fiber-optic opens a window on stream dynamics. *Geophysical Research Letters*, *33*(24). https://doi.org/10.1029/2006GL027979

Shanafield, M., Mccallum, J.L., Cook, P. G. & Noorduijn, S. (2016). Variations on thermal transport modelling of subsurface temperatures using high-resolution data. *Advances in Water Resources*, *89*. https://doi.org/10.1016/j.advwatres.2015.12.018

Slater, L., & Lesmes, D. P. (2002). Electrical-hydraulic relationships observed for unconsolidated sediments. *Water Resources Research, 38(10),* 31-1. https://doi.org/10.1029/2001WR001075

Slater, L. D., Ntarlagiannis, D., Day-Lewis, F. D., Mwakanyamale, K., Versteeg, R. J., Ward, A., … & Lane, J. W. (2010). Use of electrical imaging and distributed temperature sensing methods to characterize surface water-groundwater exchange regulating uranium transport at the Hanford 300 Area, Washington. *Water Resources Research*, *46*(10). https://doi.org/10.1029/2010WR009110

Tyler, S. W., Selker, J. S., Hausner, M. B., Hatch, C. E., Torgersen, T., Thodal, C. E., & Schladow, S. G. (2009). Environmental temperature sensing using Raman spectra DTS fiber-optic methods. *Water Resources Research*, *45*(4). https://doi.org/10.1029/2008WR007052

Villeneuve, S., Cook, P. G., Shanafield, M., Wood, C., & White, N. (2015). Groundwater recharge via infiltration through an ephemeral riverbed, central Australia. *Journal of Arid Environments, 117*, 47-58. https://doi.org/10.1016/j.jaridenv.2015.02.009

Vogt, T., Schneider, P., Hahn-Woernle, L., & Cirpka, O. A. (2010). Estimation of seepage rates in a losing stream by means of fiber-optic high-resolution vertical temperature profiling. *Journal of Hydrology*, *380*(1-2), 154-164. https://doi.org/10.1016/j.jhydrol.2009.10.033

Lyon, J. G., Trimble, S. W. & Ward, A. D. (2004). Environmental hydrology. CRC Press.

Watson, J. A., Cardenas, M. B., Ferencz, S. B., Knappett, P. S., & Neilson, B. T. (2018). The effects of floods on the temperature of riparian groundwater. *Hydrological Processes*, *32*(9), 1267-1281. https://doi.org/10.1002/hyp.11504

Westhoff, M. C., Savenije, H. H. G., Luxemburg, W. J., Stelling, G. S., Van de Giesen, N. C., Selker, J. S., ... & Uhlenbrook, S. (2007). A distributed stream temperature model using high-resolution temperature observations. *Hydrology and Earth System Sciences Discussions*, *11*(4), 1469-1480. https://doi.org/10.5194/hess-11-1469-2007

Winter, T.C. (1998). Groundwater and surface water: A single resource. *USGS Circular 1139.*

Wu, L., Singh, T., Gomez-Velez, J., Nützmann, G., Wörman, A., Krause, S., & Lewandowski, J. (2018). Impact of Dynamically Changing Discharge on Hyporheic Exchange Processes under Gaining and Losing Groundwater Conditions. *Water Resources Research*. https://doi.org/10.1029/2018WR023185

Chapter 3:
Quantification of vertical hyporheic exchange flows

Jaime Gaona [1,2,3], Jörg Lewandowski [1,4]

[1] Leibniz Institute of Freshwater Ecology and Inland Fisheries, IGB-Berlin, Müggelseedam 310, 12587, Berlin, Germany.

[2] Freie Universität Berlin, Dahlem Research School, Hittorfstraße 16, 14195, Berlin, Germany.

[3]University of Trento, Department of Civil, Environmental and Mechanical Engineering, Via Messiano 77, 31123, Trento, Italy.

[4]Humboldt University Berlin, Faculty of Mathematics and Natural Sciences, Geography Department, Rudower Chaussee 16, 12489 Berlin, Germany.

The following version is ready for submission to peer-review journals.

3.1 Abstract

Understanding flow in the hyporheic zone is essential to understand the multiple chemical and biological processes in the streambed. The aim of the present study is to compare and evaluate different methods to quantify hyporheic exchange flows. Temperature-depth profiles and multi-level pressure heads have been collected at the River Schlaube, Germany. First, we apply steady-state methods to hydraulic heads and temperature-depth profiles. We calculate point-in-time vertical flux estimates. Second, transient state thermal methods such as the analytical method VFLUX and the numerical method 1DTempPro provide time series of flux estimates able to reproduce temporal flux fluctuations. All methods are capable of providing qualitative and quantitative estimates of vertical fluxes and their depth distribution. Disagreements of values and directions of fluxes between methods suggest different impacts of heterogeneities of thermal and hydraulic sediment properties. Non-ideal natural conditions significantly increase the levels of uncertainty. Different methods to estimate vertical hyporheic exchange flows provide valuable qualitative information on the structure of the streambeds. In conclusion, quantifying hyporheic exchange flows still faces multiple challenges due to the limited applicability of the current methods under strong upwelling in heterogeneous streambeds.

3.2 Introduction

The streambed is an important compartment of rivers where many relevant biogeochemical and ecological processes take place (Lewandowski et al., 2011a). The streambed, also called hyporheic zone (HZ) (Winter, 1995), is crucial for the environmental quality of river ecosystems. Stream water entering into streambed sediments, flowing through the HZ and returning to the overlying water eventually mixing with groundwater discharge is called hyporheic exchange flow (HEF).

Numerous laboratory and modelling studies have focused on the identification of the factors controlling HEF patterns across scales. Hydrogeology defines gaining or losing conditions of a stream and hydromorphology governs the subsurface flow paths on medium to large scales (Harvey & Bencala, 1993). Pool-riffle sequences determine HEF paths on small to medium scales (Gooseff et al., 2006), while ripples, as well as obstacles, determine

the local flux patterns (Thibodeaux & Boyle, 1987). However, sediment properties, in particular hydraulic conductivity, are crucial in controlling local flux (Stonestrom & Constantz, 2004).

Several authors have studied the spatial heterogeneity of HEF (Conant, 2004, Schmidt et al., 2006) due to the variations of the hydraulic conductivity of the riverbed (Calver 2001), variable groundwater gradients in bedform sequences (Storey et al., 2003) or the influence of heterogeneous streambed topography sequences (Gooseff et al., 2006). However, given the challenging characterization of the spatial patterns of HEF across scales (Fleckenstein et al., 2006), further investigation of the spatial heterogeneity is needed.

Temporal variability induces another dimension of complexity to HEF investigation**.** For instance, daily variations of the groundwater table caused by evapotranspiration of riparian vegetation alter exchange patterns (Harvey et al., 1991). Seasonally, variations of groundwater reduce or increase HEF paths between riffles and pools (Harvey & Bencala, 1993). Moreover, even the geomorphologic evolution of the streambed can alter the exchange patterns (Wroblicky et al., 1998).

In streambeds, temperature is a natural, non-conservative tracer for water fluxes that is relatively easy to measure and model. Numerous studies have used temperature at different scales to study HEF in diverse settings. The advances in temperature logging and the increased capabilities of computer software boost the use of heat to estimate vertical fluxes in the HZ and across the groundwater-surface water interface (SWI) (Constantz, 2008). There are generally two approaches for estimating vertical flux exchanges with heat transport, either analytical solutions (Stallman, 1965, Bredehoeft & Papadopulos, 1965) or numerical models (Lapham, 1989; Healy & Ronan, 1996,).

Analytical solutions are derived from steady-state heat transport models (Bredehoeft & Papadopulos, 1965) or transient state models (Stallman, 1965) taking advantage of the different temperature propagation in the riverbed caused by upwelling or downwelling. The analytical solution proposed by (Schmidt et al., 2006) or the more recent ones by (Kurylyk et al., 2017, Anibas et al., 2009) based on the steady-state model of Bredehoeft require only discrete temperature records while the solutions derived from Stallman's transient model work with temperature profile time series. Solutions derived from (Stallman, 1965) are based

on the analysis of the amplitude attenuation and/or phase shift of the temperature signal in the streambed. This approach experienced remarkable progress due to (1) new variants of the 1D heat conduction solution (Hatch et al., 2006), (2) improvements in the data processing of times series (Keery et al., 2007), (3) the reduction of uncertainty arising from more reliable measurements of thermal properties (McCallum et al., 2012; Luce et al., 2013), (4) adaptations of sensors to high resolution in depth (Schneider et al., 2010; Briggs et al., 2012, Vogt), and (5) software developments that automatize and gather the analytical methods (Gordon et al., 2012). Data processing is a time- and expertise-demanding task. In addition, the non-ideal fluctuations of temperatures due to weather events (Webb et al., 2008) require techniques to isolate the diurnal signal from other effects modifying the temperature. In the case of the analytical methods, these difficulties are addressed by the inclusion of cosine taper band filters (Hatch et al., 2006) or Dynamic Harmonic Regression (DHR) (Keery et al., 2007). Programs such as VFLUX (Gordon et al., 2012) provide tools to facilitate the processing of temperature data.

Numerical models were developed in parallel with the first computing tools for assessing fluid and solute or energy transport in porous media (Voss, 1984). Since the interest in temperature tracing increased, numerical solutions, more adaptable to non-ideal conditions, were developed to determine vertical water fluxes (Lapham, 1989). The energy transport equation used in the current models (Healy & Ronan, 1996) is a form of the advection-dispersion equation that accounts for the changes in energy stored within a volume of porous media. This energy change is caused by the advective transport of the inflow of water with different temperature into the volume, the thermal conduction and the thermo-mechanical dispersion of heat into or out of the volume. Recent developments focus on improving model calibration and capacity to cope with heterogeneity and temporal variability (Koch et al., 2015).

The scope of the present study is to quantify vertical fluxes in the hyporheic zone with different analytical and numerical methods based on time series of temperature-depth profiles. In particular, the study aims to evaluate several quantification methods under complex field conditions. This assessment aims to identify the strengths and weaknesses of the methods as well as their applicability depending on the quality and type of data available: temperature, hydraulic and /or sediment properties.

3.3 Study site, materials and methods

The River Schlaube is a second order stream (Lewandowski et al., 2011) in a glacial valley in Brandenburg, Germany. The upper reaches of the river in 60 - 80 m.a.s.l. have carved into a sandy plateau with altitudes ranging between 100 - 150 m.a.s.l. This particular location explains the existence of high groundwater gradients, eventually causing many springs along the river banks. The River Schlaube has a larger slope (s = 0.006 m/m) than most rivers in Brandenburg and has a rather natural morphology. Sediment characteristics range from organic soft fine material to gravel. Accordingly, streambed hydraulic conductivity ranges K_s from $2.43 \cdot 10^{-4}$ to $3.32 \cdot 10^{-6}$ m s^{-1}.

The field site is located at the upper River Schlaube, upstream of the previous study site of (Lewandowski et al., 2011) and about a kilometre downstream of Lake Wirchensee which strongly regulates downstream streamflow. The 50 m long reach comprises a mix of straight, bending and meandering sections. HEFs range from very strong upwelling to slight downwelling and the geomorphology from planar and ripple sequences to bar formations. Due to the location of the study site in a pristine forest, woody debris represents a primary source of obstacles and heterogeneity in the streambed. Four transects representing different morphological features were chosen in the selected reach of the river (Figure 3.1).

3.3.1 Flux estimation based on vertical hydraulic gradients (VHG)

Hydraulic head gradients between and within the transects were measured at 70 cm depth with eight piezometers (Table 3.1) equipped with pressure transducers (Schlumberger Mini-Diver™, Texas, USA). The eight piezometers recorded sub-surface and stream water levels with a sampling rate of 15 min at three (two) locations of transects TR1, TR3, (TR4).

In addition, eight multi-level piezometers were used to measure vertical hydraulic gradients (VHG) in the streambed. These multi-level piezometers consist of a bunch of narrow (8 mm wide) transparent (HDPE) plastic tubes with filtering screens of 5 cm length in different depths from just below the sediment-water interface down to approx. 50 cm depth. The multi-level piezometers used during the summer season were inserted 20 cm upstream of the locations of the main piezometers, 55 cm deep into the sediment with six filter screens at 1, 10, 20, 30, 40, 50 cm sediment depth. For the winter season, they were upgraded to eight

levels at the same depths as the temperature lances' sensors (1, 14, 18, 23, 31, 48, 65, 82 cm). VHGs of each multi-level piezometer were manually measured with scales at millimeter resolution several times during the summer and winter season (Table 3.1), taking advantage of the visibility of high groundwater levels in the tubes above surface water levels. The Darcy equation enables vertical flux estimates based on these VHGs and the hydraulic conductivity K_s of sediment samples.

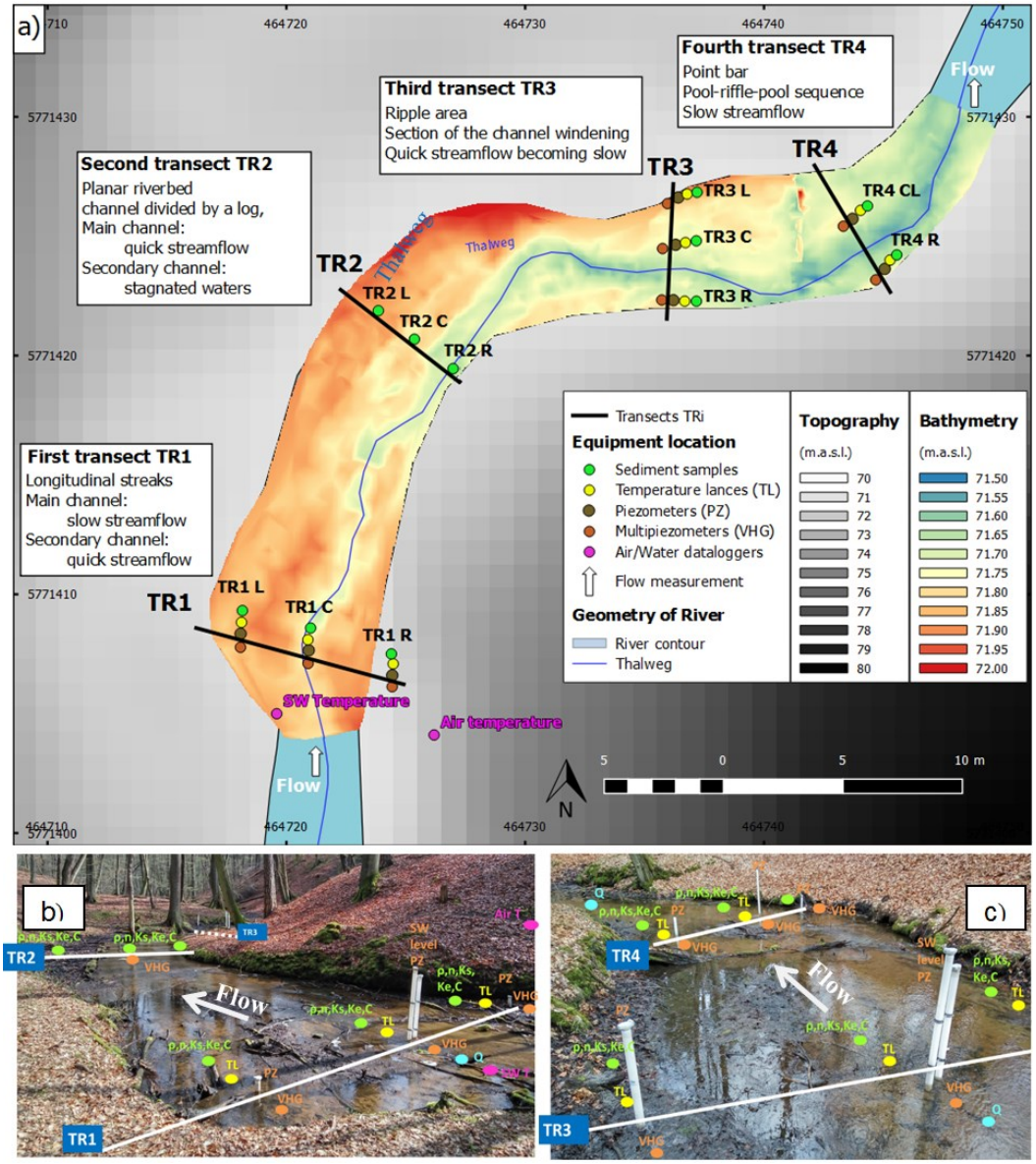

Figure 3.1: Study site and equipment installed. (a) Elevation map including the detailed bathymetry of the River Schlaube and the locations of i transects (TR) as black lines and deploying locations j in each transect (j: L=left, C=center, R=right). (b and c) Photos

showing locations of transects and measurement equipment in the study site. Initials identify locations of: temperature lances (TL), piezometers (PZ) and vented tubes for surface water level monitoring (surface water level), multi-level piezometers (VHG), sediment samples (represented by the abbreviations of some relevant sediment properties ρ, n, K_s, κ_e, C: where ρ is bulk density, n porosity, K_s hydraulic saturated conductivity, κ_e thermal diffusivity, C volumetric specific heat and λ thermal conductivity (not shown)), air and surface water temperatures (AirT, SWT) and flow measurements (Q).

Hydraulic conductivity (K_s) values were obtained from sediment cores of at least 50 cm length collected at transects TR3 and TR4 with the "KSAT" system by UMS/METER (Munich, Germany). Cores were divided into samples of 10 cm thickness. Samples of 5 cm thickness of the upper layer of sediment were collected on several locations per transect to identify the spatial variability of sediment properties (green points in Figure 3.1a and 1b). Thermal parameters needed for the analysis of temperature data, such as thermal conductivity λ, thermal diffusivity κ_e and volumetric specific heat C were obtained from the "KD2Pro" system (Decagon devices/METER, Washington, USA). Repeated measurements (>5 times) were conducted for average and standard deviation of K_s and thermal properties. In the case of K_s, the KSAT permeameter test was repeated for the same segment of the sediment core to obtain the average and standard deviation. Similarly, the KD2Pro needles were applied to different areas of the same sample to calculate average and standard deviations of the thermal properties. Finally, porosity and bulk density for the analytic and numeric thermal methods were obtained by weighting the samples under saturated and dry conditions (48 h, 105 °C).

Table 3.1: Technical specifications of instruments used in the experimental setup at River Schlaube.

Parameter	Device	Location	Details	Period collected
Temperature-depth profile	8 UIT Temperature-lances, LogTrans6 GPRS dataloggers	3 in transect 1, 3 in transect 3, 2 in transect 4	8 sensors in 1, 14, 18, 23, 31, 48, 65, 82 cm depth, Resolution: 0.004 °C, Accuracy (0 - 20 °C): 0.03 °C	7 Jul. – 15 Sep. 2016 Sampling rate: 15 min
Piezometric head (continuous measurement)	Schlumberger Mini-Diver 10 m	3 in transect 1, 3 in transect 3, 2 in transect 4	Resolution: 0.06 cm H_2O, Accuracy (0-20 °C): 0.5 cm H_2O Depth of filter screen 70cm	5 Mar. – 30 Aug. 2016 Sampling rate: 15 min

Vertical hydraulic gradients (VHG) from multi-level piezometers (point in time measurements)	Custom made, (summer type) 6 pipes 115 cm long, 1, 10, 20, 30, 40, 50 cm deep (winter type) 8 pipes 120 cm long, like temperature lances depths: 1, 14, 18, 23, 31, 48, 65, 82cm	3 in transect 1, 3 in transect 3, 2 in transect 4	Manual reading with scale of mm resolution	1 and 3 Aug. 2016, 15 Sep. 2016, 17 Jan. 2017, 20 Feb. 2017, 2 Mar. 2017
Sediment properties	UMS KSAT DECAGON K2PRO	2 sediment cores: 1 in transect 3, 1 in transect 4; 8 samples at $Tri_{,}j$	50 and 60cm depth KSAT applied each 20cm K2PRO applied each 10cm Samples at $Tri_{,}j$: 10cm depth	
Air and surface water temperature	2 HOBO Tidbits v2	Transect 1	Resolution: 0.02 °C at 25 °C Accuracy: ± 0.21 °C from 0 °C to 50 °C	5 Mar. – 30 Aug. 2016 Sampling rate: 15 min
Surface water flow	Hydromet OTT-OTT MF pro	Transect 1, Transect 3, Transect 4	Accuracy: ± 2 % flow value ± 0.015 m/s speed (0-3 m/s)	3 and 30 Aug. 2016, 15 Sep. 2016, 20 Feb. 2017, 2 Mar. 2017

3.3.2 Flux estimation based on temperature-depth profiles

We applied and compared four methods for flux estimation based on temperature-depth profiles collected with temperature lances. Eight temperature lances (TL) Logtrans 6 (multi-level temperature data logger) from UIT (Dresden, Germany) were deployed in left, centre and right locations of the three transects (Figure 3.1a) to collect time series of temperature-depth profiles. The 85 cm long devices have eight sensors in 1, 14, 18, 23, 31, 48, 65, 82 cm depth from the top. To avoid scouring in the sand-bed stream by moving bedforms the tops of the temperature lances were levelled with the SWI so that the uppermost sensor was buried 1 cm in the sediment.

The first two analytical methods (Schmidt et al., 2006, Kurylyk et al., 2017) follow the steady-state approach of calculating water flux using steady-state heat transport models (Bredehoeft & Papadopulos, 1965) while the semi-automatized analytical methods included in VFLUX (Gordon et al., 2012) enable also the estimation of temporal flux variations following the transient model derived from (Stallman, 1965). Finally, we apply also the transient-state numerical model VS2DH included in the software 1DTempPro (Koch et al., 2015).

Steady-state heat transport analytical methods

Steady-state methods use a snapshot of the temperature-depth profile to calculate fluxes. The steady-state heat and flow transport model of (Bredehoeft & Papadopulos 1965) assumes that (1) fluid flow is only vertical and (2) steady through spatially and temporally

isotropic, homogeneous properties of a semi-confined fully saturated sediment layer. These assumptions simplify the general 3D heat-transport Equation 3.1 to the one-dimensional steady heat and flux transport Equation 3.2:

Equation 3.1

$$\frac{\partial^2 T}{\partial x^2}+\frac{\partial^2 T}{\partial y^2}+\frac{\partial^2 T}{\partial z^2}-\frac{C_w \rho_w}{\lambda}\cdot\left[\frac{\partial(q_x T)}{\partial x}+\frac{\partial(q_y T)}{\partial y}+\frac{\partial(q_z T)}{\partial z}\right]=\frac{C}{\lambda}\frac{\partial T}{\partial t}$$

Equation 3.2:

$$\frac{\partial T}{\partial t}=\frac{\lambda}{C}\frac{\partial^2 T}{\partial z^2}-q\frac{C_w}{C}\frac{\partial T}{\partial z}$$

where T is the temperature (°C), z is depth (m) in the sediment, t is time (s), ρ is the density of water (kg m^{-3}), C is the volumetric heat capacity of the saturated sediment (J m^{-3} K^{-1}), C_w is the volumetric heat capacity of water, λ is the thermal conductivity of the sediment (W $m^{-1}K^{-1}$), q is the one-dimensional flux through the porous sediment (m s−1) or Darcy velocity. By applying the boundary temperatures at the sediment-water interface, Tz=0 = T_0, and at depth L (considering L the depth of sediment investigation), Tz=L = T_L, the expression becomes Equation 3.3:

Equation 3.3

$$\frac{T(z)-T_0}{T_L-T_0}=\frac{exp\left(\frac{q_z C_w}{\lambda}z\right)-1}{exp\left(\frac{q_z C_w}{\lambda}L\right)-1}$$

Schmidt et al. (2006) solve the equation using an objective function (Equation 3.4) that minimizes the error (Error(L)) between observed and simulated temperatures for n sensors *(j = 1…n)*. The homogeneous parameters of sediment and fluid properties leave the flux q_z as the variable to be optimized.

Equation 3.4:

$$Error(L)=\sum_{j=1}^{n}\left[T_j-\left(\frac{exp\left(\frac{q_z C_w}{\lambda}z\right)-1}{exp\left(\frac{q_z C_w}{\lambda}L\right)-1}(T_L-T_0)+T_0\right)\right]^2$$

Applying Equation 3.3 and Equation 3.4 results in a flux q along the entire sediment domain L. To enable the later comparison of the results with the results of the methods described below, fluxes were calculated for layers (i) of thickness $b_i = z_{i,b} - z_{i,0}$ in the domain L (Equation 3.5 3.5). The upper sensor at the top of the layer measuring temperature $T(z_{i,0}) = T_0$ and the bottom sensor recording $T(z_{i,b}) = T_b$ define the upper and lower temperature boundary conditions, while the third temperature value in between (at depth $z_{i,j}$) is the temperature $T(z_{i,j}) = T_{i,j}$ that should be fitted. Thus, the error function (Equation 3.4) to

minimize, needs to be rewritten for each separate depth segment analogous to Equation 3.5 3.5.

Equation 3.5:

$$\frac{T_{i,j}-T_0}{T_b-T_0}=\frac{\exp\left(\frac{q z_{i,j} C_w}{\lambda}\left(z_{i,j}-z_{i,0}\right)\right)-1}{\exp\left(\frac{q z_{i,j} C_w}{\lambda}\left(b_i\right)\right)-1}$$

Kurylyk et al. (2017) developed a new variant of Bredehoeft's solution (Equation 3.2) for multi-layer sediments or aquifer systems which is the base of the tool called FLUX-LM. The authors implemented the solution in a Microsoft Excel worksheet able to solve the multiple layer configurations. As in the previous method of Schmidt et al. (2006), the optimal flux minimizes the RMSE between the observed and simulated temperature values. The model assumes continuity of temperature and flux at the interface between layers. However, given the multi-layer configuration of the sediment, we apply the method in layers to obtain estimates of the potential flux at each layer. Additionally, the macro by Kurylyk et al. (2017) enables estimating Peclet numbers (Equation 3.6). The Peclet number P_e is the ratio of the rate of advection by flow to the rate of diffusion driven by the temperature gradient, and it indicates if advection or diffusion prevail in the system. The method requires a careful definition of the thickness b_i of each layer i, boundary conditions (T_0 and T_b as top and bottom temperature of the domain, respectively) and L representing the total domain depth.

Equation 3.6:

$$P_e=\frac{q_z C_w \rho_w (T_0-T_b)}{-\lambda_b\,(T_b-T_0)/L}=q_z C_w \rho_w \sum_{i=1}^{n}(b_i/\lambda_i)$$

The steady-state method of Schmidt et al. (2006) (Equation 3.5) and Kurylyk et al. (2017) were applied to the temperature-depth profiles records of 15 September 2016, 13:00 h. Flux estimations in each layer were calculated considering the segment between three time series of three consecutive sensor depths. The hydraulic gradient and K_s values of each layer were averaged proportionally to their depths.

Transient state thermal analytical approach: VFLUX

The MATLAB program toolbox VFLUX (Gordon et al., 2012) gathers four solutions (Hatch et al., 2006, Keery et al., 2007, McCallum et al., 2012; Luce et al., 2013) derived

from the 1D heat equation of (Stallman, 1965) (Equation 3.7) to estimate vertical seepage flux through saturated porous media.

Equation 3.7:

$$\frac{\partial T}{\partial t} = \kappa_e \frac{\partial^2 T}{\partial z^2} - q \frac{C_w}{C} \frac{\partial T}{\partial z}$$

In Equation 3.7, T is temperature (°C), t is time (s), κ_e is effective thermal diffusivity ($m^2\ s^{-1}$), q is fluid flux ($m\ s^{-1}$), C_w is volumetric heat capacity of water ($J\ m^{-3}\ °C^{-1}$), C is volumetric heat capacity of saturated sediment ($J\ m^{-3}\ °C^{-1}$) and z is depth (m). The values of κ_e and C determined from sediment samples collected in the field (Table 3.3 in the supporting information) are the input used for VFLUX. Required assumptions are: (1) fluid flow is only vertical, (2) steady-state flow conditions, (3) the temperature signal is sinusoidal and (4) spatially and temporally constant fluid and solid properties.

The first two solutions (Hatch et al., 2006; Keery et al., 2007) are based on the separated analysis of the amplitude ratio (A_r) and the phase shift ($\Delta\phi$) between two temperature signals dampened differently at different depths in the sediment. The other two solutions (McCallum et al., 2012; Luce et al., 2013) are based on the combined analysis of the amplitude ratio and phase shift of signals ($A_r\Delta\phi$). Hatch et al. (2006) proposed a method that isolates the diurnal signal using a cosine filter and then selects the daily temperature maximum and minimum to calculate amplitude attenuation and time lag with depth. Depths of measurement, streambed thermal parameters, and magnitude of the temperature oscillation have an impact on the reliability of Hatch's solution. The method of (Keery et al., 2007) roots from the same Stallman's equation, but applies Dynamic Harmonic Regression (DHR) (Young et al., 1999). This method enables the identification of temperature amplitudes for each sampled period of the original temperature time series, and not only for the peaks. Keery's method claims robustness against the impacts of weather conditions on the time series. (McCallum et al., 2012) developed a method able to estimate fluxes without the need to specify the effective thermal diffusivity based on the combined analysis of the dampening of the temperature amplitude and the phase shift ($A_r\Delta\phi$ *methods)*. However, the determination of the effective thermal diffusivity κ_e helps to identify periods of time when the assumptions named above (derived from Stallman's model) are violated. The fourth method proposes also a combined amplitude-phase non-dimensional solution (Luce et al., 2013). The benefit of this approach is that it performs better than previous solutions for low flow velocities. The

explicit analytical form allows an analysis of uncertainty propagation. Additionally, this last solution enables estimating scour and deposition of sediment over the profile.

VFLUX requires temperature time series from multiple depths of a vertical profile with sufficient length. The program provides tools for dealing with the uncertainty of the sediment parameters as well as for identifying unreliable time periods for flux estimation based on thermal diffusivity ranges. Time periods that include non-stationary flow conditions should be avoided due to their adverse impacts on the reliability of the estimates (Irvine et al., 2015a).

Transient state thermal numerical approach: 1DTempPro

1DTempPro is a graphical user interface (Voytek et al., 2013; Koch et al., 2015) for the numeric VS2DH code (U.S. Geological Survey) that numerically solves the flow and heat-transport equation to estimate vertical groundwater/surface-water exchange. The heat-transport equation numerical solution of VS2DH (Healy & Ronan, 1996) ran by 1DTempPro is an adjusted advection-dispersion equation (Equation 3.8). It is based on the changes of the energy stored in a volume of porous media due to the flow of water of different temperature, thermal conduction, and energy dispersion into and out of the volume. In the equation below (Equation 3.8), the left term is the change in energy stored in a volume over time. The four terms on the right correspond to the energy transport by thermal conduction, transport due to thermo-mechanical dispersion (Voss 1984), advective transport of energy and possible heat sources and sinks.

Equation 3.8: $$\frac{\partial}{\partial t}[\theta \cdot C_w + (1-\emptyset)C_s]\,T = \nabla\lambda(\theta)\nabla T + \nabla\theta C_w D_H \nabla T - \nabla\theta C_w vT + qC_w T^*$$

t is time (s), θ volumetric moisture content, C_w heat capacity of water (J m³ °C), Φ porosity, C_s heat capacity of the dry solid (J m³ °C^{-1}), λ thermal conductivity of saturated soil (W m^{-1} °C^{-1}), D_H hydro-dynamic dispersion (m² s^{-1}), v is water velocity (m s^{-1}), q is the rate of flow source (m s^{-1}) and T* is flow source temperature (°C).

1DTempPro considers discrete model domains between the uppermost and deepest temperature sensor with the sedimentary, hydraulic and thermal conditions mentioned in Equation 3.8. For each cell, homogeneous properties and no-flow lateral boundaries are considered. Nonetheless, the numerical solution allows the analysis of vertical temperature

profiles even if complex forcing mechanisms are present such as stage fluctuations or non-steady boundary conditions. Therefore, 1DTempPro shows some advantages over analytical models: the capability of incorporating head boundary conditions variable in time (e.g., water-stage fluctuations), time-varying temperature boundary conditions (e.g. solar radiation), stratified bed materials, and multidimensional flow. However, concerns about the reliability include a degrading fit to the measured data with depth caused by the multidimensional flow and the low representativeness of input data in heterogeneous media. Input parameters required for 1DTempPro include (apart from temperature series): hydraulic conductivity, porosity, thermal conductivity, bulk thermal capacity of the sediment (all of them obtained from sediment cores), plus hydraulic heads (from VHG of multi-level piezometers) in each of the sediment layers that can be defined in the sediment profile. 1DTempPro enables the calibration of flux, head data, hydraulic conductivity or other thermal properties. While the calibration process remains manual, the Levenberg-Marquardt nonlinear regression automatically iterates for the set of parameters that minimizes the sum of squared residuals between predicted and observed temperatures.

3.4. Results on sediment properties

Two cores were collected from the upper 50 cm of the streambed at the third and fourth transect (TR3C and TR4CL, Figure 3.1). According to their analysis, the streambed shows a vertical sequence of three distinct layers of different hydraulic conductivity. The upper 10 - 15 cm comprise hydraulically conductive sand deposits followed by 20 to 30 cm of finer greyish sands of low hydraulic conductivity overlying highly conductive materials ranging from coarse gravel to fine sands with woody debris at the bottom of the cores (Figure 3.2a_1 and a_2, Table 3.3 in the supporting information). The actual thickness of the bottom layer could not be determined due to the maximum sampling depth of 50 cm. Thermal properties do not show any remarkable layered sequence (Table 3.3).

3.4.1 Flux estimation by means of Darcy's Law

Applying Darcy´s law to the VHGs observed in multi-level piezometers results in moderate upwelling rates of 0.5 – 0.8 m d^{-1} for the upper layer of TR3C (0 – 20 cm depth) and up to 0.7 m d^{-1} for TR4CL (0 – 18 cm depth). In the intermediate layer (20 – 50 cm depth

in TR3C and 18 – 31 cm in TR4CL) fluxes are very low, i.e. 0 – 0.03 m d^{-1} in TR3C and 0.04 – 0.06 m d^{-1} in TR4CL. The third layer (48 – 82 cm in TR3C and 31 – 82 cm in TR4CL) reveals strong upwelling fluxes of 1.2 – 2.4 m d^{-1} in TR3C and 0.9 – 3.4 m d^{-1} in TR4CL (Figure 3.2a_2 and b_2). The differences in Darcy fluxes between TR3C and TR4CL reflect the differences in hydraulic conductivity in the streambed, known that the third and fourth transect show identical VHGs (up to 25 cm head difference between groundwater and surface water in the piezometric time series) with the same gradient towards the right bank. The eight multi-level piezometers provided VHG (Table 3.5a_1 and b_1 in the supporting information) consistent with the sequence of conductive-low conductive-very conductive materials (Figure 3.2a_1 and a_2).

3.4.2 Analytical flux estimation based on steady-state heat transport models

The temperature-depth profiles were analyzed by the approach by Schmidt et al. (2006) (Figure 3.2a_3 and b_3). The results are in agreement with the flux limitation in the intermediate layer observed when applying Darcy's law (Section 3.4.1, Figure 3.2a_2 and b_2): the upper layer exhibited medium to high fluxes (q_{TR3C} = 0.2 m d^{-1}, q_{TR4CL} = 0.13 – 0.35 m d^{-1}) followed by an intermediate layer of very low hydraulic conductivity of about q_{TR3C} = 0.003 m d^{-1} and between 24 and 65 cm in TR4CL with q_{TR4CL} = 0.035 m d^{-1}) and a deeper layer of again higher fluxes (q_{TR3C} = 0.05 m d^{-1} and q_{TR4CL} = 0.07 m d^{-1}). The values in the shallow 9 cm depth are shown in Table 3.2 and in Table 3.6 in the supporting information.

Alternatively, we applied the model FLUX-LM by Kurylyk et al. (2017). When applied to the overall domain, fluxes were smaller than expected (q_{TR3C} = -0.04 m d^{-1}, q_{TR4CL} = -0.08 m d^{-1}). Due to the flux continuity assumption, the layer with the lowest hydraulic conductivity restricts the overall vertical flux through the sediment domain. However, we also applied the method to the individual layers of different hydraulic conductivities in order to estimate the potential flux for each layer, which contributes to infer the streambed structure. The results (Figure 3.2a_4 and b_4) are in agreement both in magnitude and direction with the Darcy and Schmidt methods: larger fluxes in the upper and the bottom layers compared to low fluxes in the intermediate layers. This confirms the three-layered structure of the sediment (Figure 3.2a_1 and b_1).

3.4.3 Analytical flux estimation based on time series of temperature profiles

The deployment of temperature lances in the center (approximately in the Thalweg) (Figure 3.3a) and in the right and left part of the stream (Figure 3.3b) contribute to the understanding of the vertical thermal gradients across the streambed. The profiles located in the margins encounter higher pressure heads (Figure 3.3c) resulting in a stronger attenuation of the surface water temperature signal in the HZ (Figure 3.3a vs. b). Thus, the majority of the temperature-depth profiles located at the sides (TRiL and TRiR) become unsuitable for analytical methods based on phase lag ($\Delta\phi$) or combined amplitude ratio-phase lag ($A_r\Delta\phi$) (Briggs et al. 2014). The limited suitability of some locations for estimating fluxes is caused by the extinction depth, defined as the depth where the standard deviation of the temperature amplitude within the time series becomes lower than the accuracy of the sensor (0.1° C in the present case). According to this restriction, the application of analytical methods is only possible at sites where the extinction depth extends beyond the depth of the three shallow sensors (0.01, 0.14, 0.18 m) The period 1 – 15 September 2016 provided the deepest extinction depths in our records. In this period, the entire profiles TR1C and TR3C were above the 0.1°C threshold. However, without a sediment core from TR1C, the rest of the methods depending on sediment properties cannot be applied while the complete sediment records available for TR4CL suggest including that location despite having an extinction depth slightly under 0.18 m (Table 3.4 in the supporting information). Figure 3.2 includes results beyond the extinction depth to show the disparity of results between methods at all investigated depths. The results (Table 3.2) from the amplitude ratio (A_r) and combined methods ($A_r\Delta\phi$) incorporated in VFLUX (Hatch, Keery, McCallum and Luce solutions) report weak downwelling at location TR3C and weak upwelling at TR4CL for the uppermost depth (9 cm). They show significant agreement both in magnitude and directions. Conversely, phase shift methods (Hatch $\Delta\phi$, Keery $\Delta\phi$) disagree with the aforementioned results with much larger downwelling rates at TR3C and moderate downwelling at TR4CL. Figure 3.2a$_5$ illustrates time series of fluxes at TR3C based on the Hatch amplitude ratio (A_r) method. In TR3C, the upper two levels 9 and 18 cm deep (all levels defined as the middle point in between three sensors of the temperature lances) show low to moderate downwelling (0.07 – 0.13 m d^{-1}). Low upwelling appears at 24 cm depth (0.09 m d^{-1}).

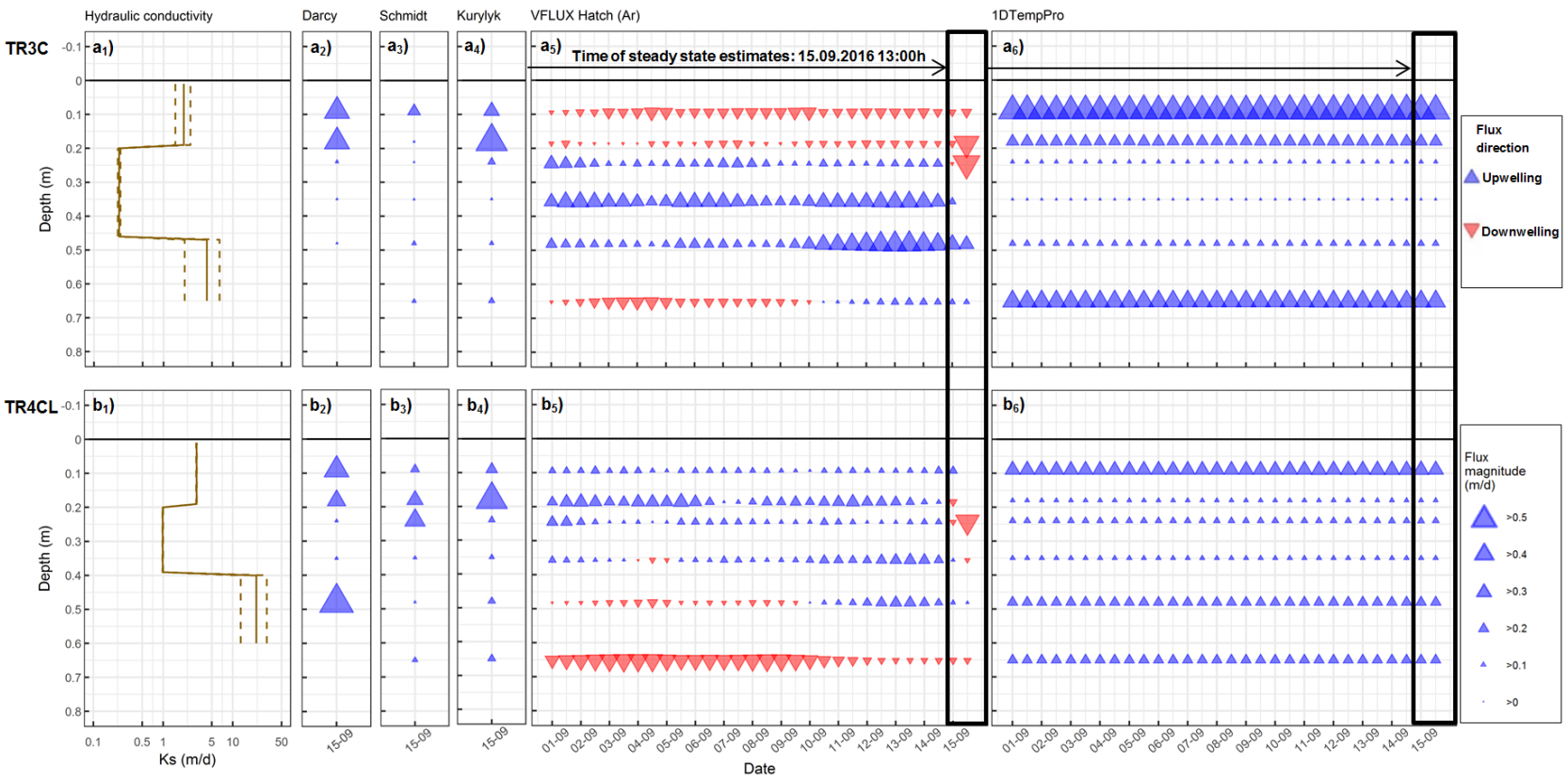

Figure 3.2: (a1, b1) Hydraulic conductivity (K_s) for the depth profiles TR3C and TR4CL with solid line representing the average and dashed lines the standard deviation. Vertical fluxes (m/d) along the temperature profiles at locations TR3C and TR4CL calculated with (a2, b2) the method of Darcy, (a3, b3) the steady-state thermal analytical method of Schmidt et al. (2006), (a4, b4) the steady-state thermal analytical method FLUX-LM (Kurylyk et al., 2017), (a5, b5) VFLUX Hatch (Ar) and (a6, b6) 1DTempPro. Temperature sensors are located in 0.09, 0.18, 0.24, 0.35, 0.48, 0.65 m depth. The black horizontal line at depth 0 m represents the river-sediment interface. Upward directed triangles (in blue) represent upwelling, downward triangles (in red) represent downwelling. The size of the triangles represents the magnitude of the flux in (m/d).

Fluxes at 35 and 47 cm depth indicate moderate upwelling (0.17 – 0.19 m d^{-1}), while downwelling (0.10 m d^{-1}) occurs in the deepest level (65 cm). TR4CL flux time series show prevailingly upwelling conditions (Figure 3.2b$_5$) throughout the entire depth profile. The levels 9 to 35 cm depth show low to moderate upwelling (0.06 – 0.13 m d^{-1}), while downwelling appearing at 47 cm depth (0.10 m d^{-1}) becomes stronger with depth (0.28 m d^{-1} at 65 cm depth).

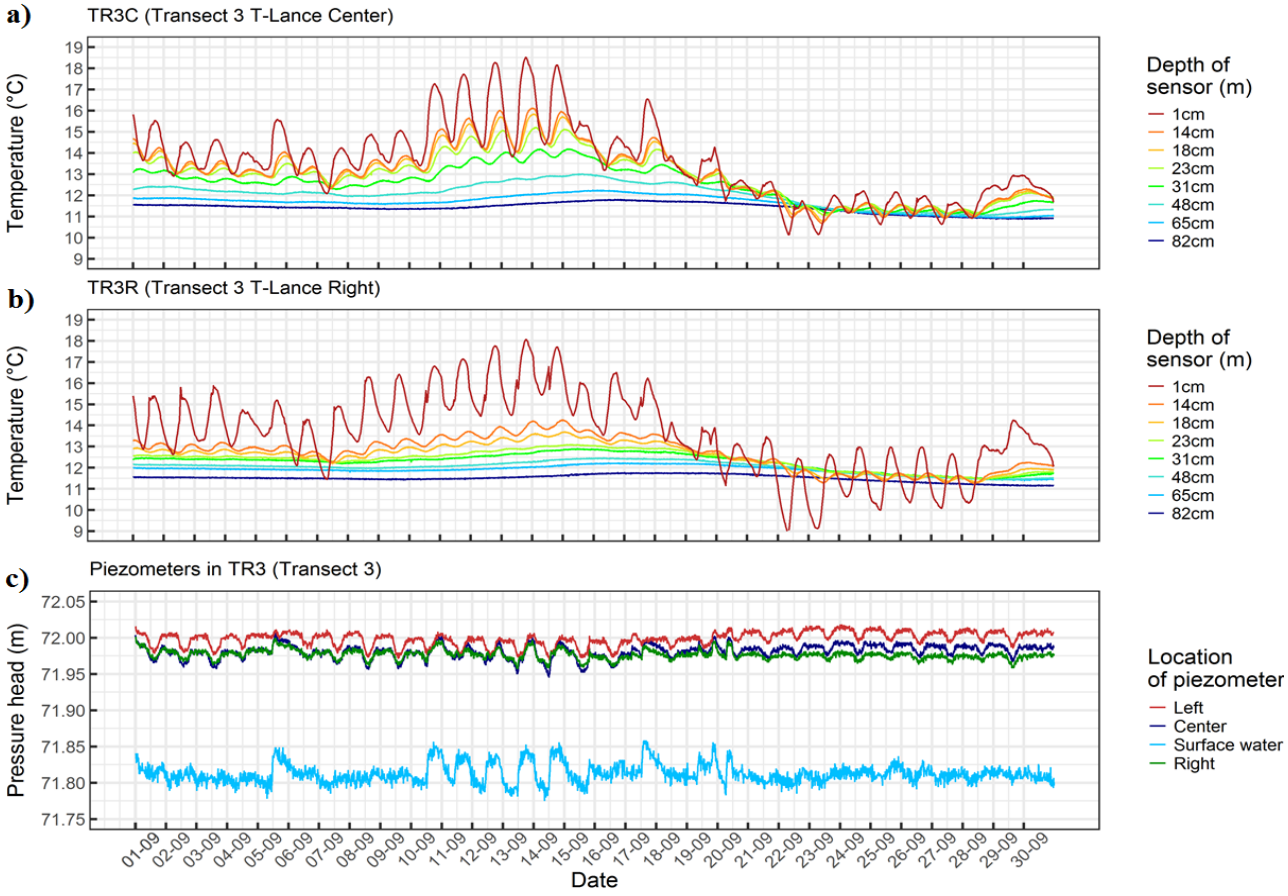

Figure 3.3: (a,b) Temperature signal transmission at two locations of the third transect TR3. The dampening of the temperature amplitude with depth is most intense at the right side of the transect (b), where a very shallow extinction depth limits the usability of the data for flux estimations with analytical methods. High-pressure heads towards the banks cause a shallower 'extinction depth' of the temperature signal in these areas. (c) Water levels of transect TR3: Groundwater levels for Left, Center, Right piezometers of transect TR3, and surface water levels for the period 1-30 September 2016. Sudden increases in the surface water levels at the 5, 10-14 and 17 of September do not correspond with rainfall events but

with weir operations at the upstream located Lake Wirchensee. The step rises of the water stage in the stream propagate to groundwater heads beneath the stream but not of the same magnitude to the groundwater heads in the margins.

Overall, the flux time series portrays substantial temporal variability. On the last day of the time series shown in Figure 3.2a_5 and b_5, enhanced upwelling occurs at TR3C and TR4CL. At this very end of the period (15 Sept 2016), an abrupt change of the flux direction occurs in several depths. A weather change inducing changes in surface temperatures may be the cause of this shift (Figure 3.3and b). In any case, the values beyond 0.09 m are mostly of qualitative nature due to the extinct tion depth but highlight the high impact of weather conditions on heat transmission.

3.4.3 Numerical flux estimation based on time series of temperature profiles

The results from the numerical method 1DTempPro differ substantially from the results of the analytical approach by VFLUX (Hatch amplitude ratio (A_r) at least for profile TR3C. Moderate upwelling (0.45 m d^{-1}) is estimated from 1DTempPro (Table 3.2) at 0.09 m depth of the profile TR3C. Between 24 and 47 cm, the values decrease sharply (0.01 – 0.07 m d^{-1}) and increase again in the deeper level of 65 cm (0.27 m d^{-1}). Upwelling fluxes at TR3C are larger than Darcy fluxes and fluxes calculated based on thermal steady-state methods (Schmidt and Kurylyk) and differ completely from the slight downwelling calculated by VFLUX Hatch amplitude ratio (A_r) method (Figure 3.2a_6 vs. a_5).

For location TR4CL, the first level in 0 – 10 cm depth shows moderate upwelling (0.21 m d^{-1}), followed by low upwelling between 18 and 35 cm (0.04 – 0.08 m d^{-1}), and finally low to moderate upwelling (0.13 – 0.18 m d^{-1}) below 35 cm (Figure 3.2b_6). This vertical flux sequence is similar to the ones observed from Darcy and analytical steady-state methods. The depth of the low-conductivity level (Figure 3.2a_6 and b_6) agrees with the depth of that level (located between 0.23 and 0.48 m) observed based on Darcy (Figure 3.2a_2 and b_2). The lowest level shows the same enhanced upwelling as Darcy-based fluxes (Figure 3.2a_2 and b_2 vs. Figure 3.2a_6 and b_6). However, 1DTempPro tends to neglect the temporal variability of fluxes when temporal fluctuations of the VHG are not available. In the present study multi-level piezometers could not be continuously monitored but were only manually read at certain dates.

Table 3.2: Vertical fluxes (m d^{-1}) (mean ± standard deviation) at 15 September 2016 at 9 cm depth with all methods of the study. This is the only depth where quantitative results of vertical flux can be provided according to the extinction depth.

		TR3C	TR4CL
Hydraulic method	Darcy	-0.43	-0.56
Steady-state analytical thermal methods	Schmidt et al. (2006)	-0.2	-0.13
	FLUX-LM	-0.25	-0.18
Transient state analytical thermal methods(VFLUX)	Hatch Ar	0.14 ± 0.04	-0.07 ± 0.02
	Hatch Δφ	0.57 ± 0.11	0.37 ± 0.13
	Keery Ar	0.14 ± 0.04	-0.07 ± 0.02
	Keery Δφ	0.58 ± 0.11	0.38 ± 0.12
	McCallum ArΔφ	0.04 ± 0.05	-0.12 ± 0.04
	Luce ArΔφ	0.04 ± 0.05	-0.12 ± 0.04
Numerical thermal method	1DTempPro	-0.45 ± 0.01	-0.21 ± 0.01

3.5. Discussion

3.5.1 Hydraulic method (Darcy)

The results of Darcy's method (Figure 3.2a_2 and b_2, Table 3.2) reflect a vertical distribution of fluxes following the hydraulic conductivity sequence observed in the sediment cores (Figure 3.2a_1 and b_1). The impact of the hydraulic gradients on the magnitude of the fluxes seems to be smaller than the effect of hydraulic conductivities differing with depth. High head differences between groundwater and surface water (groundwater heads up to 27 cm above surface water level were recorded with the piezometer at TR4R) in the whole area of the study site support this statement. Hence, the low upwelling fluxes obtained for the intermediate sediment layer are directly related to its low hydraulic conductivity measured from sediment samples. Conversely, the potential high upwelling fluxes obtained for the third layer will only occur where hydrological windows of permeable material in the intermediate layer exist. Similarly, the shallowest layer of the HZ shows strong upwelling despite the

underlying low conductivity layer limiting the supply of water from below. Groundwater discharge from the bottom of the uppermost layer through a window in the intermediate layer or local upwelling triggered by bedforms might allow such an intense upwards directed flow. Hence, the Darcy approach based on the assumption of only vertical fluxes is not adequate for complex hyporheic zones as in the River Schlaube. Especially in the shallowest layer fluxes have a large horizontal component. The distribution of the Darcy fluxes in the three sediment layers is a result of the different hydraulic conductivities with an unidentified effect of bedforms.

Darcy's method can be particularly useful at locations with moderate to strong upwelling. Such sites are unsuitable for thermal methods due to their shallow extinction depths. Unfortunately, the method is sensitive to small errors in pressure heads and sediment heterogeneities. To minimize the effects of the first issue, the use of piezometric data loggers with millimeter resolution is recommended. To reduce the problems caused by sediment heterogeneity, hydraulic conductivities should be identified with centimeter resolution along the vertical profile of interest. Another disadvantage of the method is that it only reproduces the vertical components of the fluxes. This is a problem in shallow layers of the HZ, where streamflow infiltration defines shallow paths of horizontal hyporheic flow, as reported for the River Schlaube in the past (Angermann et al., 2012a).

3.5.2 Analytical steady-state heat transport methods

The agreement between the results of Schmidt and Kurylyk (Figure 3.2a_3 - b_3 and a_4 - b_4) with the flux distribution of Darcy in the three layers of different hydraulic conductivities (Figure 3.2a_1 and b_1) verifies at least the qualitative capabilities of the thermal methods. Despite the quantitative disagreement, they concur in flux directions and magnitudes. Due to the simplicity of the assumptions needed to apply the methods, many other factors such as the heterogeneity of thermal parameters, multi-dimensionality of flow and non-ideal temperature distribution can have serious impacts on the results. The application of the methods to the entire thermal profile without a reliable consideration of the vertical stratification of the sediment properties led to a poor description of the flux patterns.

The major problems are: (1) Both methods require homogeneous thermal conductivity as input. Thus, problems arise from the necessity to find a representative

average of values from 0.6 to 3 W m^{-1} K^{-1}. (2) The one-dimensional assumption of purely vertical flow is not matched in a natural system such as the River Schlaube. Especially shallow levels are affected by hyporheic exchange fluxes forcing surface water into the streambed due to bed roughness and multidimensionality of flow. Peclet numbers given by FLUX-LM are helpful to identify the shallow and deep levels where advection can eventually prevail over conduction, which can indicate unreliable flux estimates. (3) Temperature fluctuations of the overlying water due to the irregular radiation cycle received under the forest canopy and the effect of weather trends violate the steady-state criterion for temperatures profiles. The period around the daily temperature peak can provide the most stable conditions for modelling while periods of weather trends are the least suitable.

3.5.3 Analytical transient state heat methods: VFLUX

VFLUX methods show only partial agreement with hydraulic, analytical steady-state and numerical methods (Figure 3.2a_5 and b_5, Table 3.2). Results differ both in magnitude and direction of flow, particularly the erratic results of the phase shift ($\Delta\phi$) methods due to the impact of the shallow extinction depth. Amplitude ratio (A_r) and combined methods ($A_r\Delta\phi$) agree largely in magnitude and direction. Nonetheless, flux estimates from $A_r\Delta\phi$ methods reflect lower values compared to A_r methods, also with higher susceptibility of opposite flux directions. For most sensors beyond the first 0.09 m depth, $\Delta\phi$ and $A_r\Delta\phi$ methods show more instability (i. e. missing values in the time series of flux). In view of this, we conclude that A_r methods outperform $\Delta\phi$ and $A_r\Delta\phi$ methods. Within the A_r methods, we have chosen Hatch (2006) for (Figure 3.2a_5 and b_5) because the dynamic harmonic regression (DHR) filter included in Keery (2007) causes several random values for lower depths as a consequence of a lacking diurnal daily temperature amplitude (Shanafield et al., 2011). Additionally, the three layers that have been identified by the Darcy approach and by analytical steady-state methods can be barely recognized from Hatch (A_r) results of VFLUX.

High groundwater heads (at TR3C, 15 – 20 cm higher than stream water levels, (Figure 3.3c)) almost disable $\Delta\phi$ methods and complicate the use of $A_r\Delta\phi$ methods due to the dampening and phase shift effects resulting in very low extinction depths (Figure 3.3a and b). Previous studies (Irvine & Lautz, 2015) under similar conditions show that estimates for $\Delta\phi$ methods appeared highly unreliable compared to A_r methods. Observations by (Briggs et al.,

2014) also indicated an underperformance of $A_r\Delta\phi$ methods under strong upwelling. Strong upwelling reduces both the depth of reliable flux estimates and the time window suitable for measurements. The optimal summer period of lowered groundwater levels, less intense upwelling and a deeper extinction depth is limited. Furthermore, fluxes obtained in such time periods of low groundwater heads hardly represent values of the rest of the year. The lack of resolution due to sensor spacing (Shanafield et al., 2011) is another important negative factor, which can be solved by using high-resolution vertical temperature profiles (Vogt et al. 2010).

Sediments cores showed high vertical heterogeneity of thermal and hydrological properties. For instance, sharp changes of thermal diffusivity values are observed in the transition between the intermediate low-conductive and the deep high conductive levels of TR3C and TR4CL (Table 3.3, supporting information). According to Shanafield et al., (2011), low values of thermal diffusivity (around 0.4 $m^2\ d^{-1}$) can increase the uncertainty of the flux estimates, which may explain the lack of agreement of the flux estimates of VFLUX in the deeper levels of TR3C and TR4CL with the other methods. It is known that VFLUX results can lack reliability due to the spatial heterogeneity of thermal parameters (Irvine et al., 2015). This reason, together with the fact that A_r methods can outperform $A_r\Delta\phi$ methods with regards to the uncertainty of thermal properties (Irvine & Lautz, 2015), implies to adopt the A_r–approach by Hatch et al. (2006) as the preferable transient state analytical solution.

Despite the quasi-constant environmental conditions existing in the studied period, some temporal instability was observed. Even diurnal stage fluctuations (Figure 3.3c) attributed to root uptake can cause an alteration of flux magnitude at a sub-daily scale (Larsen et al., 2014). In order to identify which episodes of temporal variability of environmental conditions have a negative impact on the estimates, VFLUX $A_r\Delta\phi$ solutions of McCallum et al. (2012) and Luce et al. (2013) facilitate the identification of the stability of the period by contrasting the estimates of thermal effective diffusivity κ_e with a range of plausible values (Gordon et al., 2012). The Peclet number also becomes a useful indicator of periods of advective prevalence in the hyporheic flow caused by river stage fluctuations (Bhaskar et al., 2012). The high temporal variability of the results of the A_r method in the upper level of the sediment can also be caused by the horizontal component of flow (Angermann et al., 2012a) when Peclet suggest prevailing advection conditions. High unreliability of the upper level of flux estimates was also reported in previous works

(Cuthbert & Mackay 2013) related to horizontal components of HEF. In conclusion, in the present case study with non-ideal conditions, the A_r method after Hatch et al. (2006) seems to be superior to $A_r \Delta\phi$ methods and shows results consistent with Darcy, steady-state analytical and numerical methods (Figure 3.2).

3.5.4. Thermal numerical method: 1DTempPro

In the present study, 1DTempPro has shown its capability to generate series of vertical fluxes that are in agreement with steady-state temperature and hydraulic methods (Figure 3.2a_6 and b_6, Table 3.2). The direction, magnitude and the general sequence of vertical fluxes (high, low and moderate to high flux from the surface to bottom) are similar. The use of known sediment properties shortens the calibration process considerably. However, the performance is low in larger sediment depth where upwelling strongly attenuates temperature signals. Despite the new temporal capabilities of the model (Koch et al., 2016) it was not possible to measure time series of VHG which is why the temporal variability of fluxes cannot be depicted here. For that reason, we suggest adopting continuous monitoring of VHG to obtain the best output from the model.

The parameters that have the largest influence on the result calculated by 1DTempPro are the hydraulic and the thermal conductivity. Despite the fact that both values can be determined quite accurately in the lab, the spatial heterogeneity of the sediment may complicate the introduction of representative values as input for the model. In fact, the sediment cores were not extracted from exactly the locations of the temperature profiles but 30 cm downstream. Furthermore, parameter calibration requires an iterative process in 1DTempPro which might be very time-consuming while the obtained result is one of many possible solutions. The automatization of this iterative loop with an optimization algorithm would be desirable, along with a ranking of performances of the obtained solutions. The third parameter of large influence is the pressure head. The 0.5 cm accuracy of our manually-observed multi-level piezometers caused significant trouble during the fitting process, because of the sensitivity of the model to centimeter step fluctuations. This sensitivity of 1DTempPro to changes in pressure head was previously reported (Briggs et al., 2014). It is recommended to pursue millimeter scale data collection. Continuous monitoring of pressure heads is recommended to enable the temporal capacity of the model.

3.5.5 Stratified sediment structure

In spite of the high hydraulic gradients that initially suggested very strong upwelling, the results of the different methods applied in this study show mostly moderate fluxes. This is in accordance with the reported decrease of hyporheic exchange due to the heterogeneity of streambed properties (Tonina et al., 2016). However, given the significant vertical heterogeneity of hydraulic conductivity at the study site, we propose a conceptual model (Figure 3.4) of the riverbed to explain the vertically stratified distribution of fluxes (Figure 3.2a$_1$ and b$_1$ and Table 3.5 in the supporting information).

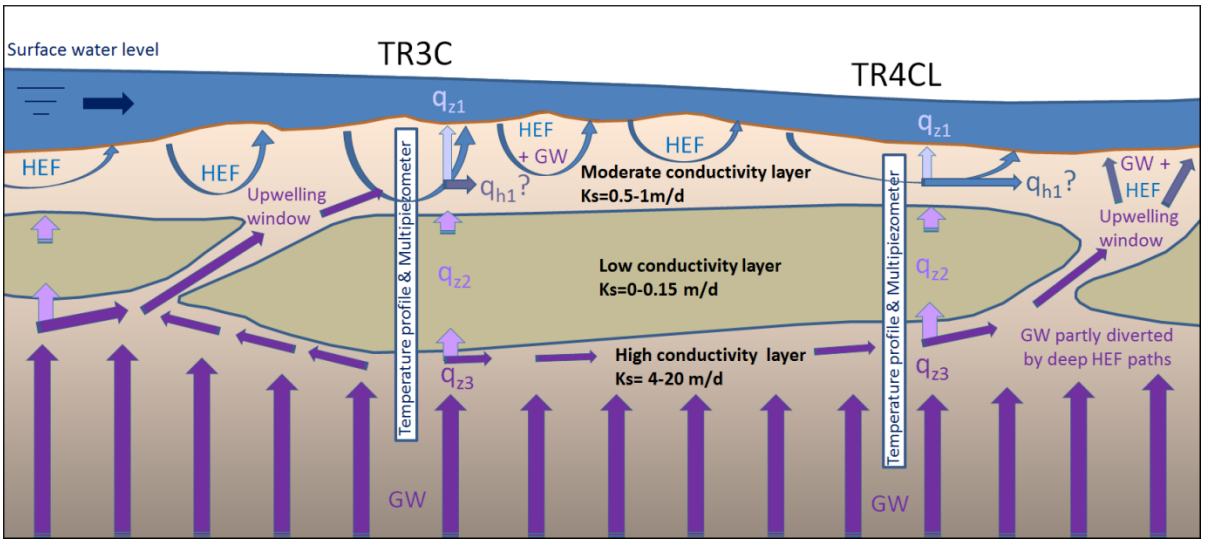

Figure 3.4: Conceptual model of the stratified structure of the sediment of the River Schlaube based on measured sediment properties and vertical flux estimates of the temperature profiles TR3C and TR4CL ($q_{z,i}$ where i defines the sediment layer identified by Ks measurements) along a pool-riffle-pool sequence. The length of the vertical arrows represents the relative magnitude of the estimated vertical fluxes q along the temperature profiles. Blue arrows in the upper layer represent surface water infiltration paths defining down/upwelling areas in the HZ. Vertical violet arrows represent groundwater paths. Intermediate colour between blue and violet represent possible mixing of water origins.

The intermediate low conductivity layer seems to control groundwater-stream water exchange. The origin of the low conductivity can be related to organic deposits in view of the dark colors observed in the sediment cores. The layer isolates the third layer of strong potential upwelling (Angermann et al., 2012b) from the upper hyporheic flow induced by

bedforms. Indeed, the blocking effect of the intermediate layer can enlarge HEF paths (Fox et al., 2014). The magnitude, the different directions and temporal variability of fluxes in the upper layer suggest that HEF is triggered by bedforms and hydraulic dynamics. This is consistent with the location of the profiles in a riffle-pool sequence that extends from upstream of TR3 to downstream of TR4. However, enhanced exchange via a high K_s window in the intermediate low conductivity layer can also contribute to the enhanced upwelling fluxes in the upper layer. Thus, the moderate values of upwelling calculated by Darcy, steady-state analytical and numerical methods in the profiles are consistent with the impact of windows of high K_s in low conductivity layers (Gomez-Velez et al., 2014).

3.6 Conclusions and outlook

The present study aimed to estimate HEF fluxes under complex natural field conditions. Non-ideal conditions, and particularly the heterogeneity of sediment properties, challenge the vertical flux estimation by hydraulic and thermal methods. Our results show the critical role of upwelling in the applicability of thermal analytical methods, in particular of the phase shift transient analytical methods included in VFLUX. Solutions based only on the amplitude ratio outperform those including phase shift analysis under strong upwelling. The dampening of the temperature signal due to strong upwelling restricts the depth down to which the method can be applied as well as the time window for flux estimation.

The non-ideal characteristics of temperature signals recorded in field studies increase the uncertainty of the flux estimates. Temperature changes due to daily fluctuations or environmental trends underline the relevance of transient methods while simultaneously demonstrating their current limitations. Steady-state methods perform reasonably well under relatively stable temperature conditions. In general, flux estimations remain challenging with every method if streambed characteristics are heterogeneous in both, vertical and horizontal directions. Hydraulic and other simple steady-state thermal analytical methods such as Schmidt et al. (2006) and Kurylyk et al. (2017) adapt reasonably well to stratified assessments of fluxes. The thermal numerical method 1DTempPro shows the most flexible and reliable performance.

Darcy and 1DTempPro are more adversely affected by streamflow dynamics than the other methods of the present study. This is due to their dependency on the time series of

hydraulic data as input. An inherent advantage of FLUX-LM and VFLUX is that they identify the temporal variability of flow. FLUX-LM and $A_r\Delta\phi$ methods of VFLUX providing the Peclet number as an indicator of the prevalence of advection over conduction are convenient to identify the periods of flux estimation with the stronger impact of flux multidimensionality.

With all that limitations in mind, we conclude that the application of 1D thermal methods to time series of temperature profiles under strong upwelling conditions allows reliable quantification of HEF fluxes in shallow depths of the sediment. This fact suggests the need to include a combination of techniques to overcome some of the current methods' limitations, deal with the heterogeneity of sediment and temporal variability of hydraulics, and investigate each factor's contribution to HEF.

Further investigation may imply the additional use of heat pulse sensors (HPS) (Lewandowski et al., 2011, Angermann et al., 2012a) able to characterize the horizontal component of fluxes, and fiber-optic distributed temperature sensing (FO-DTS) able to identify the spatial patterns of exchange fluxes. Geophysics can improve the knowledge of sediment properties heterogeneity (hydraulic and thermal properties). However, apart from coupling point and distributed techniques, modelling of specific factors and their interactions can also play a major role in improving our knowledge of HEF processes.

3.7 Acknowledgements

This research is funded by the SMART Joint Doctoral Programme (Science for MAnagement of Rivers and their Tidal systems) within the Erasmus Mundus Programme of the European Union. This project was funded with support from the European Commission, SGA 2015-1628. This publication reflects the views only of the author, and the Commission cannot be held responsible for any use which may be made of the information contained therein. We would like to thank Anne Mehrtens, Wiebke Seher and Christine Sturm for their help in fieldwork, as well as the Nature Park Schlaubetal for allowing access to River Schlaube.

3.8 References

Angermann, L., Krause, S., & Lewandowski, J. (2012a). Application of heat pulse injections for investigating shallow hyporheic flow in a lowland river. *Water Resources Research, 48*(12). https://doi.org/10.1029/2012WR012564

Angermann, L., Lewandowski, J., Fleckenstein, J. H., & Nützmann, G. (2012b). A 3D analysis algorithm to improve interpretation of heat pulse sensor results for the determination of small-scale flow directions and velocities in the hyporheic zone. *Journal of Hydrology, 475,* 1-11. https://doi.org/10.1016/j.jhydrol.2012.06.050

Anibas, C., Fleckenstein, J. H., Volze, N., Buis, K., Verhoeven, R., Meire, P., & Batelaan, O. (2009). Transient or steady-state? Using vertical temperature profiles to quantify groundwater-surface water exchange. *Hydrological Processes, 23*(15), 2165-2177. https://doi.org/10.1002/hyp.7289

Bhaskar, A. S., Harvey, J. W., & Henry, E. J. (2012). Resolving hyporheic and groundwater components of streambed water flux using heat as a tracer. *Water Resources Research, 48*(8). https://doi.org/10.1029/2011WR011784

Bredehoeft, J. D., & Papadopulos, I. S. (1965). Rates of vertical groundwater movement estimated from the Earth's thermal profile. *Water Resources Research, 1*(2), 325-328. https://doi.org/10.1029/WR001i002p00325

Briggs, M. A., Lautz, L. K., McKenzie, J. M., Gordon, R. P., & Hare, D. K. (2012). Using high-resolution distributed temperature sensing to quantify spatial and temporal variability in vertical hyporheic flux. *Water Resources Research, 48*(2). https://doi.org/10.1029/2011WR011227

Briggs, M. A., Lautz, L. K., Buckley, S. F., & Lane, J. W. (2014). Practical limitations on the use of diurnal temperature signals to quantify groundwater upwelling. *Journal of Hydrology, 519,* 1739-1751. https://doi.org/10.1016/j.jhydrol.2014.09.030

Calver, A. (2001). Riverbed permeabilities: Information from pooled data. *Ground Water, 39*(4), 546-553. https://doi.org/10.1111/j.1745-6584.2001.tb02343.x

Conant, B. (2004). Delineating and quantifying groundwater discharge zones using streambed temperatures. *Groundwater, 42*(2), 243-257. https://doi.org/10.1111/j.1745-6584.2004.tb02671.x

Constantz, J. (2008). Heat as a tracer to determine streambed water exchanges. *Water Resources Research, 44*(4). https://doi.org/10.1029/2008WR006996

Cuthbert, M., & Mackay, R. (2013). Impacts of non-uniform flow on estimates of vertical streambed flux. *Water Resources Research, 49*(1), 19-28. https://doi.org/10.1029/2011WR011587

Fleckenstein, J. H., Niswonger, R. G., & Fogg, G. E. (2006). River-aquifer interactions, geologic heterogeneity, and low-flow management. *Groundwater, 44*(6), 837-852. https://doi.org/10.1111/j.1745-6584.2006.00190.x

Fox, A., Boano, F., & Arnon, S. (2014). Impact of losing and gaining streamflow conditions on hyporheic exchange fluxes induced by dune-shaped bedforms. *Water Resources Research, 50*(3), 1895-1907. https://doi.org/10.1002/2013WR014668

Gomez-Velez, J. D., Krause, S., & Wilson, J. L. (2014). Effect of low-permeability layers on spatial patterns of hyporheic exchange and groundwater upwelling. *Water Resources Research, 50*(6), 5196-5215. https://doi.org/10.1002/2013WR015054

Gooseff, M. N., Anderson, J. K., Wondzell, S. M., LaNier, J., & Haggerty, R. (2006). A modelling study of hyporheic exchange pattern and the sequence, size, and spacing of stream bedforms in mountain stream networks, Oregon, USA. *Hydrological Processes, 20*(11), 2443-2457. https://doi.org/10.1002/hyp.6349

Gordon, R. P., Lautz, L. K., Briggs, M. A., & McKenzie, J. M. (2012). Automated calculation of vertical pore-water flux from field temperature time series using the VFLUX method and computer program. *Journal of Hydrology, 420,* 142-158. https://doi.org/10.1016/j.jhydrol.2011.11.053

Harvey, J., Bencala, K., and Zellweger, G. (1991). Preliminary investigation of the effect of hillslope hydrology on the mechanics of solute exchange between streams and subsurface gravel zones. *US Geological Survey Water Resources Investment Report, 91*(4034), 413-418.

Harvey, J. W., & Bencala, K. E. (1993). The effect of streambed topography on surface-subsurface water exchange in mountain catchments. *Water Resources Research*, *29*(1), 89-98. https://doi.org/10.1029/92WR01960

Hatch, C. E., Fisher, A. T., Revenaugh, J. S., Constantz, J., & Ruehl, C. (2006). Quantifying surface water-groundwater interactions using time series analysis of streambed thermal records: Method development. *Water Resources Research, 42*(10). https://doi.org/10.1029/2005WR004787

Healy, R. W., & Ronan, A. D. (1996). Documentation of computer program VS2DH for simulation of energy transport in variably saturated porous media: Modification of the US Geological Survey's computer program VS2DT (pp. 96-4230). *US Geological Survey.* https://pubs.usgs.gov/wri/1990/4025/report.pdf

Irvine, D. J., & Lautz, L. K. (2015a). High-resolution mapping of hyporheic fluxes using streambed temperatures: Recommendations and limitations. *Journal of Hydrology, 524,* 137-146. https://doi.org/10.1016/j.jhydrol.2015.02.030

Irvine, D. J., Lautz, L. K., Briggs, M. A., Gordon, R. P., and McKenzie, J. M. (2015b). Experimental evaluation of the applicability of phase, amplitude, and combined methods to determine water flux and thermal diffusivity from temperature time series using VFLUX 2. *Journal of Hydrology, 531,* 728-737. https://doi.org/10.1016/j.jhydrol.2015.10.054

Irvine, D. J., Cranswick, R. H., Simmons, C. T., Shanafield, M. A., & Lautz, L. K. (2015c). The effect of streambed heterogeneity on groundwater-surface water exchange fluxes inferred from temperature time series. *Water Resources Research, 51*(1), 198-212. https://doi.org/10.1002/2014WR015769

Keery, J., Binley, A., Crook, N., & Smith, J. W. (2007). Temporal and spatial variability of groundwater-surface water fluxes: development and application of an analytical method using temperature time series. *Journal of Hydrology, 336*(1), 1-16. https://doi.org/10.1016/j.jhydrol.2006.12.003

Koch, F. W., Voytek, E. B., Day-Lewis, F. D., Healy, R., Briggs, M. A., Lane, J. W., & Werkema, D. (2015). 1DTempPro V2: New Features for Inferring Groundwater/Surface-Water Exchange. *Groundwater, 54*(3), 434-439. https://doi.org/10.1111/gwat.12369

Kurylyk, B. L., Irvine, D. J., Carey, S. K., Briggs, M. A., Werkema, D., & Bonham, M. (2017). Heat as a groundwater tracer in shallow and deep heterogeneous media: Analytical solution, spreadsheet tool, and field applications. *Hydrological Processes, 31*(14), 2648-2661. https://doi.org/10.1002/hyp.11216

Lapham, W. (1989). Use of temperature profiles beneath streams to determine rates of vertical ground-water flow and vertical hydraulic conductivity (No. 2337). *Dept. of the Interior, US Geological Survey; USGPO; Books and Open-File Reports Section, US Geological Survey.* https://pubs.er.usgs.gov/publication/wsp2337

Larsen, L. G., Harvey, J. W., & Maglio, M. M. (2014). Dynamic hyporheic exchange at intermediate timescales: testing the relative importance of evapotranspiration and flood pulses. *Water Resources Research, 50*(1), 318-335. https://doi.org/10.1002/2013WR014195

Lewandowski, J., Putschew, A., Schwesig, D., Neumann, C., & Radke, M. (2011). Fate of organic micropollutants in the hyporheic zone of a eutrophic lowland stream: results of a preliminary field study. *Science of the Total Environment*, 409(10), 1824-1835. https://doi.org/10.1016/j.scitotenv.2011.01.028

Lewandowski, J., Angermann, L., Nützmann, G., & Fleckenstein, J. H. (2011). A heat pulse technique for the determination of small-scale flow directions and flow velocities in the streambed of sand-bed streams. *Hydrological Processes, 25*(20), *3244-3255.* https://doi.org/10.1002/hyp.8062

Luce, C. H., Tonina, D., Gariglio, F., & Applebee, R. (2013). Solutions for the diurnally forced advection-diffusion equation to estimate bulk fluid velocity and diffusivity in streambeds from temperature time series. *Water Resources Research, 49*(1), 488-506. https://doi.org/10.1029/2012WR012380

McCallum, A. M., Andersen, M. S., Rau, G. C., & Acworth, R. I. (2012). A 1-D analytical method for estimating surface water-groundwater interactions and effective

thermal diffusivity using temperature time series. *Water Resources Research, 48*(11). https://doi.org/10.1029/2012WR012007

Shanafield, M., Hatch, C., & Pohll, G. (2011). Uncertainty in thermal time series analysis estimates of streambed water flux. *Water Resources Research, 47*(3). https://doi.org/10.1029/2010WR009574

Schmidt, C., Bayer-Raich, M., & Schirmer, M. (2006). Characterization of spatial heterogeneity of groundwater-stream water interactions using multiple depth streambed temperature measurements at the reach scale. *Hydrology and Earth System Sciences Discussions, 3*(4), 1419-1446. https://doi.org/10.5194/hess-10-849-2006

Stallman, R. W. (1965). Steady one-dimensional fluid flow in a semi-infinite porous medium with sinusoidal surface temperature. *Journal of Geophysical Research, 70*(12), 2821-2827. https://doi.org/10.1029/JZ070i012p02821

Stonestrom, D. A., & Constantz, J.(2004). Using temperature to study stream-ground water exchanges. *Rep. 2327-6932 (No. 2004-3010).* https://pubs.usgs.gov/fs/2004/3010/

Storey, R. G., Howard, K. W., & Williams, D. D. (2003). Factors controlling riffle-scale hyporheic exchange flows and their seasonal changes in a gaining stream: A three-dimensional groundwater flow model. *Water Resources Research, 39*(2). https://doi.org/10.1029/2002WR001367

Thibodeaux, L. J., & Boyle, J. D. (1987). Bedform-generated convective transport in bottom sediment. *Nature, 325*(6102), 341-343. https://doi.org/10.1038/325341a0

Tonina, D., de Barros, F. P., Marzadri, A., & Bellin, A. (2016). Does streambed heterogeneity matter for hyporheic residence time distribution in sand-bedded streams?. *Advances in Water Resources, 96,* 120-126. https://doi.org/10.1016/j.advwatres.2016.07.009

Vogt, T., Schneider, P., Hahn-Woernle, L., & Cirpka, O. A. (2010). Estimation of seepage rates in a losing stream by means of fiber-optic high-resolution vertical temperature profiling. *Journal of Hydrology, 380*(1), 154-164. https://doi.org/10.1016/j.jhydrol.2009.10.033

Voss, C. I. (1984). A finite-element simulation model for saturated-unsaturated, fluid-density-dependent ground-water flow with energy transport or chemically-reactive single-species solute transport. *Water resources investigations report, 84*(4369), 409.

Voytek, E.B., Drenkelfuss, A., Day-Lewis, F.D., Healy, R., Lane, J.W. Jr., & Werkema, D. (2013). 1DTempPro: Analyzing temperature profiles for groundwater/surface‐water exchange. *Groundwater 52*, 2: 298‐302. https://doi.org/10.1111/gwat.12051.

Webb, B. W., Hannah, D. M., Moore, R. D., Brown, L. E. & Nobilis, F. (2008). Recent advances in stream and river temperature research. *Hydrological Processes, 22*(7), 902-918. https://doi.org/10.1002/hyp.6994

White, D. S. (1993). Perspectives on Defining and Delineating Hyporheic Zones. *Journal of the North American Benthological Society*, *12*(1), 61–69. https://doi.org/10.2307/1467686

Winter, T. C. (1995). Recent advances in understanding the interaction of groundwater and surface water. *Reviews of Geophysics*, *33*(S2), 985-994. https://doi.org/10.1029/95RG00115

Wroblicky, G. J., Campana, M. E., Valett, H. M., & Dahm, C. N. (1998). Seasonal variation in surface-subsurface water exchange and lateral hyporheic area of two stream-aquifer systems. *Water Resources Research, 34*(3), 317-328. https://doi.org/10.1029/97WR03285

Young, P. C., Pedregal, D. J., & Tych, W. (1999). Dynamic harmonic regression. *Journal of Forecasting, 18*(6), 369-394. https://doi.org/10.1002/(SICI)1099-131X(199911)18:6<369::AID-FOR748>3.0.CO;2-K

3.9 Supporting information

Table 3.3: Tables of hydraulic and thermal properties in the transects third (a1-b1) and fourth (a_2-b_2).The values of hydraulic conductivity indicate three distinct levels: an upper level corresponding to a sandy level of new sedimentation, an intermediate level of lower hydraulic conductivity that corresponds to the cores of fine sand with high organic content, and a bottom level with more hydraulic conductivity in respect to the other two, caused by levels of gravel and coarse sand with big pieces of organic debris embedded.

a_1) Saturated hydraulic conductivity in sediment core of TR3C

Core depth (cm)	Hydraulic conductivity $K_{25°C}$ (m s^{-1})	Hydraulic conductivity $K_{25°C}$ (m d^{-1})	Hydraulic conductivity $K_{10°C}$ (m s^{-1})	Hydraulic conductivity $K_{10°C}$ (m d^{-1})
TR3 5-10 TR3 10-20	$2.27 \times 10^{-5} \pm 5.54 \times 10^{-6}$	1.96 ± 0.48	$1.67 \times 10^{-5} \pm 3.86 \times 10^{-6}$	1.44 ± 0.27
TR3 20-35 TR3 35-47	$2.72 \times 10^{-6} \pm 1.50 \times 10^{-7}$	0.23 ± 0.01	$1.93 \times 10^{-6} \pm 1.03 \times 10^{-7}$	0.17 ± 0.01
TR2 47-58 TR3 58-65	$4.86 \times 10^{-5} \pm 2.54 \times 10^{-5}$	4.20 ± 2.19	$7.78 \times 10^{-5} \pm 5.66 \times 10^{-5}$	6.72 ± 4.89

a_2) Saturated hydraulic conductivity from sediment core of TR4CL

Core depth (cm)	Hydraulic conductivity $K_{25°C}$ (m s^{-1})	Hydraulic conductivity $K_{25°C}$ (m d^{-1})	Hydraulic conductivity $K_{10°C}$ (m s^{-1})	Hydraulic conductivity $K_{10°C}$ (m d^{-1})
TR4 0-10 TR4 10-20	$3.50 \times 10^{-5} \pm 3.61 \times 10^{-7}$	3.02 ± 0.03	$2.49 \times 10^{-5} \pm 2.51 \times 10^{-7}$	2.15 ± 0.02
TR4 20-30 TR4 30-40	$1.15 \times 10^{-5} \pm 1.00 \times 10^{-7}$	0.99 ± 0.01	$8.52 \times 10^{-6} \pm 4.04 \times 10^{-8}$	0.74 ± 0.01
TR4 40-50 TR4 50-60	$2.52 \times 10^{-4} \pm 1.02 \times 10^{-4}$	21.80 ± 8.84	$1.81 \times 10^{-4} \pm 7.54 \times 10^{-5}$	15.61 ± 6.51

b_1) Thermal properties from the sediment core of TR3C

Core depth (cm)	Thermal conductivity λ (W m K^{-1})	Volumetric Specific Heat C (MJ m^{-3} K^{-1})	Thermal diffusivity κ (mm^2 s^{-1})	Thermal resistivity ρ (°C cm W^{-1})
TR3 5-10	2.54 ± 0.02	2.92 ± 0.04	1.06 ± 0.02	34.73 ± 0.45
TR3 10-20	1.49 ± 0.006	3.48 ± 0.05	0.66 ± 0.10	46.04 ± 3.88
TR3 20-35	2.63 ± 0.02	2.78 ± 0.05	0.55 ± 0.12	52.48 ± 5.54
TR3 35-47	2.20 ± 0.03	2.99 ± 0.04	0.42 ± 0.18	82.27 ± 23.67
TR3 47-58	1.46 ± 0.02	2.96 ± 0.05	0.79 ± 0.04	41.226 ± 1.44
TR3 58-65	0.73 ± 0.02	3.95 ± 0.02	0.40 ± 0.04	73.72 ± 4.75

b_2)

Thermal properties from the sediment core of TR4CL				
Core depth (cm)	Thermal conductivity λ (W m K^{-1})	Volumetric Specific Heat C (MJ m^{-3} K^{-1})	Thermal diffusivity κ (mm^2 s^{-1})	Thermal resistivity ρ (°C cm W^{-1})
TR4 0-10	2.77 ± 0.04	2.70 ± 0.04	1.07 ± 0.003	34.58 ± 0.40
TR4 10-20	2.09 ± 0.01	3.21 ± 0.02	0.66 ± 0.004	47.98 ± 0.11
TR4 20-30	2.11 ± 0.09	1.41 ± 0.06	0.55 ± 0004	47.55 ± 1.97
TR4 30-40	2.46 ± 0.01	2.55 ± 0.03	0.97 ± 0.01	38.01 ± 0.29
TR4 40-50	0.67 ± 0.08	4.13 ± 0.47	0.16 ± 0.02	151.07 ± 19.34
TR4 50-60	2.41 ± 0.23	2.59 ± 0.17	0.94 ± 0.13	41.80 ± 4.15

Table 3.4: Choice of suitable temperature profile locations for flux estimation with both analytical and numerical methods along the period 1 September to 15 September 2016. The driest conditions of this period caused the depletion of the extinction depths, so that it becomes possible to study the locations TR1C, TR3C, TR4CL (locations of neutral, downwelling and upwelling transects) until the third, fourth and second sensor depth respectively.

01-15Sep2016	Standard deviation (°C) of temperature amplitude per transect location							
Depth (cm)	TR1L	TR1C	TR1R	TR3L	TR3C	TR3R	TR4CL	TR4R
1	**0.159**	0.551	**0.214**	**0.130**	0.502	**0.196**	0.338	0.369
14	0.047	0.189	0.039	0.054	0.204	0.028	**0.117**	**0.111**
18	0.035	**0.126**	0.036	0.037	0.174	0.016	0.082	0.085
23	0.026	0.061	0.017	0.026	**0.115**	0.004	0.054	0.058
31	0.014	0.025	0.005	0.014	0.054	0.002	0.027	0.036
48	0.004	0.007	0.001	0.004	0.007	0.000	0.004	0.012
65	0.001	0.001	0.000	0.000	0.000	0.000	0.000	0.000
82	0.000	0.000	0.000	0.000	0.000	0.000	0.000	0.000

Table 3.5: Vertical hydraulic gradients (VHG) of transects TR3 and TR4 between the two sediment depths reported in the first column. Average vertical fluxes calculated from the VHGs and hydraulic conductivities (Table $3a_1$-a_2) for summer (a) and winter (b). Note the different distribution of multi-level piezometer ports in summer and winter due to the improvement of the devices. Negative values stand for upwelling. Darker colour visualizes more intensity of the flow. Note that the 50 cm depth summer's version of multi-level piezometers barely reached the third level, while the longer (80cm depth) version of them

reflects the high conductivity of the third level (the deep level beyond 48 cm depth).

a$_1$) **a)**

Average VHG (m/m) in transect Tri-i

Depth(cm)	TR3-L	TR3-C	TR3-R	TR4-L	TR4-CL	TR4-R
0-10	-0.150	-0.233	-0.317	-0.058	-0.108	-0.383
10-20	-0.150	-0.333	-0.367	-0.025	-0.033	-0.233
20-30	-0.100	-0.217	-0.137	-0.050	-0.058	-0.133
30-40	-0.235	-0.067	-0.223	-0.083	-0.083	-0.233
40-50	-0.190	-0.025	-0.123	-0.100	-0.083	-0.167

a$_2$) **b)**

Average VHG (m/m) in transect Tri-i

Depth(cm)	TR3-L	TR3-C	TR3-R	TR4-L	TR4-CL	TR4-R
1-14	-0.027	-0.027	-0.054	-0.027	-0.054	-0.089
14-18	-0.094	-0.469	-0.094	-0.156	-0.125	-0.250
18-23	-0.400	-0.150	-0.050	-0.200	-0.100	-0.450
23-31	-0.313	-0.281	-0.031	-0.156	-0.094	-0.500
31-48	-0.147	-0.162	-0.066	-0.022	-0.221	-0.044
48-65	-0.132	-0.176	-0.088	-0.022	-0.118	-0.191
65-82	-0.044	-0.353	-0.013	-0.074	-0.059	-0.103

b$_1$)

Average q (m/d) in transect Tri-i

Depth(cm)	TR3-L	TR3-C	TR3-R	TR4-L	TR4-CL	TR4-R
0-10	-0.227	-0.502	-0.828	-0.150	-1.516	-0.101
10-20	-0.227	-0.811	-1.066	-0.059	-0.269	-0.281
20-30	-0.136	-0.224	-0.098	-0.037	-0.043	-0.098
30-40	-0.054	-0.027	-0.044	-0.061	-0.061	-0.172
40-50	-0.040	-0.007	-0.028	-1.561	-1.301	-2.602

b$_2$)

Average q (m/d) in transect Tri-i

Depth(cm)	TR3-L	TR3-C	TR3-R	TR4-L	TR4-CL	TR4-R
1-14	-0.037	-0.049	-0.060	-0.069	-0.750	-0.023
14-18	-0.135	-0.676	-0.135	-0.369	-1.009	-0.301
18-23	-0.067	-0.025	-0.008	-0.147	-0.074	-0.331
23-31	-0.052	-0.047	-0.005	-0.115	-0.069	-0.368
31-48	-0.025	-0.027	-0.011	-0.344	-3.443	-0.689
48-65	-0.890	-1.186	-0.593	-0.344	-1.836	-2.984
65-82	-0.297	-2.372	-0.089	-1.148	-0.918	-1.607

Table 3.6: Vertical fluxes of transects TR3C and TR4CL obtained from the analytical steady-state heat transport methods of (Schmidt et al. 2006) and FLUX-LM (Kurylyk et al. 2017) for the profile levels 0.09, 0.14,0.18, 0.24, 0.35,0.48 and 0.65.

Vertical flux estimates with the steady-state thermal method (Schmidt et al. 2006)

TR3C	Vertical flux		Daily flow
(cm)	q_z (m s^{-1})	q_z (m d^{-1})	Q_z (L d^{-1})
9	-2.32E-06	-0.201	200.6
18	-3.61E-08	-0.003	3.1
24	-3.19E-09	-0.000	0.3
35	-5.89E-08	-0.005	5.1
48	-6.52E-07	-0.056	56.4
65	-5.41E-07	-0.047	46.8

TR4CL	Vertical flux		Daily flow
(cm)	q_z (m s^{-1})	q_z (m d^{-1})	Q_z (L d^{-1})
9	-1.54E-06	-0.133	133.4
18	-3.10E-06	-0.268	268.3
24	-4.01E-06	-0.346	346.1
35	-4.00E-07	-0.035	34.6
48	-1.50E-07	-0.013	13.0
65	-7.96E-07	-0.069	68.8

Vertical flux estimates with FLUX-LM steady-state thermal method (Kurylyk et al. 2017)

TR3C	Vertical flux		Daily flow
(cm)	q_z (m s^{-1})	q_z (m d^{-1})	Q_z (L d^{-1})
9	-2.93E-06	-0.253	253
18	-6.33E-06	-0.547	547
24	-1.22E-06	-0.105	105
35	-1.16E-07	-0.010	10
48	-5.32E-07	-0.046	46
65	-9.26E-07	-0.080	80

TR4CL	Vertical flux		Daily flow
(cm)	q_z (m s^{-1})	q_z (m d^{-1})	Q_z (L d^{-1})
9	-2.11E-06	-0.182	182
18	-6.28E-06	-0.543	543
24	-1.04E-06	-0.090	90
35	-7.41E-07	-0.064	64
48	-1.17E-06	-0.101	101
65	-1.28E-06	-0.111	111

Chapter 4: Upscaling of hyporheic estimations

Flow and heat transport modelling in the hyporheic zone based on high-resolution temperature and geophysics datasets.

Jaime Gaona [1,2,3], Alberto Bellin [3]

[1] Leibniz Institute of Freshwater Ecology and Inland Fisheries, IGB-Berlin, Müggelseedam 310, 12587, Berlin, Germany.

[2] Freie Universität Berlin, Dahlem Research School, Hittorfstraße 16, 14195, Berlin, Germany.

[3]University of Trento, Department of Civil, Environmental and Mechanical Engineering, Via Messiano 77, 31123, Trento, Italy.

The following version is ready for submission to peer-review journals.

4.1 Abstract

Modelling flow and heat exchanges between the stream and the underlying hyporheic zone is essential for the study of the physical, chemical and biological hyporheic processes. The quantification of the spatial patterns of these flows within the hyporheic zone remains a challenge for the traditional flow and transport models particularly if based on point measurements. Distributed sensing techniques may contribute significantly to overcome this difficulty, thereby providing valuable information to make modelling more effective.

In particular, the spatial temperature patterns at the sediment-water interface observed with fiber-optic distributed temperature sensing are valuable datasets for the validation of heat transport models. In addition, electromagnetic induction (EMI) geophysics allow to map the distribution of electrical conductivity and through petrophysical relationship infer hydraulic property variations, whose impact on flow and heat transport patterns can be significant in heterogeneous sand bed streams such as the study site at River Schlaube (Germany).

The present study proposes a fully distributed three-dimensional modelling approach to estimate hyporheic flows based on a validated multiphysics flow and heat transfer model applied to the densely monitored reach of the Schlaube River. We apply MODFLOW - MT3D-USGS through the graphical interface FREEWAT and the python suite FloPy, whose flexibility facilitates the complex geometric definition of the heterogeneity of hydraulic properties recognized by the geophysics and the calibration of the model based on vertical hydraulic gradients and validated based on temperature at the sediment-water interface provided by fiber-optic distributed temperature sensing.

The objective of the present work is to upscale and investigate hyporheic processes by a combination of distributed three-dimensional multiphysics modelling and distributed sensing as provided by accurate fiber-optic distributed temperature sensing and electromagnetic induction geophysics surveys. The high resolution of the model discretization and data input enables a detailed identification of the sediment-water interface exchange patterns while allows the evaluation of the influence of the input's spatial resolution in the validity of the model, in particular of the key factor of subsurface heterogeneity.

4.2 Introduction

The indirect characterization of the hydrological conditions of a stream using point or/and distributed measurements of temperature is relatively easy, economic and non-invasive. We described in previous chapters the potential of distributed measurements for distinguishing the spatial patterns of hyporheic exchange flows (HEF) and the capabilities for calculating vertical flux estimates from temperature profiles. Conversely, at heterogeneous sites, we need alternatives to the one-dimensional (1D) methods for calculating HEF (Irvine et al., 2015). We require methods able to determine the three-dimensional (3D) nature of exchange (Lautz & Siegel, 2006; Ferguson & Bense, 2011) with sufficient reliability at the sediment-water interface (Brookfield & Sudicky, 2012; Shanafield et al., 2016).

The study of groundwater-surface water interactions by using fully-distributed 3D groundwater flow modelling allows evaluating the spatial distribution neglected by 1D models. By calibrating over sufficiently complete datasets of hydraulic heads and gradients, it is possible to reliably quantify HEF and residence times (Harvey & Bencala, 1993; Wondzell a& Swanson, 1996). Moreover, 3D modelling allows displaying the spatial variability of the interactions across the range of scales of the model (Gooseff et al., 2006; Cardenas & Wilson, 2007) which is of great advantage for upscaling (Lautz et al, 2006). The process-based perspective of groundwater flow models compared to the tracer models (Packman & Bencala, 2000) allows studying the impact of the factors governing exchanges (Storey et al., 2003; Kasahara & Wondzell, 2003; Cardenas et al., 2004).

However, 3D modelling has been traditionally impacted by the lack of detailed data on variables such as hydraulic heads and subsurface properties, particularly when defining realistic boundary conditions (Shanafield et al., 2016). Despite the still limited possibility to obtain sufficiently detailed hydraulic heads, the availability of high resolution distributed data of the subsurface properties can significantly improve the accuracy of the model. Geophysical techniques are increasingly used in hydrogeological studies (Rosenberry et al., 2017) due to their capabilities to identify and quantify the variability of subsurface properties in a non-invasive, quick and distributed way. Known that large errors are possible when neglecting the geologic heterogeneity of the subsurface (Schornberg et al., 2010) and the significant impact of shallow sediment heterogeneity in HEF estimations (Cardenas et al.

2004; Salehin et al. 2004; Schmidt et al. 2006), including geophysical data can increase the accuracy of the models. Furthermore, using EMI geophysics data to improve the detail on the subsurface parametrization can help to constrain the non-uniqueness of the model's solutions (Zheng & Wang, 1999). In the case of FO-DTS, including high-resolution temperature datasets solves the traditional scarcity of data for verification of the models (Wroblicky et al., 1998; Kasahara & Wondzell, 2003; Storey et al., 2003). There are a few studies using temperature as datasets for 3D flow and transport models in streambeds. Brookfield et al. (2009) applied this approach with success on identifying the exchange patterns previously determined by Conant (2004) but with limited capability to quantify the flux rates, attributed to the impact of heterogeneity. At a much smaller scale, Shope et al. (2012) applied flow and heat transport modelling for the investigation of the influence of bars on exchanges. In conclusion, integrating distributed measurements from fiber-optic distributed temperature sensing (FO-DTS) and geophysics into 3D models opens opportunities to increase the accuracy of hyporheic modelling, particularly for upscaling.

Our approach is coupling a 3D groundwater flow MODFLOW model with a heat transport MT3D-USGS model to simulate HEF in heterogeneous streambeds. The use of MODFLOW is common on hydrogeologic studies (Barlow & Harbaugh, 2006; Furman, 2008) but there are only a few applications on hyporheic studies (Lautz & Siegel, 2006, Wondzell et al., 2009). Known the thermal capabilities of MT3D-USGS for modelling dispersive and advective heat transport, we test (1) its capabilities to reproduce the spatial distribution of temperature patterns attributed to GW-SW interactions and quantify the exchanges. Afterwards, we aim to (2) compare the flow results with those of 1D heat transport models described in the previous chapter in order to discuss the factors causing discrepancies. Furthermore, we take advantage of the high-resolution geophysical data to test (3) the influence of heterogeneity in the accuracy of the flow and heat transport estimate. For this purpose, the results from a uniform model defined based on hydraulic conductivity values from bibliography and a model defined based on hydraulic conductivities extracted from soil samples are compared with the ones of a model defined based on geophysical data. In this way, we evaluate the impact of heterogeneity on the performance of 3D flow and heat transport models of the hyporheic zone.

4.3 Methods

4.3.1 The case study: River Schlaube study site

This small stream of prevailing GW contribution (further details are described in sections "Study site", Figure 1, Chapter 2 and Figure 3.3) provides a set of characteristics interesting for modelling GW-SW interactions. Thanks to the topography of the valley (funnel type) groundwater tables are high, which prevents the river from a disconnection between GW and SW (Figure 4.1). Figure 4.1 illustrates the steep slopes of the margins of River Schlaube limiting the extent of the hyporheic zone to the width of the channel. The absence of bedrock allows studying the influence of deep sedimentary heterogeneity in the transmission of groundwater to the stream. Finally, the stream is very shallow which facilitates the immediate propagation of flow and heat changes to the hyporheic zone. Thus, River Schlaube provides favourable particularities to model the HZ (Wondzell et al., 2010): highly constrained boundary conditions and constant head boundary of streamflow close to the part of the model domain where we wish to estimate flux. Furthermore, River Schlaube is particularly suitable for modelling steady-state conditions given the natural regulation caused by the upstream lake and the prevalence of GW contribution over runoff. The highly monitored characteristics of the study site facilitate incorporating different data sources to parametrize, calibrate and validate the model.

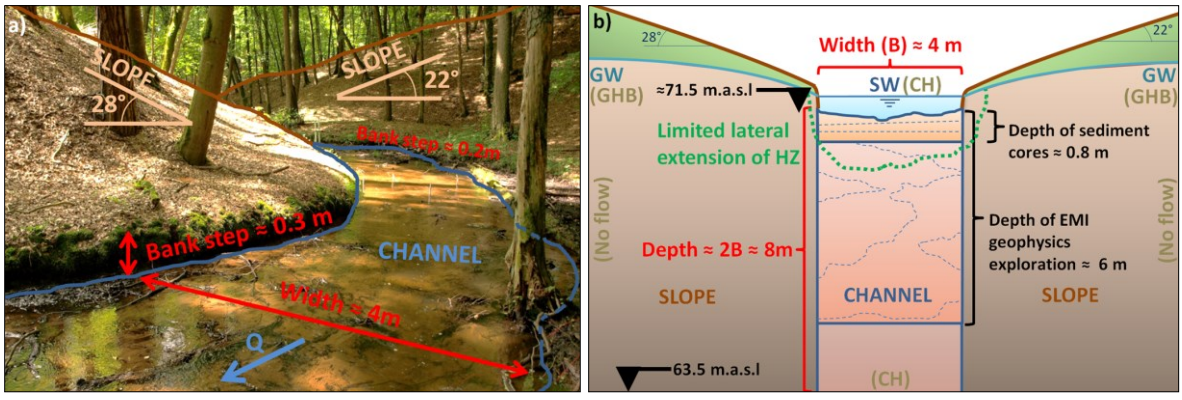

Figure 4.1: (a) Image from the study site illustrating the lateral constraint of the channel due to the steep slopes. This fact, together with the high GW heads existing in the margins, allows assuming that HEF is mainly constrained to the width of the channel. Thus, the sketch in (b) shows the model domain including the channel and the slopes with a depth of two

times the width of the channel. Considering the variable altitude of the streambed along the reach, depth is approximately 8 meters from the sediment-water interface to the bottom of the domain fixed at 63.5 m.a.s.l.. Bottom boundary condition assumes initial head levels of 80 m.a.s.l.. The top boundary condition of surface water (SW) is of variable altitude according to the elevation of the water surface at each section along the reach. The lateral boundary conditions in the slope are defined as general head boundaries (GHB). The sides of the domain are defined as no-flow conditions. Figure (b) also indicates the depth of investigation of subsurface hydraulic conductivity conducted in previous chapters using sediment cores and EMI geophysics.

4.3.2 Point data

Piezometers / Well network

The network of piezometers used to define the hydraulic heads in the model was the one of the hand-made multi-level piezometers shown in Table 1, Chapter 2 and Figure 3.1 (also described in detail in Section 3.3.1). The eight depths where these piezometers measured hydraulic heads represent a big advantage over piezometers without multiple levels. Deploying the piezometers in cross sections facilitates incorporating the longitudinal but also transversal variability of hydraulic heads of the study site. The data from each level of these ten multi-level piezometers was interpolated with the inverse distance weight (IDW) method to obtain a surface of hydraulic heads at their corresponding 1, 8, 14, 23, 31, 48, 65, 82 cm deep. The interpolated piezometric surfaces were applied to the different layers of the model as initial conditions of hydraulic head. The period of data selected for modelling lasts from 29 June 2017 to 2 July 2017, the period immediately before the artificial flow events triggered for the identification of local HEF in Chapter 2.The network of manually-observed multi-level piezometers was completed with a network of piezometers and surface water monitoring wells continuously monitored with data loggers (Table 3.1). The data from deep levels of these additional piezometers was incorporated into the IDW interpolation of piezometric surfaces. Conversely, the data from surface water levels, whose level barely show changes according to Figure 4, Chapter 2, was used together with the topographic survey of the surface water to define the top constant head boundary condition. The level of

stream water serves as an approximation of hydraulic heads along and across the whole channel due to the slow speed of flow throughout the study site.

Soil properties

Soil properties were obtained from the analysis of the 24 surface samples indicated in Table 1, Chapter 2 and the two cores situated at Transects TR3C and TR4C indicated in Table 3.1. The instruments and methods used for analyzing these samples are reported in Table 1, Chapter 2 and Table 3.1. Several of the sediment properties play a prominent role in the parametrization. Hydraulic conductivity, porosity and thermal conductivity define the differences in the definition of heterogeneity of the three models tested in this study: the uniform, multi-layered and distributed models. Despite the point nature of the samples, they describe the sufficient spatial and in-depth variability of sediment properties to define heterogeneous fields of hydraulic conductivity or porosity across the river. The interpolation is conducted using the IDW method between the sample locations of the same depth level. Models including the interpolated surfaces of this data outperform models using spatially averaged values (Anderson & Woessner, 1992). In the case of the model defined with distributed geophysics data, the soil definition is described in the section below explaining distributed data from geophysics.

All cells of the model located outside the volume explored from soil samples are defined with values of hydraulic and thermal properties typical of sand (Domenico & Schwartz, 1990). The cells calibrated for hydraulic conductivity correspond to those behind the channel and below the levels of properties determined by sediment samples or geophysics. The cells outside the channel in the slopes are not calibrated and remain with the values of hydraulic and thermal properties of fine sands from Domenico & Schwartz (1990). Values of specific yield and storage required for cell definition in MODFLOW are extracted from sand values of Lohman (1972). There, the values of total (N_t) and effective porosity (N_e) are indicated with values of N_t =25% and N_e=20%. Values of porosity obtained from sediment cores are incorporated to the area below the channel leaving literature values for the area of slopes. From the same reference, the specific yield (S_y) is considered 20% and the value of specific storage (S_s) is 0.0002 for medium sands, applied to all cells of the domain.

Regarding thermal properties, some authors indicate the small impact of including average values of thermal properties in the models (Rau et al., 2014), especially taking into consideration the much wider range of variability of hydraulic conductivity values (Anderson, 2005). However, we included in our multi-layered and distributed models the spatial variability of the thermal properties observed in the multiple sediment samples, which ensures a lower impact of thermal properties heterogeneity in the accuracy of our results. The most influential thermal parameter in the model is the coefficient of thermal diffusivity. We derived the mean value of $7.5 \cdot 10^{-7}$ m²/s value from the results of thermal diffusivity conducted with K2PRO (Table 1, Chapter 2, or Table 3.3) on sediment samples.

Temperature profiles

Temperature profiles were continuously recorded with the multi-level temperature data loggers detailed in Table 3.1 at the same depths of multi-level piezometers. This coincidence helps to define the initial conditions of temperature for the layers defined from sediment cores. Similarly to hydraulic data, we generate interpolated fields of temperature at the corresponding depths of the sediment (using IDW) (Figure 4.4). These temperature profiles enabled obtaining 1D flux estimations of the exchanges in the sediment, but additionally can be used to identify steady periods and scour/deposition (Luce et al., 2013).

4.3.3 Distributed data

FO-DTS

Based on the temperature-dependent back-scattering of a laser pulse in a fiber-optic cable, fiber-optic distributed temperature sensing (FO-DTS) provided high-resolution measurements of the temperature at the sediment-water interface at multiple scales (all figures Chapter 2). Further details on the deployment of this technique at the study site are described in the Section "Fiber-optic distributed temperature sensing" of Chapter 2. With the experimental setup covering the whole channel with more than 3600 points, the interpolated field of temperatures of the uppermost level of sediment (at the depth where cables of FO-DTS are buried) conserves to a great extent the high-resolution of FO-DTS data. This interpolated field is the dataset used for validation of MT3D-USGS heat transport models. The two heat boundary conditions required for MT3D-USGS are surface water temperature

and groundwater temperature respectively located at the top and at the bottom of the model domain. The top boundary condition was considered constant throughout the study site from the records of several meters of FO-DTS cable exposed to the current in the vicinity of Transect TR2 (Table 1, Chapter 2). However, the bottom boundary condition could not be directly measured in depth of the sediment. Despite the quasi-constant temperature of the deepest levels of the temperature lances, the true constant GW temperature seems to be located beyond the depth of 80 cm. We adopt the temperature collected by a datalogger buried in depth of a powerful GW spring located in the nearby.

Geophysics

Electromagnetic induction (EMI) enabled a non-invasive exploration of the sediment texture based on the different response of sediment to the primary and secondary magnetic fields (Figure 4.2). Electrical conductivity (*EC*) fields depending on sediment texture (when pore water *EC* variability is not of great influence) can provide preliminary estimations of hydraulic conductivity (K_s) fields. This study aims to define the hydraulic parameters of the cells of the model in a distributed manner based on EMI geophysics data. The first step on this purpose requires interpolating *EC* for the areas in between the *EC* profiles (Figure 5, Chapter 2) using 3D ordinary kriging interpolation (function defined in the R package gstat).

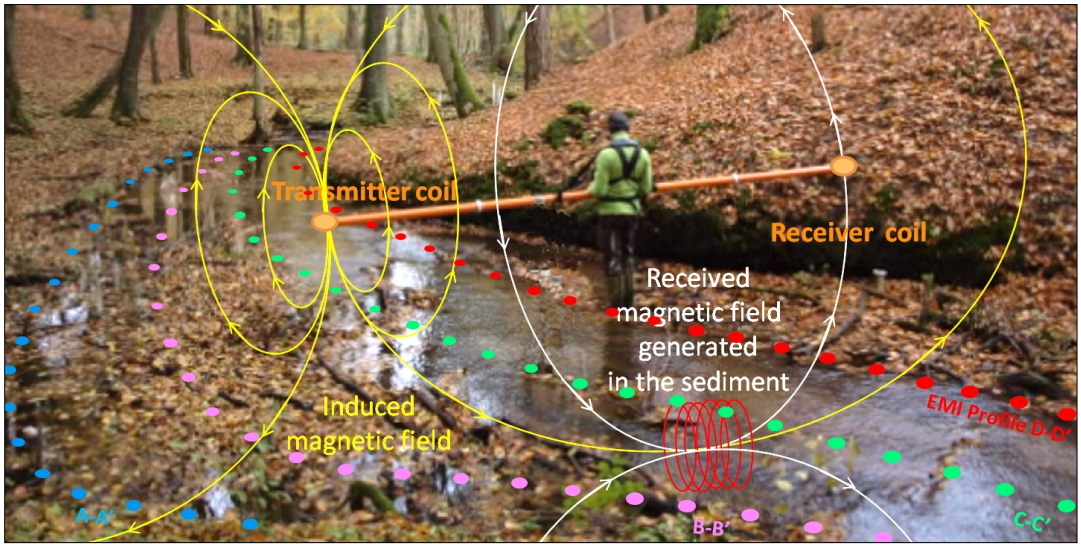

Figure 4.2: EMI geophysics survey at River Schlaube depicting the span of the CMD GF instruments device and illustrating the introduction of the magnetic field into the sediment with its subsequent magnetic response measured back in the device.

A petrophysical relation is used to translate *EC* values into values of hydraulic conductivity (K_s). The use of petrophysical relations is possible in cases of particularly inverse conditions of the *EC*- K_s due to the presence of clay. That was the case of our study site as described in the Section "FO-DTS differentiation of local SW down-/upwelling during floods". Once adjusted the inverse relation between *EC* and K_s from the data of EMI geophysics and core samples, the relation is applied to transform the 3D field of EC into K_s. We classify the range of K_s obtained from the transfer function in groups of similar K_s called hydrofacies. The histogram of K_s suggests the definition of three main hydrofacies for the most prevalent low, medium and high K_s values. Later on, calibration results suggested including two additional hydrofacies to split the range of high K_s values for some specific areas. Each hydrofacies adopts the mean of all their K_s as the initial value for calibration.

4.3.4 The time period of study

All data incorporated into the model correspond to the period of study between 29 June 2017 and 2 July 2017 under quasi-steady conditions of streamflow and groundwater discharge as described in Chapter 2, Section "FO-DTS based identification of groundwater and interflow discharge". The interflow discharge recognized and discussed in the results of that cited section are not the focus of the modelling goals of this study given the lack of hydraulic, temperature, soil and geophysics data from the slopes.

4.3.5 Modelling tools

Flow model: MODFLOW

To estimate streamflow and groundwater exchanges through the channel bed three models (uniform, layered and distributed) were created using MODFLOW (Harbaugh, 2005). MODFLOW finite differences program calculates flux numerically in and out of each cell of the domain to provide the general flow budget. In order to properly capture the up-/downwelling areas at the sediment-water interface (Wondzell et al., 2009), the models incorporate the topography of the streambed. The size of the cells adopts the resolution of the topographic survey (approx. 0.2 x 0.2 m). This small cell size is sufficient to capture the ripples and other bedforms occurring in the streambed and contribute to increase flux budgets (Anderson & Woessner, 1992). In addition to the small cell size, the model layers have

variable altitude (Figure 4.4). Each of these layers is defined following the downstream slope and the altitudinal levels where multi-level piezometers, temperature profiles and soil cores occur in the subsurface (i.e. the level at 14 cm depth). In this way, the model needs dealing with an unstructured grid of cells (which is identified with the term "USG"). Graphical interfaces such as FREEWAT (Rossetto et al., 2018) are required to handle the geometric complexity of an MODFLOW-USG model.

Interface: FREEWAT

FREEWAT graphical interface is an open source composite plugin for the desktop GIS software QGIS (https://qgis.org). Multiple QGIS tools together with some special utilities of FREEWAT are needed for editing the raster and vector GIS layers defining the complex geometry of layers of variable altitude and thickness. The geometric configuration of the model is stored in a SQLite database. The module incorporates not only the possibility to define completely the core MODFLOW module (MODFLOW-2005, Harbaugh, 2005) but also many of the related software of the MODFLOW environment such as MODFLOW-NWT (Niswonger et al., 2011), MODFLOW-OWHM (Hanson et al., 2014), MODPATH (Pollock, 2017), SEAWAT (Langevin et al., 2007), MT3D-USGS (Bedekar et al., 2016) and UCODE_2014 (Poeter et al., 2014). In our particular case, we use FREEWAT's OBS module to include the observed data (e.g. multi-level head records), the UCODE module for calibration and sensitivity analysis of hydraulic conductivities of the layers beyond the depth of observations, and MT3D-USGS module to conduct heat transport modelling. All the implemented programs and modules of MODFLOW included in FREEWAT run in Python using the Python package FloPy (Bakker et al., 2016).

Editing and postprocessing: FloPy

Flopy Python package works internally in FREEWAT utilities but can also be used externally to modify the parametrization of the model, change the solvers and process the results. Additionally, the scripting nature of FloPy facilitates recording the construction, running and post-processing of the model (Bakker et al., 2014) which is convenient for repetitive actions. Here, this advantage was used for checking the model geometry, testing the performance of different solvers for the unstructured grid and for plotting the multiple layers of the model (e.g. Figures 4.6-4.9).

Transport model: MT3D-USGS

Once MODFLOW provides the flux and head results for the models, MT3D-USGS (Bedekar et al., 2016) can be incorporated to simulate the three-dimensional transport model of temperature. Temperature is the only transport species consider in this study. MT3D-USGS requires the values of flow velocities from each cell's face as input to solve the classical advection-dispersion transport equation of MT3DS (Zheng, 1990, Zheng & Wang, 1999). The interaction of MT3D-USGS with MODFLOW occurs within FREEWAT through the LMT module, although it can also be run from FloPy. MT3D-USGS provides several transport solution methods that are also included in FREEWAT interface: the fully implicit finite difference method (FDM), the particle-tracking based method of characteristics (MOC) and its variants (hybrid HMOC), and a third-order total variation diminishing (TVD) for limiting numerical dispersion. In our case, the FDM solver proves more stable than MOC, HMOC and TVD methods.

Calibration

In our case, the calibration was conducted iteratively between the hydraulic and thermal model (i.e from MODFLOW to MT3D-USGS models) with help of the Fortran-based calibration method **UCODE** developed by Poeter & Hill (1999). This is a code in for solving problems with less number of parameters than observations. The code performs inverse modelling using nonlinear regression that minimizes the weighted least-squares objective function using a Gauss-Newton method. The code allows flexible definition of the parameters to calibrate; whose evaluation can be conducted analyzing different statistic variables (e.g composite scaled statistics (CSS) and parameters correlation coefficients (PCC)) about their sensitiveness and individual contribution to the uncertainty of the model. The UCODE Python-based version included in FREEWAT is UCODE_2014 (Poeter et al., 2014). UCODE is used to calibrate the hydraulic conductivities of the layers below the depth of sediment cores defined in the multi-layered model and the hydrofacies defined based on EMI geophysics data in the distributed model.

4.3.6 Model definition

Geometrical definition of the multi-layered and distributed models for comparison

Three 3D models are defined for this study: one uniform model defined based on literature values for hydraulic and thermal properties of the sediment, a second model defined in multiple layers in the HZ using the hydraulic conductivity from sediment cores and a third model defined in semi-distributed volumes of similar sediment properties (i.e. hydrofacies) using the hydraulic conductivities derived from EMI geophysics. Despite the different inputs for the parameters of sediment properties, all models are defined with the same number of layers (21) in order to allow the comparison of results cell by cell (Figure 4.3 and 4.4).

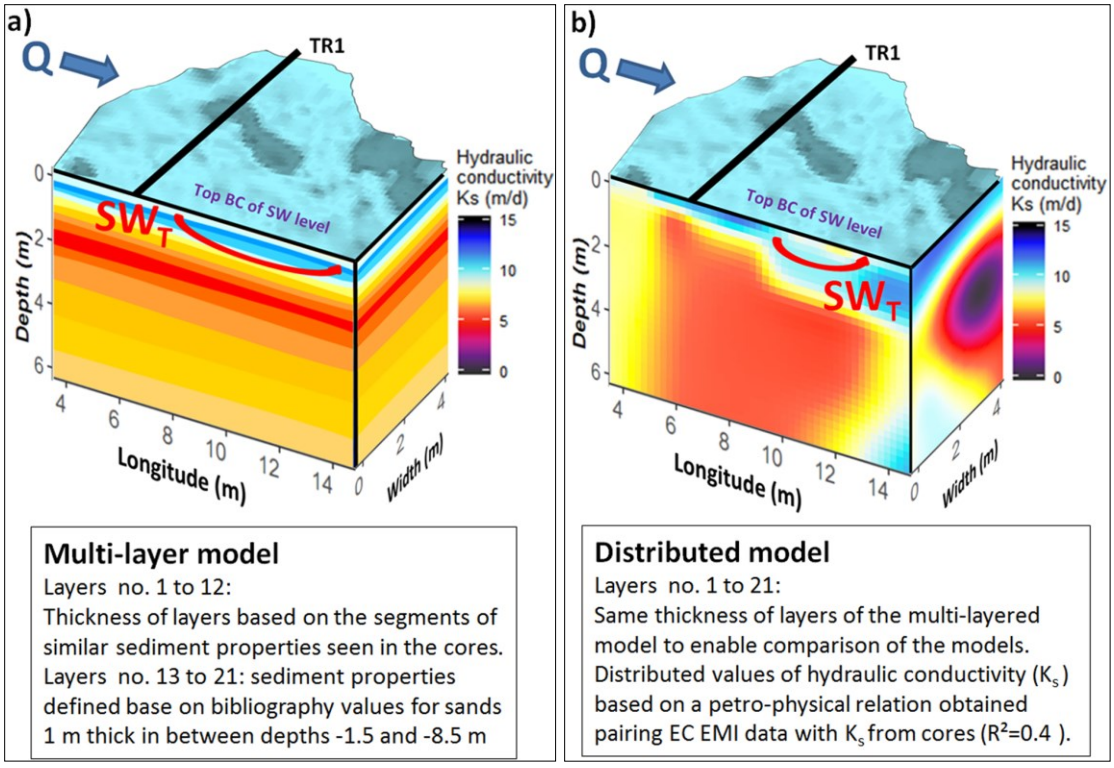

Figure 4.3: Layering definition of the channel region (see Figure 4.1) of the (a) multi-layered model and the (b) distributed model based on the different sources of information of sediment properties. The uniform model is not shown given its simplicity, based on a unique hydraulic conductivity value, to give room for illustrating the other more complex models. In (a) the multi-layered model illustrates the different thickness of each layer defined based on the segments of sediment cores of similar sediment properties. The differences in the thickness of layers concentrate in the upper 12 layers, where there is centimetre information

from the sediment cores. Layers from -1.5 to -8.5 m show regular thickness of 1 m. The distributed model displayed in (b) adopts the same thicknesses of layers but incorporating in slices the values of hydraulic conductivity given by the petrophysical relation obtained by pairing the values of EC-K_s of point and distributed data.

Thickness and altitude of the layers are common between the three models. The upper layers have a thickness in between 4 and 16 cm, while those -0.8 m below the sediment-water interface become progressively wide from 28 cm of layer 13 to 150 cm of layers below -3 m. The increasing thickness with depth responds to the need to identify smaller patterns of heterogeneity in the upper layers compared to patterns in the lower ones. Not only sediment cores but also the EMI geophysics datasets provide higher definition in the upper levels compared to the lower ones, which supports adopting an increasing thickness of layers. Additionally, the small thickness in the upper levels contributes to a better estimation of the flux when the vertical flow component is significant (Brunner et al., 2010). The last layer adopts a thickness of up to 1.6 m in order to reach the desired depth of the model domain of 8 m, which is approximately twice the width of the channel (Figure 4.1b). The increasingly wide thickness of layers can be observed in Figure 4.3a and with more detail in Figure 4.4.

The area immediately below the channel is defined by the data from sediment samples /geophysics while the area below the slopes is defined by the data from literature values as detailed in Sections 4.3.2 and 4.3.3 and on Figure 4.1 and 4.4. The parametrization of the area below the slopes is not calibrated. In the layered model, only the hydraulic conductivities (K_s) of the layers before the level of sediment cores (below -0.8 m) are calibrated for both the flow and heat transport models. In the distributed model, only the K_s area where geophysics exploration occurred is calibrated for the flow model. As shown in Figure 4.1, the hydrofacies definition extends only to the depth of the geophysics exploration. Values of K_s of each hydrofacies group are calibrated in the distributed model,to refine the preliminary K_s estimations provided by the inverse linear relation EC- K_s.

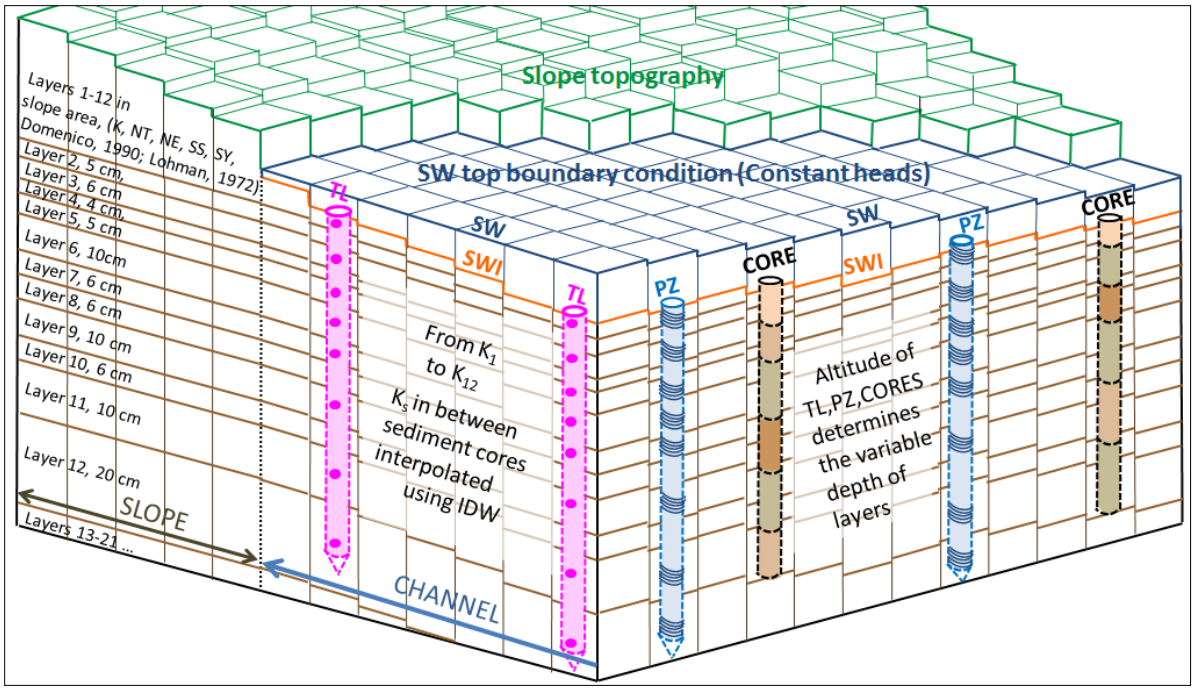

Figure 4.4: Unstructured grid of the MODFLOW model determined by the depths of the devices collecting data in profiles. TL identifies the temperature lances which measure temperatures at eight depths. PZ represents the multi-level piezometers used to measure the vertical hydraulic gradients (VHG) at the same depths of TL. Cores identify the changes in sediment properties. SWI identifies the sediment-water interface. SW depicts surface water.

The model domain extends 45 meters from West to East and 25 meters from North to South. The cell size adopted is 0.2 x 0.2 m to capture the small heterogeneity of exchanges occurring in the sediment-water interface, where bedforms rarely exceed these horizontal dimensions. With these domain and cell dimensions, the model domain contains 29375 cells per layer. Considering the 21 layers, the number of total cells is 616875. From above, the shape of the models is rectangular and comprises the stream a bit in diagonal due to the orientation of the slopes (Figure 1, Chapter 2). The altitudinal range varies from the 63.5 m.a.s.l. of the bottom of the domain up to a maximum of 82 m.a.s.l. in the slopes while the streambed altitude ranges from 71.6 m.a.s.l. to 71.9 m.a.s.l.

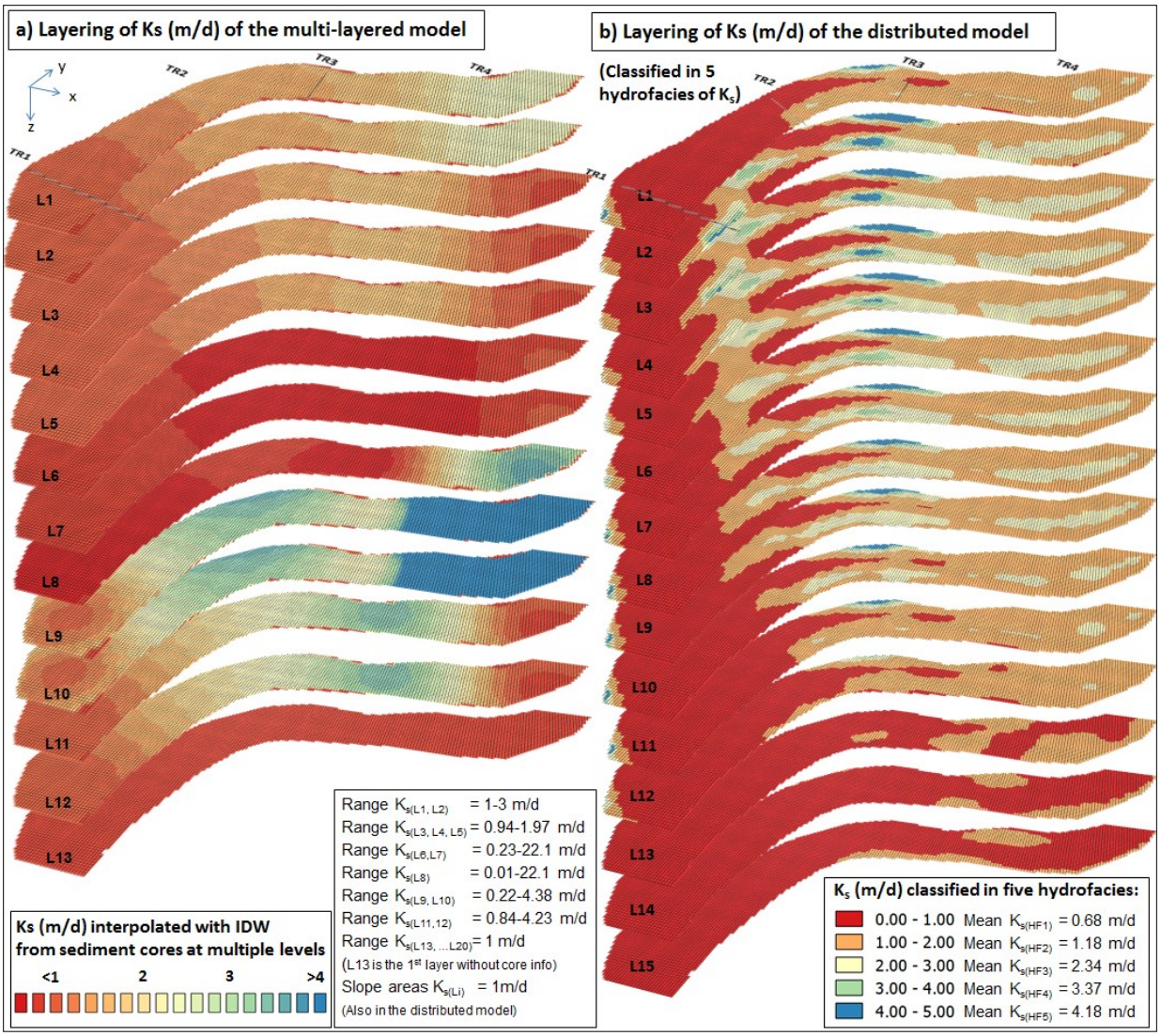

Figure 4.5: Definition of hydraulic conductivity (K_s) of the models. (a) The multi-layered model incorporates K_s data interpolating the values obtained from sediment cores between cores locations for the 12 layers covering the first meter of depth of the sediment. Layer 13-20 adopt a uniform value of K_s =1m/d. The IDW interpolation generates K_s fields of round shapes and long transitions between the locations of the cores. (b) The distributed model incorporates the K_s values transformed from the 3D electrical conductivity dataset measured with EMI geophysics. The optimal number of hydrofacies (HF) for modelling performance is five, which is the case represented in this Figure 4.5b. The starting values adopted are the mean values of all K_s existing on each hydrofacies. L16 and L17 of similar prevailing low-conductive (K_s <1m/d) materials to the L15 showed for the distributed model are not shown.

Layers are plotted in the vertical dimension without regard to their thickness and real separation to facilitate the visualization of changes in K_s.

Boundary conditions

In terms of hydraulic boundary conditions, both multi-layered and distributed models were defined with no-flow boundary conditions in the upstream and downstream face of the model. The hydraulic lateral boundary conditions for the river are defined with general head boundary conditions (GHB). The period chosen for the simulation, date of a rainfall event of great magnitude (Figure 3, Chapter 2), facilitates adopting high hydraulic heads in the lateral faces of the slopes as general head boundary conditions (GHB) (Figure 4.1). The high hydraulic heads for these GHB are iterated based on the optimal misfit statistics of the UCODE flow model calibration. The optimal values obtained are of 2.5 and 3.5 m below surface in the outer left and right slope margins of the model domain. The head value adopted for the bottom no-flow boundary conditions is 80 m.a.s.l. This value was calculated by applying the hydraulic gradient observed in the lowest level of multi-level piezometers to the depth not observed with multi-piezometers. The hydraulic top boundary condition is the quasi-constant stream water level surveyed at centimetre resolution with the total station Leica TPS1200 together along with the levels recorded in pressure transducers at transects TR1 and TR3 (Table 1, Chapter 2). This top boundary condition is usually considered as an internal boundary (Wondzell et al., 2009) due to its easiness of measurement and vicinity to the cells of the domain facilitate obtaining accurate model predictions (Rubin & Dagan, 1992). The thermal boundary conditions adopted are GW temperature for the bottom and the SW temperature for the top one. GW temperatures are recorded at a nearby groundwater spring (T=10°C) and SW temperatures from the Line 2 of FO-DTS exposed to the streamflow in the vicinity of Transect TR3 (Figure 3, Chapter 2). The data from the 3611 points of FO-DTS temperature measurement at the SWI is reserved for the validation of MT3D-USGS.

Assumptions

The models defined for our study comprise three main assumptions. We consider the stream in the study site completely hydraulically connected given the higher elevation of hydraulic heads compared to streambed elevation (Brunner et al., 2010) along and across the

river reach. Secondly, we assume isotropic K_s values after some sensitivity analysis with UCODE which produced better fits than considering the horizontal hydraulic conductivity K_h larger than the vertical one K_v. K_v values were the K_s obtained from the laboratory analysis of hydraulic conductivity with KSAT (Table 2, Chapter 2, Table 3.1). Finally, we considered values of longitudinal dispersivity of ΔL=0.05 m for the transport modelling extracted from literature (Gelhar et al., 1992).

The metrics for comparison

The models are compared for three main types of results: hydraulic heads, flux estimates and temperature estimates. First, the hydraulic head estimates are compared for all models with the head observations from the multi-level piezometers and wells to evaluate the fit of the models. In total, there are 99 estimates of heads available for comparison at 8 different levels down to -0.8 m in the sediment. Secondly, flux estimates are compared by comparing the net budget of water exchange of the cells representing the sediment-water interface with the gain of stream flow measured with the OTT device (Table 2, Chapter 2) between the upstream and downstream endpoints of the reach. Finally, the estimates of temperature provided by MT3D-USGS at the uppermost layer of the models are compared with temperature values of the sediment-water interface observed with FO-DTS. In the case of temperatures estimates, also the spatial distribution is compared to the spatial distribution of temperatures from the FO-DTS records, especially regarding the location, area and temperature anomaly of the regions of preferential exchange.

Afterwards, the multi-layered and distributed models are compared with the aim of evaluating the influence of the type of hydraulic conductivity (K_s) distribution in the subsurface. In particular, we check the influence of defining K_s in layers compared to the distributed definition based on hydrofacies. In this case, we evaluate the differences between models by comparing their misfit statistics for hydraulic heads and temperature estimates and patterns of temperature distribution in the sediment-water interface.

4.4 Results

4.4.1 Groundwater flow MODFLOW models

The observed vs. simulated head values have residual RMS of 0.018 for the uniform model, 0.007 for the multilayered and 0.0004 for the distributed model (Table 4.1). For both the multi-layered and distributed models calibrated for K_s using UCODE the residuals are certainly accurate (Table 4.1). In view of the lower order of magnitude of the uniform model compared to the multilayered and distributed models, the uniform model is discarded for further analysis. The lowest values of misfit prevail in the upper levels of the subsurface, closer to the constant head boundary condition of the stream water surface. Table 4.1 shows how these values remain similar for the temporal validation dates of 18 Jan 2017 and 3 Mar 2017. The differences in misfit of simulated versus observed heads between the multi-layered and the distributed model differ in almost an order of magnitude, with values below or around the millimeter in the case of the distributed model (Table 4.1).

Table 4.1: Table of misfit statistics of hydraulic heads against observed heads in multi-level piezometers and wells for the multi-layered and distributed models the 1 Jul 2017.

	UCODE calibration residuals with 9 head observations (m) from piezometers (PZ)	UCODE calibration residuals of 99 head observations (m) from 9 piezometers (PZ) + 10 Multi-level piezometers (MPZ)		
	UNIFORM MODEL			
Date	Calibration 2 Jul 2017	Calibration 2 Jul 2017	Validation 18 Jan 2017	Validation 3 Mar 2017
SD	0.052	0.033	0.041	0.041
RMS	**0.039**	**0.018**	**0.021**	**0.015**
Avg	0.038	0.018	0.021	0.015
Max	0.127	0.127	0.089	0.094
Min	-0.089	-0.081	-0.146	-0.141
	MULTILAYERED MODEL			
SD	0.033	0.031	0.046	0.044
RMS	**0.018**	**0.007**	**0.009**	**0.006**
Avg	0.018	0.007	-0.009	-0.006
Max	0.075	0.079	0.090	0.090
Min	-0.055	-0.111	-0.130	-0.159
	DISTRIBUTED MODEL			
SD	0.033	0.027	0.029	0.042
RMS	**0.018**	**0.0004**	**0.001**	**0.001**
Avg	0.018	0.0005	-0.001	-0.001
Max	0.075	0.052	0.059	0.09
Min	-0.055	-0.102	-0.125	-0.151

The lowest residuals occur for both models in the uppermost level (Layer 1, z=-0.05 m) as shown in Figures 4.6a$_1$ and b$_1$. The highest head residuals tend to be concentrated in the lowest levels of the multi-piezometers (82 and 65cm deep), as shown for Layer 11 (level z=-0.8m) (Figure 4.6a$_2$ and b$_2$). The distributed model shows generally lower residuals than the multi-layered model, as illustrated with the abovementioned layers L1 and L12 in Figure 4.6. In the same figures can be appreciated how, in general, the heads of the areas between transects TR1 and TR3 tend to show higher residuals than areas around TR2 and TR4. Once calibrated, the K_s values from the optimal configuration of five hydrofacies of the distributed model change from those indicated in Figure 4.5b to 0.27, 1.07, 2.17, 3.00, 4.08 m/d.

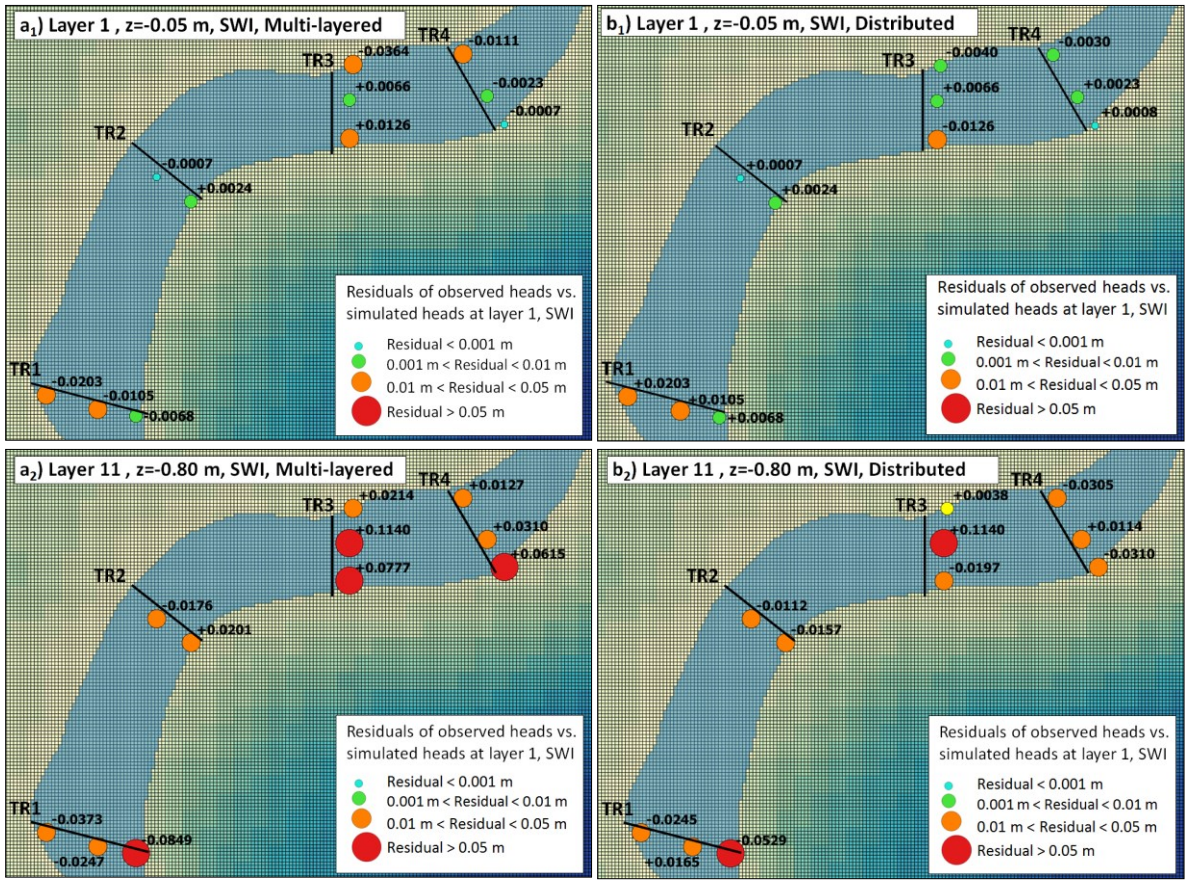

Figure 4.6: Differences of residuals of observed vs simulated heads (m) at the uppermost and lowest levels of multi-level piezometers for the multi-layered (a$_1$, a$_2$) and distributed models (b$_1$, b$_2$). Layer L1 of both models comprises the lowest residuals while Layer L11 shows the highest. Distributed model shows lower residuals than the multi-layered model.

The uppermost layer of both the multi-layered and distributed models display a concentration of upwelling in the area between transects TR3 and TR4 (Figure 4.7a). Areas between TR1 and TR2 remain mostly neutral, which highlights the heterogeneity in the spatial distribution of GW-SW interactions. Considering the global net exchange of the cells of the uppermost level, groundwater contributed to the stream with a gain of about 5.8 L/s and 8.6 L/s in the multi-layered and distributed model respectively. Results are on the same magnitude to those measured from differential stream gauging (10 L/s on the 2 Jul 2017) but lower than the ones obtained using 1D vertical methods. The extrapolation of 1D methods' results to the whole SWI would generate over 100 L/s, results an order of magnitude higher.

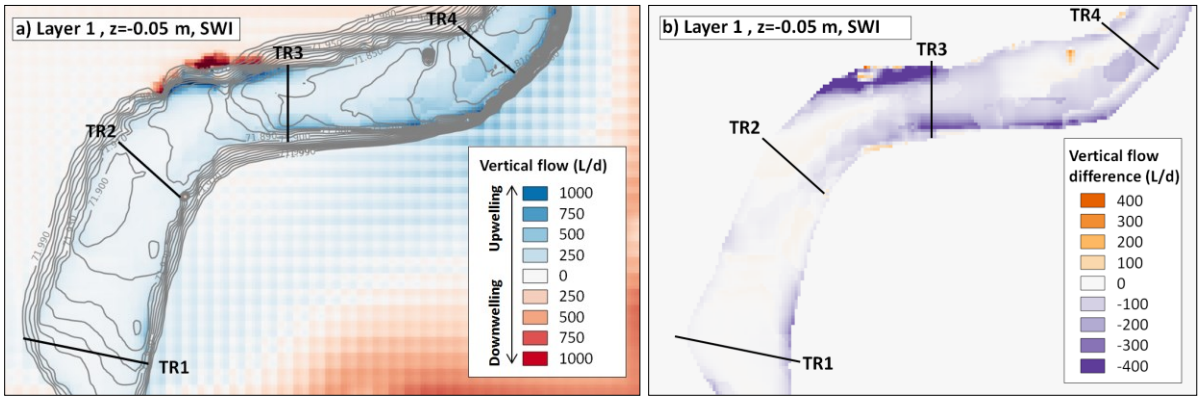

Figure 4.7: (a) Estimates of vertical flow of the distributed model. High upwelling values concentrate in blues along TR3 and TR4. (b) Flow differences between the distributed and multi-layered models. The distributed model shows higher daily vertical discharge than the multi-layered one in TR3 and TR4 (negative values). Along TR1-TR2 slightly orange colours identify where the distributed model reduces the upwelling in respect to the multi-layered model in agreement with the clogging conditions identified before along TR1-TR2.

The model is also able to identify the highly variable direction of the horizontal component of HEF in the upper levels of the sediment caused by the interaction of groundwater gradients and riverbed forms (Figure 4.8a). These changes on the direction of flux do not consider the influence of streamflow dynamics. The influence of bedforms decreases with depth leaving groundwater gradients as the main driver of the direction and magnitude of fluxes below the depth of 1m (Figure 4.8a vs. Figure 4.8b). The lower layers show the tendency of GW to shortcut the curves of the stream, particularly when the curve is located over the left margin, whose topography and GW gradients show less steep slopes.

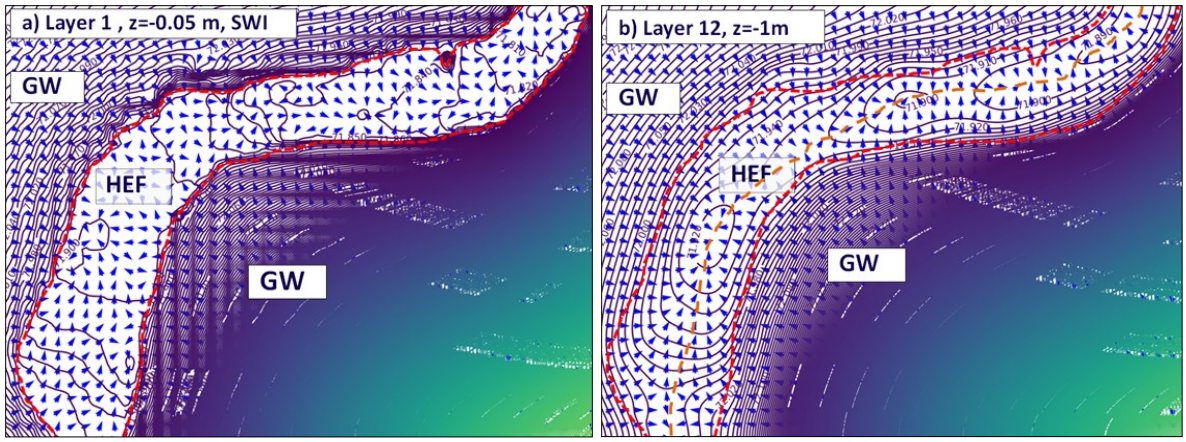

Figure 4.8: (a) Potentiometric surface & flow direction of the multi-layered model at Layer L1 (z=-0.05m) and (b) at L12 (z=-1m) of the distributed model. Due to the influence of bedforms, the flow direction in L1 is very variable, representative of HEF complexity. The area of the channel where this occurs is delimited with a red contour. Flow direction outside of this area is determined by groundwater gradients labelled with "GW". (b) The bedform influence disappears with depth, and deeper than Layer 12 only the gradients of GW define the direction of flow. The red contour no longer identifies the transition between oriented and variable flow. The orange line illustrates the direction division generated by the confronting groundwater gradients from slopes.

4.4.2 Heat transport MT3D-USGS models

Once the multilayered and distributed models become calibrated for the 99 multi-level heads with UCODE, forward heat transport modelling can be conducted and evaluated. To validate the models we compare the simulated temperatures in the uppermost layer of the sediment with the temperatures observed by FO-DTS at the sediment-water interface (SWI) (Figure 4.9). Both the multi-layered and the distributed models prove able to qualitatively reproduce the general configuration of the temperature anomalies at the SWI (Figures 4.9a and b). Both models simulate areas along TR1 and TR2 without significant cold temperature anomalies attributable to GW. The distributed model is more accurate in reproducing SWI temperature along these areas closer to the SW temperature value of 15.7°C (areas red in colour along TR1 and TR2). Both models locate the mean cold anomalies attributed to GW discharge along TR4, and less accurately at TR3. The anomaly in TR3 is largely overlooked by the multi-layered model while seems slightly better reproduced by the distributed model.

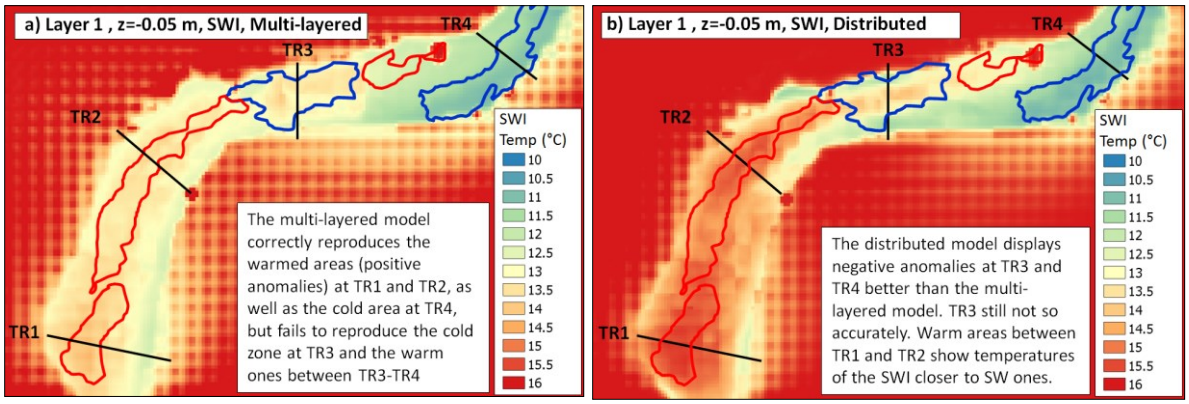

Figure 4.9: Temperature maps at the sediment-water interface (SWI), where the cable was buried, from MT3D-USGS forward runs of (a) multi-layered and (b) distributed models. The warm / cold anomalies identified from FO-DTS analysis in Figure 2, Chapter 2, are displayed as red and blue contours overlapping the modelled SWI temperatures for comparison. Red contours represent the shallow areas suffering higher temperatures influenced by radiation and air temperature (Areas type Ei and Si, Figure 2, Chapter 2). The blue contour represents anomalies attributed to groundwater discharge (Areas GW3 and GW4, Figure 2, Chapter 2).

Quantitative assessment of models' capability to reproduce the thermal patterns in the SWI has been conducted by comparing the simulated temperature anomalies at the SWI to the measured temperature anomalies at the SWI using FO-DTS (Table 4.2). Residuals of the difference of temperature anomalies of the multi-layered model are higher at each transect TRi than the corresponding ones of the distributed model. The distributed model outperforms the multi-layered model especially at the areas TR1 and TR2, where simulated anomalies are barely half a degree below the values observed by FO-DTS. However, residuals remain high at TR3 and TR4 denoting the tendency of both models to overestimate those cold anomalies.

Table 4.2: Residuals statistics of the difference of the simulated temperature anomalies A_T (°C) and the observed temperature anomalies measured with FO-DTS.

MULTI-LAYERED MODEL Residual statistics of temperature anomalies A_T (°C) at the SWI of transects Tri				
	TR1	TR2	TR3	TR4
SD	0.598	1.208	1.945	1.151
Avg	**-2.168**	**-1.727**	**-1.923**	**-2.422**
Max	-0.819	4.262	5.565	1.647
Min	-4.477	-4.567	-4.333	-4.698

DISTRIBUTED MODEL Residual statistics of temperature anomalies A_T (°C) at the SWI of transects Tri				
	TR1	TR2	TR3	TR4
SD	0.940	1.190	2.211	1.289
Avg	**-0.357**	**-0.516**	**-1.206**	**-2.064**
Max	0.769	4.053	5.808	1.536
Min	-3.590	-3.830	-4.656	-5.356

Differences of the simulated temperature anomalies at the SWI of the multi-layered and distributed models to the temperature anomalies observed with FO-DTS (Figure 2, Chapter 2) are also shown in Figures 4.10a and b. The multi-layered model (Figure 4.10a) tends to underestimate all temperatures (blue color representing negative sign) at the SWI, both in neutral areas between TR1 and TR2 and in area TR4 (difference up to -4°C). At TR3 both models show areas in red in the center of TR3 illustrating overestimation of the temperatures and areas in blue in the margins illustrating underestimation. These complex patterns of underestimation and overestimation of temperatures seem more accentuated in the distributed model than in the multi-layered model while the mean residual is lower in the first case (-2.064 °C) than in the second (-2.422°C). Areas TR1-TR2 are better reproduced in the distributed model than in the multi-layered one as illustrated in blue colors for the Figure 4.10c comparing models (blue colors identify where the multi-layered model underestimates compare to the distributed one. In any case, both models lack accuracy in the area of TR3.

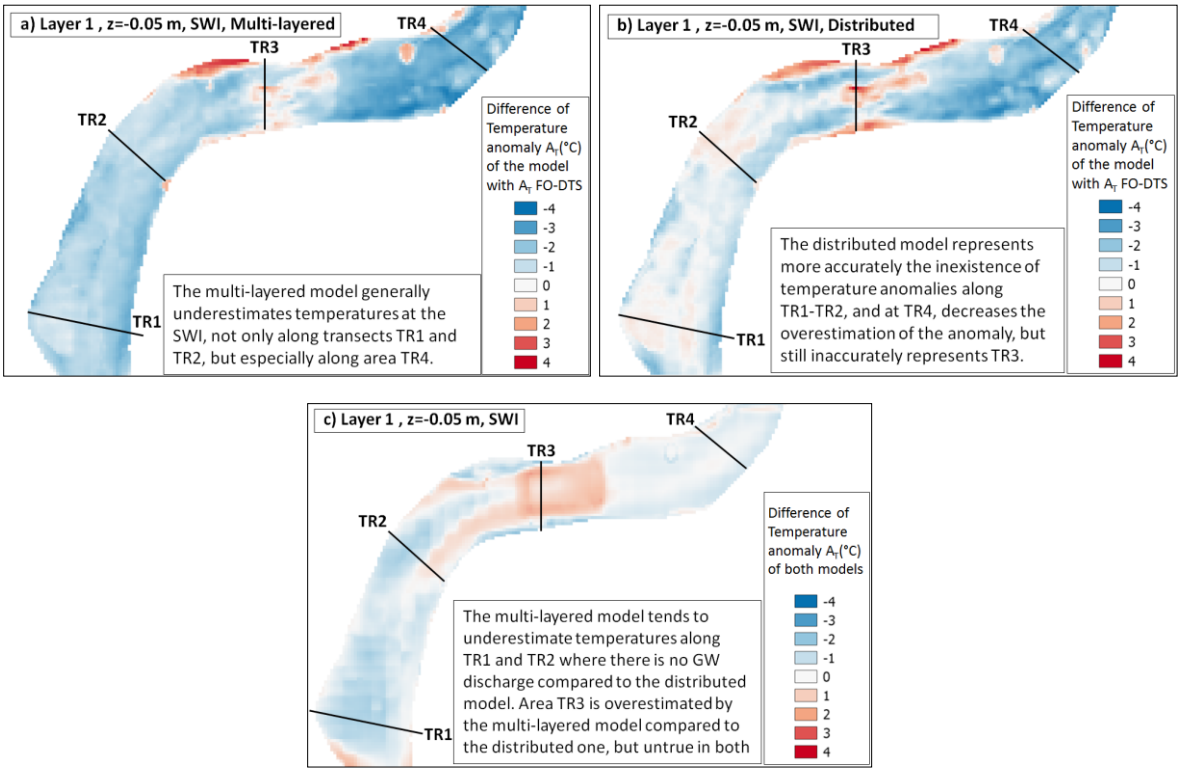

Figure 4.10: Differences of temperature anomaly A_T (°C) of the (a) multi-layered model and (b) distributed model with the A_T (°C) observations measured using FO-DTS. (c) Difference in estimates of A_T (°C) between the multi-layered and distributed models.

4.5 Discussion

The calibrations of the hydraulic heads of the models show particularly low residuals in the case of the multi-layered and distributed models. Furthermore, the goodness of fit remains consistently similar when the model is applied to other periods of steady-state conditions (18 Jan 2017 and 2 March 2017) (Table 4.1). There are several factors with a positive impact on the accuracy of the fit. The first factor is the possibility to calibrate over a set of head observations at multiple levels provided by multi-level piezometers. The results of the models calibrated with multiple levels of heads significantly outperform those calibrated with only one head level from normal piezometers (Table 4.1). Secondly, the shallowness of the river narrows the distance between the constant head boundary condition of surface water level and the layers of interest of the sediment in the upper subsurface. This proximity becomes beneficial for accurate reproduction of heads as reported by Wondzell et al. (2009). The decreasing proximity of the head observations with depth from the top boundary condition of SW can explain the increase of residuals described in Figure 4.6. Wondzell et al. (2009) also indicate how the application of groundwater models in areas of narrow valleys facilitates a tighter bond of the model with the lateral boundary conditions. This is the case of River Schlaube where slopes tightly delimit the boundaries of the hyporheic area (Figure 4.1), improving the fit of the estimated versus the observed heads. The strong influence of slopes on head levels can also

The spatial patterns of exchange revealed by the models in the sediment-water interface are in agreement with the spatial and in-depth configuration of hydraulic gradients. Neutral areas along transects TR1 and TR2 (in grey in Figure 4.7a) correspond well to the areas where hydraulic gradients concentrate at the deep levels of multi-level-piezometers. The existence of such high hydraulic gradients in deep levels suggests the blockage of exchanges in an intermediate level of the sediment (intermediate in respect to the length of multi-level piezometers) as shown in Figure 3.4. Conversely, upwelling areas along Transects TR3 and especially TR4 (in blue in Figure 4.7a) are in agreement with the high groundwater gradients observed in the uppermost levels of multi-level piezometers at these locations. At TR3 and TR4, additionally, groundwater heads at level z = - 0.82 m are

significantly over SW level (up to 25 cm) with gradients concentrated immediately below the sediment-water interface.

The choice of the cell size at the approximate size of bedforms enables small scale (sub-meter) identification of upwelling and downwelling areas such as the localized strong downwelling in the left margin between TR2 and TR3 (Figure 4.7a). This small downwelling point is located where transient FO-DTS analysis located interflow discharge (Figure 2 and 3, Chapter 2). The 0.2 x 0.2 m cell size also allows characterization of the small scale heterogeneity of groundwater gradients in the uppermost layer of the sediment-water interface. This gradient heterogeneity causing high variability on the direction of the flux exchanges at the sediment-water interface (Figure 4.8) can be attributed to the interaction of streambed morphology (bedforms) and groundwater heads. High-resolution surveys of the streambed are already feasible with techniques such as laser-scanner (Brasington et al., 2012) but additional high-resolution measurements of head data would be necessary to capture the sub-meter scale variability of hydraulic gradients in the sediment-water interface. The microgravity techniques able to measure head variations can still only operate at the aquifer scale (Piccolroaz et al., 2015), far from the sub-meter scale required for HEF. Meanwhile, densifying the network of piezometers (especially with multi-level piezometers) in areas of sharper longitudinal and transversal groundwater gradients would improve the accuracy of the small scale estimates. The indirect identification of areas of higher groundwater levels with techniques such as FO-DTS (as described in Chapter 2) could help to identify the optimal location for the densified network of piezometers.

The difference between the multi-layered and the distributed models is greater in the spatial distribution of the flux than in the values of flux (Figure 4.7b). The distributed model that integrates distributed heterogeneity data from geophysics outperforms the multi-layered model defined based only on a few profiles from the shallower subsurface (down to -0.8 m) on reproducing the neutral areas along TR1 and TR2 and the exchange area of TR3 and especially of TR4. Thus, the detail on heterogeneity provided by EMI geophysics, even after classifying K_s in hydrofacies, favours the distributed model. These results are consistent with previous studies Conant (2004) and Brookfield & Sudicky (2012). The net upwelling flow of the reach of the study was 5.8 L/s in the multi-layered model and 8.6 L/s in the distributed model close to the 10 L/s measured with differential gauging. The difference in flux

simulations favourable for the distributed model is also described by the negative values of Figure 4.7b. These results are consistent with previous studies (Wondzell et al., 2009), where models with more detailed spatial distributions of K also have higher estimates of hyporheic exchange flows.

The results of heat transport modelling with MT3D-USGS provide also insights into the reliability of the simulations. The simulated spatial patterns of temperatures in the sediment-water interface (Figure 4.9) are in good agreement with the observed in the temperature maps of FO-DTS, particularly for the areas of anomalies identified in Figure 2, Chapter 2, regions delimited in blue and red in Figure 4.9. The multi-layered model shows lower capabilities than the distributed model to reproduce both the areas without anomalies along TR1 and TR2 and the temperature anomalies related to groundwater discharge at TR4 and in particular at TR3. The difference is likely related to the more realistic definition of the hydraulic conductivities in the distributed case. Since EMI geophysics can identify vertical structures of hydraulic conductivity favourable for groundwater discharge at Transects TR3 and TR4, the distributed definition likely outperforms the layered definition thanks to including the vertical preferential paths of exchange (Figure 4.5). This capability also serves to properly identify the regions without vertical connectivity. In between TR1 and TR2 the distributed model shows warmer temperature anomalies than the multi-layered model (Figure 4.9b), indicating the capability of the first to better recognize the clogging conditions preventing exchange. In terms of quantifying the simulated temperatures at the sediment-water interface, again the distributed model provides better results. The temperatures at the areas of groundwater discharge are less underestimated by the distributed model (Figure 4.10a and b). Conversely, both the multi-layered and distributed model tend to underestimate the cold temperature anomaly at TR3.

Neglecting the influence of streamflow in the temperatures of the sediment-water interface is likely the reason for this underestimation. Streamflow velocities in the downstream face of the point-bar/dune at TR3 may pump GW discharge increasing the anomaly. Brookfield et al. (2009) already indicated this effect for the upstream face of bedforms, where the advection of warm stream water entering the streambed tends to heat the shallow subsurface. Furthermore, the existence of hyporheic paths due to stream water inflow into the sediment may create concentrated regions of groundwater discharge (Brookfield &

Sudicky, 2012). In areas TR3 and TR4 there is an overlap of groundwater discharge areas with regions of quick streamflow. The plume-like appearance of this groundwater discharge areas from above (especially visible in Figure 2, Chapter 2) is likely linked to the existence of important horizontal hyporheic flows. This is consistent with the studies highlighting the key role of streamflow and bedform morphology interaction in the definition of flux exchanges (Boano et al., 2006; Cardenas & Wilson, 2007). These limitations related to streamflow could be avoided by adopting modules of MODFLOW capable to model streamflow (Surface-Water Routing module (SWR)) (Langevin et al., 2012) or by using models able to handle streamflow influence such as Hydrogeosphere (Therrien et al., 2006). The discussion about the difficulties modelling the discharges in the margins of the stream reported by Brunner et al. (2010) is also present in our study.

Regarding thermal properties, some authors indicated the small impact of including average values of thermal properties in the models (Rau et al., 2014), especially taking into consideration the much wider range of variability of hydraulic conductivity values (Anderson, 2005). However, we included in our multi-layered and distributed models the spatial variability of the thermal properties interpolated from the multiple sediment samples, which ensured a lower impact of thermal properties heterogeneity in the accuracy of our results. Sensitivity analysis was performed to identify the most influential thermal parameter in the model which is the coefficient of thermal diffusivity. However, sensitivity analysis indicated no significant impact of thermal diffusivity within the range of values obtained from sediment cores (Table 3.3) on the goodness of fit of the simulations, which allows neglecting the impact of thermal heterogeneity.

To conclude with, we realize that every model is just an inaccurate representation of the reality (Anderson & Woessner, 1992) whose results must be considered as a tool to understand the modelling domain (Kasahara & Wondzell, 2003). Thus, the present study outlines the worth of integrating data from distributed measurement techniques such as FO-DTS and EMI geophysics into 3D modelling of flow and transport of the HZ. EMI geophysics lessens the level of uncertainty related to subsurface heterogeneity in flow models while FO-DTS data allows fine evaluation of heat transport models. These benefits should encourage the hyporheic community to integrate distributed measurements into 3D modelling of hyporheic processes. Future steps should address 3D hyporheic modelling with distributed

data in transient conditions and the improvement of quantification capabilities of the models towards the upscaling of groundwater-surface water interactions.

4.6 Conclusions

The capabilities of 3D groundwater flow and heat transport numerical modelling to reproduce GW-SW interactions increase with the integration of point and distributed data. The contribution of distributed geophysical data to improve modelling capabilities is evaluated comparing a uniform model, a multi-layered model defined in layers based on sediment samples and a distributed model defined by geophysics. The results show how the uncertainty of homogenous models sharply reduces with the integration of head and temperature multi-level point data. A distributed model based on EMI geophysics outperforms both the uniform model and the model defined in multiple layers in reproducing the spatial variability of GW-SW exchanges. The distributed model including structures of vertical hydraulic conductivity indicated by EMI geophysics reproduces better the patterns of temperature anomalies corresponding to areas of concentrated GW discharge, but also those where interactions are prevented due to clogging. These results are in good agreement with the spatial distribution of temperature patterns shown by FO-DTS. Thanks to the high spatial resolution of FO-DTS data, the study identifies limitations of the models on reproducing the temperature patterns of exchange at bedform scale related to the interaction of streamflow dynamics with streambed morphology. To sum up, the study demonstrates the utility of numerical modelling to provide not only better understanding on the influence of multiple factors, such as heterogeneity, on GW-SW interactions but also to expand the identification and quantification of water exchanges beyond point locations. Finally, the study highlights the advantage of integrating point and distributed data to evaluate the performance of the models. These results should encourage hyporheic scientists to integrate point and distributed techniques with 3D heat and transport modelling of the HZ to improve our understanding of GW-SW interactions.

4.7 Acknowledgements

This research is funded by the SMART Joint Doctoral Programme (Science for MAnagement of Rivers and their Tidal systems) within the Erasmus Mundus Programme of

the European Union. This project was funded with support from the European Commission, SGA 2015-1628. I would like to thank Alberto Bellin for all the expertise and guidance provided. His help was always crucial to face the challenges existing in this complex discipline of groundwater modelling.

4.8 References

Anderson, M. P., & Woessner, W. W. (1992). *Applied groundwater modelling. 381* p. Academic, San Diego, California.

Anderson, M. P. (2005). Heat as a Ground Water Tracer. *Groundwater, 43*: 951-968. https://doi.org/10.1111/j.1745-6584.2005.00052.x

Bakker, M. (2014). Python Scripting: The Return to Programming. *Groundwater*, 52: 821-822. https://doi.org/10.1111/gwat.12269

Bakker, M., Post, V., Langevin, C. D., Hughes, J. D., White, J. T., Starn, J. J., & Fienen, M. N. (2016). Scripting MODFLOW Model Development Using Python and FloPy. *Groundwater*, *54*(5), 733-739. https://doi.org/10.1111/gwat.12413

Barlow, P. M., & Harbaugh, A. W. (2006). USGS directions in MODFLOW development. *Groundwater, 44*(6), 771-774. https://doi.org/10.1111/j.1745-6584.2006.00260.x

Bedekar, V., Morway, E.D., Langevin, C.D., and Tonkin, M., (2016). MT3D-USGS version 1: A U.S. Geological Survey release of MT3DMS updated with new and expanded transport capabilities for use with MODFLOW. *U.S. Geological Survey Techniques and Methods* 6-A53, 69 p. https://doi.org/10.3133/tm6A53

Boano, F., Camporeale, C., Revelli, R., & Ridolfi, L. (2006). Sinuosity‐driven hyporheic exchange in meandering rivers. *Geophysical Research Letters, 33*(18). https://doi.org/10.1029/2006GL027630

Brasington, J., Vericat, D., & Rychkov, I. (2012). Modelling river bed morphology, roughness, and surface sedimentology using high-resolution terrestrial laser scanning. *Water Resources Research, 48*(11). https://doi.org/0.1029/2012WR012223

Brookfield, A. E., Sudicky, E. A., Park, Y. J., & Conant Jr, B. (2009). Thermal transport modelling in a fully integrated surface/subsurface framework. *Hydrological Processes, 23*(15), 2150-2164. https://doi.org/10.1002/hyp.7282

Brookfield, A. E., & Sudicky, E. A. (2012). Implications of hyporheic flow on temperature-based estimates of groundwater/surface water interactions. *Journal of Hydrologic Engineering*, *18*(10), 1250-1261. https://doi.org/10.1061/(ASCE)HE.1943-5584.0000726

Brosten, T. R., Day-Lewis, F. D., Schultz, G. M., Curtis, G. P., & Lane Jr, J. W. (2011). Inversion of multi-frequency electromagnetic induction data for 3D characterization of hydraulic conductivity. *Journal of Applied Geophysics,* 73(4), 323-335. https://doi.org/10.1016/j.jappgeo.2011.02.004

Brunner, P., Simmons, C. T., Cook, P. G., & Therrien, R. (2010). Modelling surface water-groundwater interaction with MODFLOW: some considerations. *Groundwater*, *48*(2), 174-180. https://doi.org/10.1111/j.1745-6584.2009.00644.x

Cardenas, M. B., Wilson, J. L., & Zlotnik, V. A. (2004). Impact of heterogeneity, bed forms, and stream curvature on subchannel hyporheic exchange. *Water Resources Research, 40*(8). https://doi.org/10.1029/2004WR003008

Cardenas, M. B., & Wilson, J. L. (2007). Thermal regime of dune-covered sediments under gaining and losing water bodies. *Journal of Geophysical Research: Biogeosciences*, *112*(G4). https://doi.org/10.1029/2007JG000485

Conant Jr, B. (2004). Delineating and quantifying groundwater discharge zones using streambed temperatures. *Groundwater*, *42*(2), 243-257. https://doi.org/10.1111/j.1745-6584.2004.tb02671.x

Domenico, P. A., & Schwartz, F. W. 1990. *Physical and chemical hydrogeology*.

Ferguson, G., & Bense, V. (2011). Uncertainty in 1D heat‐flow analysis to estimate groundwater discharge to a stream. *Groundwater, 49*(3), 336-347. https://doi.org/10.1111/j.1745-6584.2010.00735.x

Furman, A. (2008). Modelling coupled surface-subsurface flow processes: A review. *Vadose Zone Journal, 7*(2), 741-756. https://doi.org/10.2136/vzj2007.0065

Gaona, J., Meinikmann, K.,& Lewandowski, J. (2019). Identification of groundwater exfiltration, interflow discharge and hyporheic exchange flows by fiber-optic distributed temperature sensing supported by electromagnetic induction geophysics. *Hydrological Processes*. https://doi.org/10.1002/hyp.13408

Gelhar, L. W., Welty, C., & Rehfeldt, K. R. (1992). A critical review of data on field-scale dispersion in aquifers. *Water Resources Research*, *28*(7), 1955-1974. https://doi.org/10.1029/92WR00607

Gooseff, M., Anderson, J., Wondzell, S., LaNier, J., and Haggerty, R. A. (2006) modelling study of hyporheic exchange pattern and the sequence, size, and spacing of stream bedforms in mountain stream networks. *Hydrological Processes*, *20*, 2443–2457. https://doi.org/10.1002/hyp.6349

Hanson, R. T., Boyce, S. E., Schmid, W., Hughes, J. D., Mehl, S. W., Leake, S. A., ... & Niswonger, R. G. (2014). One-water hydrologic flow model (MODFLOW-OWHM) (No. 6-A51). US Geological Survey.

Harbaugh, A. W. (2005). MODFLOW-2005, the US Geological Survey modular ground-water model: the ground-water flow process (p. 253). Reston, VA. *US Department of the Interior, US Geological Survey*.

Harbaugh, A.W., Langevin, C.D., Hughes, J.D., Niswonger, R.N., and Konikow, L. F., 2017, MODFLOW-2005 version 1.12.00, the U.S. Geological Survey modular groundwater model. *U.S. Geological Survey Software Release*, 03 February 2017.

Harvey, J. W., & Bencala, K. E. (1993). The effect of streambed topography on surface‐subsurface water exchange in mountain catchments. *Water Resources Research, 29*(1), 89-98. https://doi.org/10.1029/92WR01960

Irvine, D. J., Lautz, L. K., Briggs, M. A., Gordon, R. P., & McKenzie, J. M. (2015). Experimental evaluation of the applicability of phase, amplitude, and combined methods to determine water flux and thermal diffusivity from temperature time series using VFLUX 2. *Journal of Hydrology*, *531*, 728-737. https://doi.org/10.1016/j.jhydrol.2015.10.054

Kalbus, E., Schmidt, C., Molson, J. W., Reinstorf, F., & Schirmer, M. (2009). Influence of aquifer and streambed heterogeneity on the distribution of groundwater discharge. *Hydrology and Earth System Sciences*, *13*(1), 69-77.

Kasahara, T., & Wondzell, S. M. (2003). Geomorphic controls on hyporheic exchange flow in mountain streams. *Water Resources Research*, *39*(1), SBH-3. https://doi.org/10.1029/2002WR001386

Langevin, C.D., Thorne, D.T., Jr., Dausman, A.M., Sukop, M.C., and Guo, W., 2007, SEAWAT Version 4: A Computer Program for Simulation of Multi-Species Solute and Heat Transport. *U.S. Geological Survey Techniques and Methods*. Book 6, Chapter A22, 39 p.

Lohman, S. W. (1972). Ground-water hydraulics. US Geological Survey Professional Paper, 708.

Lautz, L. K., & Siegel, D. I. (2006). Modelling surface and groundwater mixing in the hyporheic zone using MODFLOW and MT3D. *Advances in Water Resources*, *29*(11), 1618-1633. https://doi.org/10.1016/j.advwatres.2005.12.003

McLachlan, P.J., Chambers, J.E., Uhlemann, S.S. & Binley, A. (2017). Geophysical characterisation of the groundwater-surface water interface. *Advances in Water Resources*, *109*, 302-319. https://doi.org/10.1016/j.advwatres.2017.09.016

Niswonger, R.G., Panday, Sorab, and Ibaraki, Motomu, 2011, MODFLOW-NWT, A Newton formulation for MODFLOW-2005. *U.S. Geological Survey Techniques and Methods*. 6-A37, 44 p.

Noorduijn, S. L., Shanafield, M., Trigg, M. A., Harrington, G. A., Cook, P. G., & Peeters, L. (2014). Estimating seepage flux from ephemeral stream channels using surface water and groundwater level data. *Water Resources Research, 50*(2), 1474-1489. https://doi.org/10.1002/2012WR013424

Packman, A. I., & Bencala, K. E. (2000). Modelling methods in the study of surface-subsurface hydrologic interactions. *In Streams and Ground Waters* (pp. 45-80). Academic Press.

Piccolroaz, S., Majone, B., Palmieri, F., Cassiani, G., & Bellin, A. (2015). On the use of spatially distributed, time‐lapse microgravity surveys to inform hydrological modelling. *Water Resources Research, 51*(9), 7270-7288. https://doi.org/10.1002/2015WR016994.

Poeter, E. P., & Hill, M. C. (1999). UCODE, a computer code for universal inverse modelling. *Computers & Geosciences*, *25*(4), 457-462. https://doi.org/10.1016/S0098-3004(98)00149-6

Poeter, E., Hill, M.C., Lu, D., Tiedeman, C.R., & Mehl, M. (2014). UCODE_2014, with new capabilities to define parameters unique to predictions, calculate weights using simulated values, estimate parameters with SVD, evaluate uncertainty with MCMC, and more. *Integrated Groundwater Modelling Center Report Number* GWMI 2014-02

Pollock, D.W. (2016). User guide for MODPATH Version 7 - A particle-tracking model for MODFLOW. *U.S. Geological Survey Open-File Report* 2016-1086, 35 p.. https://doi.org/10.3133/ofr20161086

QGIS Development Team (2019). QGIS Geographic Information System. Open Source Geospatial Foundation Project. http://qgis.org".

Rau, G. C., Andersen, M. S., McCallum, A. M., Roshan, H., & Acworth, R. I. (2014). Heat as a tracer to quantify water flow in near-surface sediments. *Earth-Science Reviews*, *129*, 40-58. https://doi.org/10.1016/j.earscirev.2013.10.015

Rosenberry, D.O., Briggs, M.A., Voytek, E.B., & Lane, J.W. (2016). Influence of groundwater on the distribution of dwarf wedgemussels (Alasmidonta heterodon) in the upper reaches of the Delaware River, northeastern USA. *Hydrology and Earth System Sciences,20*(10): 4323–4339. https://doi.org/10.5194/hess-20-4323-2016

Rossetto, R., De Filippis, G., Borsi, I., Foglia, L., Cannata, M., Criollo, R., & Vázquez-Suñé, E. (2018). Integrating free and open source tools and distributed modelling codes in GIS environment for data-based groundwater management. *Environmental Modelling & Software, 107*:210-230. https://doi.org/10.1016/j.envsoft.2018.06.007

Rubin, Y., & Dagan, G. (1992). A note on head and velocity covariances in three‐dimensional flow through heterogeneous anisotropic porous media. *Water resources research, 28*(5), 1463-1470. https://doi.org/10.1029/92WR00107

Salehin, M., Packman, A. I., & Paradis, M. (2004). Hyporheic exchange with heterogeneous streambeds: Laboratory experiments and modelling. *Water Resources Research, 40*(11). https://doi.org/10.1029/2003WR002567

Schmidt, C., Bayer-Raich, M., & Schirmer, M. (2006). Characterization of spatial heterogeneity of groundwater-stream water interactions using multiple depth streambed temperature measurements at the reach scale. *Hydrology and Earth System Sciences Discussions, 3*(4), 1419-1446. https://doi.org/10.5194/hess-10-849-2006

Schornberg, C., Schmidt, C., Kalbus, E., & Fleckenstein, J. H. (2010). Simulating the effects of geologic heterogeneity and transient boundary conditions on streambed temperatures—Implications for temperature-based water flux calculations. *Advances in Water Resources, 33*(11), 1309-1319. https://doi.org/10.1016/j.advwatres.2010.04.007

Shanafield, M., McCallum, J. L., Cook, P. G., & Noorduijn, S. (2016). Variations on thermal transport modelling of subsurface temperatures using high-resolution data. *Advances in Water Resources*, *89*, 1-9. https://doi.org/10.1016/j.advwatres.2015.12.018

Shope, C. L., Constantz, J. E., Cooper, C. A., Reeves, D. M., Pohll, G., & McKay, W. A. (2012). Influence of a large fluvial island, streambed, and stream bank on surface water‐groundwater fluxes and water table dynamics. *Water Resources Research, 48*(6). https://doi.org/10.1029/2011WR011564

Storey, R. G., Howard, K. W., & Williams, D. D. (2003). Factors controlling riffle‐scale hyporheic exchange flows and their seasonal changes in a gaining stream: A three-dimensional groundwater flow model. *Water Resources Research*, 39(2). https://doi.org/10.1029/2002WR001367

Therrien, R., McLaren, R. G., Sudicky, E. A., & Panday, S. M. (2010). HydroGeoSphere: A three-dimensional numerical model describing fully-integrated subsurface and surface flow and solute transport. Groundwater Simulations Group, University of Waterloo, Waterloo, ON.

Wondzell, S. M., & Swanson, F. J. (1996). Seasonal and storm dynamics of the hyporheic zone of a 4th-order mountain stream. I: Hydrologic processes. *Journal of the North American Benthological Society, 15*(1), 3-19. https://doi.org/10.2307/1467429

Wondzell, S. M., LaNier, J., & Haggerty, R. (2009). Evaluation of alternative groundwater flow models for simulating hyporheic exchange in a small mountain stream. *Journal of Hydrology*, *364*(1-2), 142-151. https://doi.org/j.jhydrol.2008.10.011

Wroblicky, G. J., Campana, M. E., Valett, H. M., & Dahm, C. N. (1998). Seasonal variation in surface‐subsurface water exchange and lateral hyporheic area of two stream‐aquifer systems. *Water Resources Research, 34*(3), 317-328. https://doi.org/10.1029/97WR03285

Zheng, C. (1990). MT3D. A modular three-dimensional transport model for simulation of advection, dispersion, and chemical reactions of contaminants in groundwater systems. *Report to the Kerr Environmental Research Laboratory*. US Environmental Protection Agency. Ada, Oklahoma.

Zheng, C., & Wang, P. P. (1999). MT3DMS: a modular three-dimensional multispecies transport model for simulation of advection, dispersion, and chemical reactions of contaminants in groundwater systems. *Documentation and user's guide*. Alabama Univ University.

Chapter 5: General discussion

5.1 Rationale and research aims

The number of studies on GW-SW interfaces (hyporheic zones) increased significantly during recent decades due to the extraordinary relevance of the HZ for many hydrological, biogeochemical and ecological processes in adjacent compartments (Boulton et al., 1998). Increasing research efforts focus on water exchange in the HZ and on factors governing exchange across multiple spatial and temporal scales (Palmer, 1993; White, 1993). Combining different techniques is required to investigate HEF across scales (Krause et al., 2010). Adopting this approach resulted in the sequence of hyporheic studies of the present thesis. Although the number of studies applying the multi-technique approach is increasing, most of them focus on the individual aims of identifying, quantifying or modelling HEF (e.g. Lautz & Siegel, 2006; Hare et al., 2015; Gonzalez-Pinzón et al., 2015). There is need for studies merging all the activities required for HEF investigation from measurement to simulation. The chapters of the present PhD thesis focus on compiling the three main tasks required for full HEF characterization: identification, quantification and upscaling of HEF across scales. This sequence provides an overview of the advances and limitations of the techniques applied for each of the three tasks and their combinations. Additionally, general implications for hyporheic investigation are described. The following section describes briefly the contributions of each chapter.

5.2 Key research findings

The present thesis shows the advantages and limitations of combining different techniques for identification, quantification and upscaling of HEF with a multi-scale approach. The thesis reveals (1) the possibility to distinguish the different components of GW-SW interactions, (2) the capabilities and limitations of 1D methods for estimating vertical fluxes at locations with strong upwelling in heterogeneous streambeds, and (3) the opportunity to upscale the characterization of GW-SW interactions across scales by means of numerical modelling. The sequence of results successfully compiles the activities required for HEF investigation as pursued. The key findings of each chapter are detailed below:

Chapter 2

The combination of two distributed techniques enables the differentiation of different components of GW-SW interaction based on their spatial and temporal patterns. Fiber-optic distributed temperature sensing (FO-DTS) is capable to capture spatial and temporal temperature patterns at the sediment-water interface while electromagnetic induction geophysics (EMI) provides a distributed characterization of the subsurface patterns of hydraulic conductivity.

iv. The first component of GW-SW interaction identified using FO-DTS is groundwater discharge, which creates permanent cold temperature anomalies during summer and warm temperature anomalies during winter. The areas of permanent temperature anomalies tend to be located where EMI geophysics detects subsurface structures of high hydraulic connectivity.

v. Interflow discharge can be identified based on the temporal evolution of the patterns of the temperature anomalies present close to the shoreline of the river after episodes of heavy rainfall. During such events, these temperature anomalies show sharp increases of area and magnitude, which fade away within days or weeks after the rain events.

vi. The third component of HEF identifiable with FO-DTS is local downwelling during floods. FO-DTS is able to capture the sudden temperature changes in temperature at certain areas of the sediment-water interface caused by the infiltration of SW with altered temperature into the hyporheic zone. By calculating the rates of temperature change of the sediment-water interface it is possible to identify the local downwelling areas quickly adopting the altered temperature of SW. The spatial distribution of these patterns is in agreement with the distribution of downwelling determined by bedforms.

Chapter 3

The evaluation of several 1D methods for estimating the vertical component of HEF identifies their advantages and limitations and provides insight into the factors impacting HEF.

i. 1D methods provide at least valuable qualitative recognition of exchanges in the HZ. The methods concur in the vertical distribution of flux exchanges, whose vertical sequence

allows interpreting the structure of the uppermost meter of the HZ. Disagreement increases when comparing the flux magnitudes. Particularly arguably are the results from the analytical solutions based on the phase-shift of the temperature signal. Complex hyporheic conditions still challenged flux quantification by 1D methods.

ii. Determining sediment properties contributed largely to the reliability of the methods of flux estimation. Methods demanding fewer sediment data are the ones less in agreement with the distribution and magnitude of fluxes compared to the methods demanding more data (e.g. 1DTempPro).

iii. The strong upwelling reduces the downward directed penetration depth of thermal signals. As a consequence, the temperature signal in the sediment might be insufficient for calculating vertical fluxes based on temperature-depth profiles even at the uppermost sensors of the temperature profiles. Conversely, under upwelling conditions, the vertical hydraulic methods exhibit larger data to noise ratios, which despite the method's low resolution enhance the performance up to the accuracy of thermal methods.

iv. The heterogeneous patterns of hydraulic and thermal depth gradients in the HZ are caused by HEF and subsurface anomalies. Hydraulic and temperature gradients characterize vertical flux in steady upwelling areas, but the range of vertical fluxes from neutral and downwelling areas may be biased without repeated measurements. Indeed, the temporal variability of fluxes shown in the results of transient thermal methods recommends collecting time series not only of temperature but also of hydraulic gradients.

v. The horizontal flow component strongly reduces the reliability of vertical flux estimates. Few methods can evaluate this impact based on the alterations of thermal diffusivity. Thus, qualitative identification of the sediment structures prone to advective influence is beneficial.

Chapter 4

The integration of point and distributed data into three-dimensional (3D) numerical models of flow and heat transport enable reproducing GW-SW interactions. Modelling enables the upscaling of HEF estimates and the evaluation of the influence of hyporheic drivers on HEF.

i. The vertical hydraulic heads significantly improve model calibration. The performance of multi-layered models based on sediment profiles is superior to the uniform models but inferior to models defined based on geophysics data.

ii. Distributed data of EMI geophysics and FO-DTS is also beneficial for HZ models. The distributed model defined with EMI data shows better fitting statistics compared to the ones of the multi-layered model based on sediment cores. The distributed model outperforms the multi-layered model on reproducing the temperature patterns at the sediment-water interface, both in area and magnitude of GW anomalies.

iii. Flux estimates of 3D heat and transport models can be compared with those of 1D methods. Compared to the restrictive assumptions of 1D methods, the detailed parametrization of 3D models provides a realistic framework for estimating HEF. Net flux balance of the reach of the 3D models is similar to the streamflow gain obtained from differential gauging, while the net balance of the1D methods differs in an order of magnitude. Modelling can additionally describe flux direction, the horizontal component of HEF and the depth and width of the HZ.

iv. 3D flow and heat transport modelling enables upscaling of water exchanges in the HZ. While the accuracy of the estimates is still restricted to the range of scales of the input data and the resolution of the model domain, modelling allows quantifying HEF at any location.

5.3 Specific implications for multi-scale hyporheic characterization

The set of key findings described above aim to help hyporheic scientist to design the optimal approach for the identification, quantification and simulation of HEF. Particular implications of the results of the present thesis are discussed below.

5.3.1 Identification of the spatiotemporal patterns of the components of HEF

One objective of the present study is to identify the different patterns of HEF with distributed techniques. The study illustrates the multiple capabilities of fiber-optic distributed temperature sensing (FO-DTS) for investigations of surface water-groundwater interactions. FO-DTS has sufficient resolution and accuracy at both spatial and temporal scales to determine different components of HEF (Gaona et al., 2019). While the identification of

spatial patterns of groundwater discharge has been reported in previous studies (Lowry et al., 2007; Krause et al., 2012; Leonard et al., 2018), the interflow discharge has only been described using another thermal distributed technique: thermal infrared reflectometry (TIR) (Hare et al., 2015). However, this TIR application did not report the temporal evolution of temperature anomalies after rains. Furthermore, the local patterns of temperature related to upwelling and downwelling sites were long ago reported from individual riffle locations (White et al., 1987; Evans & Petts, 1997). However, using FO-DTS we offer a systematic method for identifying such patterns simultaneously across the whole river reach. Thus, the main contribution of the published second chapter of the present thesis (Gaona et al., 2019) is to identify different components of exchange based on their distinct spatiotemporal patterns of temperature anomalies.

The applicability range of FO-DTS (Tyler et al., 2009) facilitates the observation of the thermal footprints left by HEF at different scales at the sediment-water interface. Results of Chapter 2 demonstrate the capability of the technique to measure from sub-meter to hundreds of meters scale (Selker et al., 2006a). Additionally, the use of densified layouts (i.e. in multiple transversal lines of fiber-optic cable across the stream (Figure 1, Chapter 2) proves convenient for identifying the spatiotemporal patterns of temperature anomaly in the sediment-water interface attributed to the distinct components of HEF. Most of the existing studies only deployed one or a few lines along the river (e.g. Selker et al., 2006b; Lowry et al., 2007; Westhoff et al., 2011; Krause et al., 2012), which proves insufficient to cover the 2D nature of HEF at the sediment-water interface, particularly for the sub-meter local patterns of downwelling. We recommend adopting a densified layout in transversal direction to capture the spatial heterogeneity of GW-SW interactions.

Furthermore, Chapter 2 also shows the convenience of collecting FO-DTS time series of the sediment-water interface to identify the HEF components of relevant temporal variability such as interflow and local SW downwelling (Gaona et al., 2019). However, the sudden nature of floods can challenge scientist's capacity to prepare FO-DTS measurement in the few hours before the flood arrival. In order to facilitate capturing the short-term variability of HEF processes such as floods, we recommend configuring FO-DTS devices with remote control capabilities for long-term monitoring such as the one developed by Kurth et al. (2013). Despite the generation of big amounts of data, the analysis of long FO-

DTS time series would improve our understanding of the temporal dynamics of interflow and the distribution of up-/downwelling areas across the streambed. Furthermore, the integration of FO-DTS HEF measurements in real-time hydrological observation networks would help water managers to improve the policies for the effective control of environmental flows, aquifer recharge, etc., in the same way, they proved useful for evaluating the effectiveness of river restoration (Kurth et al., 2015).

The other distributed techniques used in Chapter 2 (Gaona et al., 2019), EMI geophysics, provides helpful insights into the impacts of heterogeneity on the distribution of HEF. This is in line with previous works (Binley et al., 2015). The exploration of the subsurface at the reach scale with the CMD-explorer shown in Figure 5 of Chapter 2 illustrates mainly the geological heterogeneity and its impact on the distribution of HEF patterns. The interpretation of EMI data as patterns of hydraulic conductivity largely concurs with the identification of patterns of GW-SW interaction based on FO-DTS. Thus, the technique is consistently able to support other non-geophysical techniques for hyporheic investigations, in agreement with previous studies (Rosenberry et al., 2016; Busato et al., 2018). The combined interpretation (Gaona et al., 2019) of EMI and FO-DTS, additionally provides helpful insights to improve the experimental design, particularly to decide the optimal locations for estimating HEF with 1D vertical methods. However, the EMI geophysics exploration included in Chapter 2 evidences the need to explore also the local heterogeneity related to bedform morphology in the shallower part of the HZ. The application of EMI devices of better resolution in the shallow subsurface would be particularly valuable at sites with natural conditions such as the River Schlaube where woody debris significantly impacts sediment and HEF patterns (Lautz et al., 2006a). The application of geophysical devices adapted to larger scales should also be encouraged. Boaga, (2017) reports the possibility to explore the subsurface from sub-meter to hundreds of meters, a range that would facilitate identifying subsurface structures from bedforms to watersheds (Abdu et al., 2008). Agencies are devoting significant efforts to apply these tools to larger scales (i.e. CSIRO: English et al., 2004). There are still challenges on the feasibility of using them beyond research but there is also great interest in these developments which have the potential to upscale the characterization of GW-SW interactions on basin scales. The

popularization of this type of data would spread the application of hydrogeophysics among hyporheic scientist.

5.3.2 Quantification of the vertical component of HEF

Chapter 3 illustrates the advantages and limitations of using the point techniques to quantify HEF. Depth profiles are useful to capture the in-depth variability of HEF due to sediment heterogeneities (Krause et al., 2012). Our study shows the usefulness of vertical hydraulic and thermal gradients in the HZ to estimate vertical fluxes with 1D analytical and numerical methods, which is in agreement with multiple previous studies (Conant, 2004; Schmidt et al., 2006; Gordon et al., 2012; Bhaskar et al., 2012). However, we also remark the limited accuracy of these methods under complex HZ conditions (Rau et al., 2015), particularly under strong upwelling restricting the propagation of the temperature signal (Briggs et al., 2014) or when the assumption of pure vertical flux neglects the multi-dimensionality of HEF (Irvine et al., 2015; Munz et al., 2016). Collecting temperature profiles at milimeter resolution with high precision could solve the issue of limited propagation of the temperature signal, e.g., by coiling the FO-DTS cable round a stick to measure depth profiles (Vogt et al., 2010). Unfortunately, this alternative which would have solved the limitations of our sensor spacing (Shanafield et al., 2011) insufficient for the shallow extinction depth (Briggs et al., 2014) was not applied at our study site.

Despite multiple limitations, the present study shows the benefits of calculating HEF time series by VFLUX (Irvine et al., 2015b) and 1DTempPro (Koch et al., 2015). The reliability of the estimates can be evaluated based on the stability of thermal parameters along the time series. Other improvements of the vertical models have been developed to handle nonlinear temperature depth-profiles (Kurylyk, 2017) and multiple frequencies of temperature signals (Luce et al., 2017). However, further research is required to improve the capability of 1D models to deal with the complexity of HEF (Rau et al., 2015). An alternative to overcome the limitations of the unrealistic assumptions of the vertical 1D methods is heat-pulse methods capable to define the direction and velocity of hyporheic flow by processing the breakthrough curves of temperature pulses emitted and measured by the device (Lewandowski et al., 2011; Banks et al., 2018).

Finally, the present study demonstrates that on the one hand, point techniques (Figure 3.4) are of great value to identify subsurface structures (Schmidt et al., 2006), and can support the interpretation of exchange patterns identified with distributed techniques. On the other hand, distributed techniques can be used to find the optimal places for point measurements. This interdependency highlights the benefit of combining point and distributed techniques to untangle the complex patterns of HEF across scales (Gonzalez-Pinzón et al., 2015).

5.3.3 Modelling of flow and heat transport of the HZ

The fourth chapter of the present PhD thesis evaluates the capabilities of 3D numerical modelling of flow and heat transport in the HZ. The model aims to assess the benefits of integrating point and distributed data in the 3D models, serve as a tool for studying the impact of individual factors such as sediment heterogeneity on HEF, and upscale HEF estimations.

Our modelling approach illustrates the possibility to integrate point and distributed measurements into the model parametrization and calibration. Despite the challenge of adapting the geometry and parametrization of the model to the data, the flexibility of current models (e.g. able to handle irregular gridding and zonification) represents a barely explored opportunity (Shanafield et al., 2016). The increasing customization capabilities of models help to adopt a multi-scale combination of techniques to study the HZ (Krause et al., 2011; Gonzalez-Pinzón et al., 2015). The integration of the observed hydraulic and thermal gradients in the models improve their performance and facilitates evaluating how hydraulic gradients drive HEF at different depths, which also allows determining the depth of the HZ. Including detailed planimetry of the riverbed into the models allows modelling the spatial patterns of hydraulic gradients caused by bedforms in the uppermost centimeters of the HZ (Figure 4.8a), which has not been frequently done yet based on field data (Gooseff et al., 2006). However, only computational fluid dynamics (CFD) methods can reproduce the dynamic interactions of bedforms and hydraulic gradients (Trauth et al., 2013).

The spatial patterns of hydraulic gradients can also be caused by subsurface heterogeneity. Comparing a 3D MODFLOW model with uniform sediment definition and 3D MODFLOW models with layered or distributed definition of the subsurface hydraulic

conductivity provides valuable insights about the influence of layering and heterogeneity. The distributed model including a detailed definition of the sediment heterogeneity outperforms the layered and uniform flow models on reproducing the areas of preferential GW-SW interactions (Table 4.1, Figure 4.9 and 4.10), results in line with previous studies investigating the impact of heterogeneity (Lautz & Siegel, 2006; Wondzell et al., 2006).

Additionally, the integration of distributed geophysical data enhances the capability of the MT3D-USGS model to reproduce the spatial distribution of temperature patterns observed in the sediment-water interface with FO-DTS. The heat transport capabilities of our model are in agreement with the capabilities of Hydrogeosphere (Brookfield & Sudicky, 2012; Shanafield et al., 2016). Models adjusted for the reproduction of temperatures in the sediment-water interface enhance the reliability of HEF estimates (Shanafield et al., 2016). This allows evaluating the estimates calculated with 1D vertical methods Brookfield & Sudicky (2012), which improves our understanding of the factors impacting the reliability of 1D methods.

In any case, the possibility to estimate HEF values at any location in the modelled space from the scale of the model cells to the entire model domain opens the path for upscaling. The opportunity to upscale HEF quantification and to expand our understanding of hyporheic processes should encourage hyporheic scientist to embrace modelling activities (Gomez-Velez & Harvey, 2015). However, efforts would be necessary to adapt the modelling tools to challenges such as big datasets generated from data-intense hyporheic investigations (Vogel et al., 2015).

5.4 General implications: benefits of a multiscale interdisciplinary approach

Results from the research presented in this PhD thesis illustrate the convenience of a multi-scale interdisciplinary approach to improve our understanding of the complexity of HEF. Up to now, there are only very few studies using such multi-scale approaches (Magliozzi et al., 2017). Tasks of the present thesis were to identify, quantify, interpret and reproduce the spatial and temporal variation of HEF. Combining the results and insights from these tasks helps to link the fragmentary hyporheic knowledge across scales. The nested

nature of hyporheic processes advocates for adopting techniques able to investigate factors simultaneously on different scales (Gomez-Velez & Harvey, 2014). The present PhD thesis exemplifies this with the multi-scale capability of FO-DTS to distinguish the different components of HEF (groundwater, interflow and local exchange) occurring simultaneously at different spatial and temporal scales (Gaona et al., 2014).

Although the capability of techniques to monitor temporal variability of HEF is always advantageous, scientists have to assess the need to collect temporal data of each variable of interest. Factors such as the subsurface heterogeneity observed with EMI geophysics do not require temporal resolution but conversely demand more effort to combine the results with data from other techniques. The present PhD thesis shows how HEF measurements using point and distributed techniques can be integrated into modelling of the HZ to improve the characterization of the hyporheic processes. The insights provided by that multi-scale and multi-technique approach of the present PhD thesis should encourage hyporheic scientist to use similar combinations of methods. This approach is of special interest regarding the increasing need to integrate different sources of data such as biogeochemical and ecological data with hydrological data in hyporheic investigations (Malcolm et al., 2008b).

Additionally, integrating multiple data sources enhances the reliability of the hyporheic assessments, which can expand the use of hyporheic knowledge to other potential applications. Considering hyporheic processes can help to define water management policies and restoration protocols (Mendoza-Lera & Datry, 2017) able to mitigate the hydrological, biogeochemical and ecological alterations humans cause on rivers.

5.5 Conclusions

The investigation of GW-SW interactions with a multi-technique and multi-scale approach is advantageous for full characterization of HEF from the sub-meter to the reach scale. The present study exemplifies the benefits of combining point and distributed techniques to identify and quantify GW-SW interactions but also for process understanding. Heterogeneous HEF patterns are recognized across a range of scales. The integration of measured field data of the present PhD thesis into a model allows detailed parametrization and calibration of the model which increase its reliability. Models enable the evaluation of

GW-SW interactions beyond the scale of observation and constitute a tool for assessing the factors governing the hyporheic zone processes. Several challenges remain unsolved such as the improvement of the point and distributed techniques, the optimal use of their combination, the integration of their data into modelling and the reliability and power of the models. However, the multi-technique and multi-scale approaches pave the way for an integrative investigation of GW-SW interaction, from the local identification and quantification of the patterns of exchange to their upscaling.

5.6 References

Abdu, H., Robinson, D. A., Seyfried, M., & Jones, S. B. (2008). Geophysical imaging of watershed subsurface patterns and prediction of soil texture and water holding capacity. *Water resources research*, *44*(4). https://doi.org/10.1029/2008WR007043

Banks, E. W., Shanafield, M., Noorduijn, S., McCallum, J., Lewandowski, J., & Batelaan, O. (2018). Active heat pulse sensing of 3-D-flow fields in streambeds. *Hydrology and Earth System Science, 22*, 1917-1929. https://doi.org/10.5194/hess-22-1917-2018

Bhaskar, A. S., Harvey, J. W., & Henry, E. J. (2012). Resolving hyporheic and groundwater components of streambed water flux using heat as a tracer. *Water Resources Research, 48*(8). https://doi.org/10.1029/2011WR011784

Binley, A., Hubbard, S. S., Huisman, J. A., Revil, A., Robinson, D. A., Singha, K., & Slater, L. D. (2015). The emergence of hydrogeophysics for improved understanding of subsurface processes over multiple scales. *Water Resources Research*, *51*(6), 3837-3866. https://doi.org/10.1002/ 2015WR017016

Boaga, J. (2017). The use of FDEM in hydrogeophysics: A review. *Journal of Applied Geophysics*, *139*, 36-46. https://doi.org/10.1016/j.jappgeo.2017.02.011

Boulton, A. J., Findlay, S., Marmonier, P., Stanley, E. H., & Valett, H. M. (1998). The functional significance of the hyporheic zone in streams and rivers. *Annual Review of Ecology and Systematics*, *29*(1). https://doi.org/59-81. 10.1146/annurev.ecolsys.29.1.59

Briggs, M. A., Lautz, L. K., Buckley, S. F., & Lane, J. W. (2014). Practical limitations on the use of diurnal temperature signals to quantify groundwater upwelling. *Journal of Hydrology, 519*, 1739-1751. https://doi.org/10.1016/j.jhydrol.2014.09.030

Brookfield, A. E., & Sudicky, E. A. (2012). Implications of hyporheic flow on temperature-based estimates of groundwater/surface water interactions. *Journal of Hydrologic Engineering*, *18*(10), 1250-1261. https://doi.org/10.1061/(ASCE)HE.1943-5584.0000726

Busato, L., Boaga,J., Perri, M.T., Majone, B., Bellin, A., Cassiani, G., (2018). Hydrogeophysical characterization and monitoring of the hyporheic and riparian zones: The Vermigliana Creek case study. *Science of the Total Environment*, *648*, 1105-1120. https://doi.org/10.1016/j.scitotenv.2018.08.179

Conant Jr, B. (2004). Delineating and quantifying groundwater discharge zones using streambed temperatures. *Groundwater, 42*(2), 243-257. https://doi.org/10.1111/j.1745-6584.2004.tb02671.x

English, P., Richardson, P., Glover, M., Cresswell, H., & Gallant, J. (2004). Interpreting airborne geophysics as an adjunct to hydrogeological investigations for salinity management: Honeysuckle Creek catchment, Victoria. *Technical Report. CSIRO Land and Water*, *18*(4).

Gaona, J., Meinikmann, K., Lewandowski, J. (2019). Identification of groundwater exfiltration, interflow discharge and hyporheic exchange flows by fiber-optic distributed temperature sensing supported by electromagnetic induction geophysics. *Hydrological Processes*. https://doi.org/10.1002/hyp.13408

González-Pinzón, R., Ward, A. S., Hatch, C. E., Wlostowski, A. N., Singha, K., Gooseff, M. N., ... & Brock, J. T. (2015). A field comparison of multiple techniques to quantify groundwater-surface water interactions. *Freshwater Science*, *34*(1), 139-160. https://doi.org/10.1086/679738

Gordon, R. P., Lautz, L. K., Briggs, M. A., & McKenzie, J. M. (2012). Automated calculation of vertical pore-water flux from field temperature time series using the VFLUX

method and computer program. *Journal of Hydrology*, 420, 142-158. https://doi.org/10.1016/j.jhydrol.2011.11.053

Gooseff, M. N., Anderson, J. K., Wondzell, S. M., LaNier, J., & Haggerty, R. (2006). A modelling study of hyporheic exchange pattern and the sequence, size, and spacing of stream bedforms in mountain stream networks, Oregon, USA. *Hydrological Processes*, 20(11), 2443-2457. https://doi.org/10.1002/hyp.6349

Hare, D. K., Briggs, M. A., Rosenberry, D. O., Boutt, D. F., & Lane, J. W. (2015). A comparison of thermal infrared to fiber-optic distributed temperature sensing for evaluation of groundwater discharge to surface water. *Journal of Hydrology, 530*, 153-166. https://doi.org/10.1016/j.jhydrol.2015.09.059

Irvine, D. J., Lautz, L. K., Briggs, M. A., Gordon, R. P., & McKenzie, J. M. (2015). Experimental evaluation of the applicability of phase, amplitude, and combined methods to determine water flux and thermal diffusivity from temperature time series using VFLUX 2. *Journal of Hydrology, 531*, 728-737. https://doi.org/10.1016/j.jhydrol.2015.10.054

Koch, F. W., Voytek, E. B., Day‐Lewis, F. D., Healy, R., Briggs, M. A., Lane Jr, J. W., & Werkema, D. (2016). 1dtemppro v2: New features for inferring groundwater/surface‐water exchange. *Groundwater, 54*(3), 434-439. https://doi.org/10.1111/gwat.12369

Krause, S., Hannah, D. M., Fleckenstein, J. H., Heppell, C. M., Kaeser, D., Pickup, R., Pinay, G., Robertson, A. L. and Wood, P. J. (2011). Inter-disciplinary perspectives on processes in the hyporheic zone. *Ecohydrology, 4*: 481-499. https://doi.org/10.1002/eco.176

Krause, S., Blume, T., & Cassidy, N. J. (2012). Investigating patterns and controls of groundwater up-welling in a lowland river by combining Fiber-optic Distributed Temperature Sensing with observations of vertical hydraulic gradients. *Hydrology and Earth System Science, 16*, 1775-1792. https://doi.org/10.5194/hess-16-1775-2012, 2012.

Kurth, A.-M., Dawes, N., Selker, J., & Schirmer, M. (2013). Autonomous distributed temperature sensing for long-term heated applications in remote areas. *Geoscientific Instrumentation Methods and Data Systems, 2*, 71-77. https://doi.org/10.5194/gi-2-71-2013

Kurth, A.M., Weber, C., & Schirmer, M. (2015). How effective is river restoration in re-establishing groundwater-surface water interactions? – A case study. *Hydrology and Earth System Sciences, 19*, 2663-2672. https://doi.org/10.5194/hess-19-2663-2015, 2015

Kurylyk, B. L., Irvine, D. J., Carey, S. K., Briggs, M. A., Werkema, D., & Bonham, M. (2017). Heat as a groundwater tracer in shallow and deep heterogeneous media: Analytical solution, spreadsheet tool, and field applications. *Hydrological Processes*, 31(14), 2648-2661. https://doi.org/10.1002/hyp.11216

Lautz, L. K., Siegel, D. I., & Bauer, R. L. (2006a). Impact of debris dams on hyporheic interaction along a semi-arid stream. *Hydrological Processes, 20*(1), 183-196. https://doi.org/10.1002/hyp.5910

Lautz, L. K., & Siegel, D. I. (2006b). Modelling surface and groundwater mixing in the hyporheic zone using MODFLOW and MT3D. *Advances in Water Resources*, *29*(11), 1618-1633. https://doi.org/10.1016/j.advwatres.2005.12.003

Leonard, R. M., Kettridge, N., Devito, K. J., Petrone, R. M., Mendoza, C. A., Waddington, J. M., & Krause, S. (2018). Disturbance Impacts on Thermal Hot Spots and Hot Moments at the Peatland-Atmosphere Interface. *Geophysical Research Letters, 45*(1), 185-193. https://doi.org/10.1002/2017GL075974

Lewandowski, J., Angermann, L., Nützmann, G., & Fleckenstein, J. H. (2011). A heat pulse technique for the determination of small‐scale flow directions and flow velocities in the streambed of sand‐bed streams. *Hydrological Processes*, *25*(20), 3244-3255. https://doi.org/10.1002/hyp.8062

Lowry, C. S., Walker, J. F., Hunt, R. J., and Anderson, M. P. (2007). Identifying spatial variability of groundwater discharge in a wetland stream using a distributed temperature sensor. *Water Resources Research, 43*, W10408. https://doi.org/10.1029/2007WR006145

Luce, C. H., Tonina, D., Applebee, R., & DeWeese, T. (2017). Was that assumption necessary? Reconsidering boundary conditions for analytical solutions to estimate streambed fluxes. *Water Resources Research*, 53, 9771– 9790. https://doi.org/10.1002/ 2017WR020618

Mendoza-Lera, C., & Datry, T. (2017). Relating hydraulic conductivity and hyporheic zone biogeochemical processing to conserve and restore river ecosystem services. *Science of the Total Environment*, 579, 1815-1821. https://doi.org/10.1016/j.scitotenv.2016.11.166

Munz, M., Oswald, S. E., & Schmidt, C. (2016). Analysis of riverbed temperatures to determine the geometry of subsurface water flow around in-stream geomorphological structures. *Journal of Hydrology, 539*, 74–87. https://doi.org/10.1016/j.jhydrol.2016.05.012

Palmer, M.A. (1993). Experimentation in the hyporheic zone: challenges and prospectus. *Journal of the North American Benthological Society, 12*.1: 84-93. https://doi.org/10.2307/1467689

Rau, G. C., Cuthbert, M. O., McCallum, A. M., Halloran, L. J., & Andersen, M. S. (2015). Assessing the accuracy of 1-D analytical heat tracing for estimating near-surface sediment thermal diffusivity and water flux under transient conditions. *Journal of Geophysical Research: Earth Surface, 120*(8), 1551-1573. https://doi.org/10.1002/2015JF003466

Rosenberry, D. O., Briggs, M. A., Voytek, E. B., & Lane, J. W. (2016). Influence of groundwater on the distribution of dwarf wedgemussels (Alasmidonta heterodon) in the upper reaches of the Delaware River, northeastern USA. *Hydrology and Earth System Sciences*, *20*(10), 4323-4339. https://doi.org/10.1016/j.scitotenv.2018.08.179

Shanafield, M., Hatch, C., and Pohll, G. (2011). Uncertainty in thermal time series analysis estimates of streambed water flux. *Water Resources Research, 47*(3), W03504. https://doi.org/10.1029/2010WR009574

Shanafield, M., Banks, E. W., Arkwright, J. W., & Hausner, M. B. (2018). Fiber-optic sensing for environmental applications: Where we have come from and what is possible. *Water Resources Research, 54*, 8552‐8557. https://doi.org/10.1029/2018WR022768

Schmidt, C., Bayer-Raich, M., & Schirmer, M. (2006). Characterization of spatial heterogeneity of groundwater-stream water interactions using multiple depth streambed temperature measurements at the reach scale. *Hydrology and Earth System Sciences Discussions*, *3*(4), 1419-1446. https://doi.org/10.5194/hess-10-849-2006

Selker, J. S., Thévenaz, L., Huwald, H., Mallet, A., Luxemburg, W., Van De Giesen, N., ... & Parlange, M. B. (2006a). Distributed fiber-optic temperature sensing for hydrologic systems. *Water Resources Research*, *42*(12). https://doi.org/10.1029/2006WR005326

Selker, J., van de Giesen, N., Westhoff, M., Luxemburg, W., …& Parlange, M. B. (2006b). Fiber-optics opens a window on stream dynamics. *Geophysical Research Letters*, 33, L24401. https://doi.org/10.1029/2006GL027979

Tyler, S. W., Selker, J. S., Hausner, M. B., Hatch, C. E., Torgersen, T., Thodal, C. E., & Schladow, S. G. (2009). Environmental temperature sensing using Raman spectra DTS fiber-optic methods. *Water Resources Research*, *45*(4). https://doi.org/10.1029/2008WR007052

Vogel, R. M., Lall, U., Cai, X., Rajagopalan, B., Weiskel, P. K., Hooper, R. P., & Matalas, N. C. (2015). Hydrology: The interdisciplinary science of water. *Water Resources Research*, *51*, 4409–4430. https://doi.org/10.1002/2015WR017049.

Vogt, T., Schneider, P., Hahn-Woernle, L., & Cirpka, O. A. (2010). Estimation of seepage rates in a losing stream by means of fiber-optic high-resolution vertical temperature profiling. *Journal of Hydrology, 380*(1-2), 154-164. https://doi.org/10.1016/j.jhydrol.2009.10.033

Westhoff, M. C., Gooseff, M. N., Bogaard, T. A., and Savenije, H. H. G. (2011), Quantifying hyporheic exchange at high spatial resolution using natural temperature variations along a first-order stream. *Water Resources Research, 47*, W10508. https://doi.org/10.1029/2010WR009767

White, D. S., Elzinga, C. H., & Hendricks, S. P. (1987). Temperature patterns within the hyporheic zone of a northern Michigan river. *Journal of the North American Benthological Society, 6*(2), 85-91. https://doi.org/10.2307/1467218

White, D.S. (1993). Perspectives on defining and delineating hyporheic zones. *Journal of the North American Benthological Society, 12*.1: 61-69. https://doi.org/10.2307/1467686

Wondzell, S. M., LaNier, J., & Haggerty, R. (2009). Evaluation of alternative groundwater flow models for simulating hyporheic exchange in a small mountain stream. *Journal of Hydrology, 364*(1-2), 142-151. https://doi.org/10.1016/j.jhydrol.2008.10.011

Keywords

Chapter 2

Fiber-optic distributed temperature sensing; groundwater exfiltration; interflow discharge; hyporheic exchange flows; temperature anomaly; flood; electromagnetic induction geophysics; sediment structure.

Chapter 3:

Groundwater-stream water interactions; hyporheic exchange flows, temperature profiles, hydraulic gradients; FLUX-LM; VFLUX; 1DTempPro; vertical sediment heterogeneity.

Chapter 4:

Three-dimensional flow and heat transport, MODFLOW, MT3D-USGS, groundwater-stream water interactions; hyporheic exchange flows, UCODE, PEST, heterogeneity, upscaling.

Statement of academic integrity

I hereby certify that the submitted thesis "Groundwater-stream water interactions: point and distributed measurements and innovative upscaling techniques" is my own work and that all published or other sources of material consulted in its preparation have been indicated. I have clearly pointed out any collaboration that has taken place with other researchers and stated my own personal share in the investigations in the Thesis Outline. I confirm that this work has not been submitted to any other university or examining body for a comparable academic award.

Berlin, 23.04.2019

Jaime Gaona

Acknowledgements

I must start with thanks to the SMART academic board, in particular to Guido Zolezzi and Aureliano Cerreti who notify me the possibility to join the program and tolerate to accept my confirmation and supply of my documents from my sister while I was uncommunicated in Ussuriland. Similarly, I must continue giving thanks to our efficient and helpful secretaries in Berlin and Trento. Firstly to Ina Severin, who so thoughtfully guide me through the admission process regardless of the distance difficulties of the beginning or the intricate bureaucratic steps required for a novice in Berlin. And finally to Marina Rogato in Trento for the multiple occasions she solved so efficiently any issue with the most careful attention.

Then is turn for my main supervisor Jörg Lewandowski for all his guidance during the multiple challenging steps of the PhD, from the experimental to the writing and publishing tasks, and particularly for his patience and approachability at any time, despite his very always busy agenda. I realize some of his virtues already shape my academic profile, and I think I will keep him as reference in all these aspects. Secondly, thanks to my second supervisor Alberto Bellin for his unparalleled kindness despite my delays, and especially for his impressive wisdom and expertise, crucial several times for developing the contents of the fourth chapter of this thesis.

Thanks now turn to the assistants at fieldwork: Wiebke Seher for her many extra hours at Schlaube, Jason Galloway for his always generous help with topography and EMI geophysics, Amaia Marruedo Arricibita for her intuition of the worth of the field site, Birgit Müller and Hanna Schulz for their interest to help on electrical conductivity survey and especially to Anne Mehrtens and Christine Sturm for their modelic cheerful attitude regardless the complex, tiring and time demanding fieldwork at Schlaube. The success of this thesis belongs to a great extent to you two. Finally to Karin Meinikmann for her availability for help during logistics preparations, for the rescue on the mud-incident with the car at the banks of river Schlaube, and for her multiple constructive suggestions to the manuscripts.

Thanks to Klement Tockner for agreeing to review this thesis.

A lot of thanks go to the SMART family in Berlin, from Oleksandra Shumilova who introduced me to the IGB life, to Maja Grubisic for her crucial intuition when my claim for help passed unnoticed to all, or to Abel de Souza Machado for his inspiring joviality in our time as neighbours at Villa Ehrlich. Thanks to the other friends at IGB, in special to all the ambassadors of Spanish happiness at IGB. My core in Berlin could not be completed without my best thanks to my Lewandowski's group family. Thanksgiving start with Anna Jäger and Jason Galloway for their friendly and always familiar company in our office and follows with Amaia Marruedo Arricibita who mastered on guiding me through the first experimental steps of the PhD. I must end up with our own 花木兰, the resilient and always wise and reliable friend Liwen Wu, to whom I must praise her many meaningful lessons about academy and life.

Then thanksgiving extends to Trento, firstly to Alyssa Serlet for her friendship and inspiring mindful and balanced attitude towards PhD and life, and to Gregor Lopez-Moreira Mazzacotte for all his friendly company in the office and his kind invitations to discover the magic charm of Dolomites. I must also give thanks to Milad Niroumand for the funny office times both in Berlin and in Trento, and to Valentina Premier for her kind neighbourhood in Berlin and her friendly local guidance in Trento. Finally, to all my multinational friends at the Babel tower of San Bartolomeo Studentato: Giorgio Massa, Mastad Ahmed, Alfred Mudonhi, Gias Uddin, Abdul Hannah Azzad-Niti Rahman, Maaz Jan and Nandu C Nair.

Even the landscapes deserve some thanks. Firstly to the wilderness of River Schlaube for having provided such an interesting and complex study site for my research. Secondly to the lakes and forest of Berlin which give relief to my homesickness. Thirdly, to the unforgettable views of the Adige's glacial valley while working in Trento that gave me inspiration for some of the contents included in this text. Finally, to my cold highlands of Iberia, where I left my siblings of green blood, whose blooming, fruiting and leaf-shedding I miss so much when abroad.

Then I must follow with thanks to my elusive rivers of faith, who will remain named as Cadagua, Elbe, Isarco, Ithikkara, Tevere and Paraguaçu. I bless their source of inspiration despite the droughts and the floods, hoping that their fountains keep crystalline giving relief to the tired explorers in their odyssey of seeking their own spring of happiness.

Finally, this thesis is dedicated to my family for being the support in the distance, the energy in the dismay, the advice in the doubt, the guide in the darkness and the hope in the uncertainty. My success with this PhD thesis is the success of my parents Feli and Carlos for their effort during my 32 years old journey and a great success of my sister Cristina who lead us all. This work belongs to them as much as it belongs to me.